Relations between GammaRay Burst time estimators and their implications

A Thesis

Submitted to the Graduated School of Science

Department of

Physics

in

Astrophysics

by

Nicolas Vasquez Pazmino

TOKYO INSTITUTE OF TECHNOLOGY

February , 2011

Examining Committee:

(chair) Nobuyuki Kawai, Ph.D.

Toshio Terasawa, Ph.D.

Akio Hosoya, Ph.D.

Tadayasu Dotani, Ph.D.

Fumio Kakimoto,Ph.D.

Abstract

Gamma-ray bursts (GRBs) have been proven to be cosmological objects that release a huge amount of energy in a relatively short time. Nevertheless the canonical classification of bursts is usually in the observer frame, giving birth to a bimodal distribution of GRBs, long and short. Recently, an intermediate class of bursts have been proposed and the intermediate class of GRBs is a recurrent topic of debate. The studies on the group of GRBs were renewed by the classification in the burst frame, as a first result of bimodal behavior of the cosmologically corrected Auto-Correlation Function (ACF) was reported. Following the recent classification trend, a sample of 15 GRBs with known redshift detected by Swift and Suzaku satellites is analyzed in this work. The simultaneous detection of long GRBs by the mentioned satellites offers the opportunity to study the prompt emission of GRBs in a broad energy band range (15-5000 keV). Using the duration time to release the 50% of the total fluence (T_{50}), the ACF evaluated at the full-width at half maximum and the emission time of the 50% of the total fluence (t_{50}) as temporal parameters first a possible sub-class of long GRBs is discussed when the temporal parameters are measured in the GRB frame. The three temporal parameters characterize a time interval of the same physical process, but they are not completely equivalent although they are strongly correlated. The relation is linear between T_{50} and t_{50} as well as ACF and t_{50}. In the time-space plane, 4 GRBs are have longer values of time estimators and they are relatively close suggesting a subclass of long GRBs. To elucidate if there is or not real evidence of this special class of bursts, temporal values were combined with the energy parameters to look for their spectra and energy counterparts. Extending the validity of the Yonetoku relation for the studied sample of bursts, we found that in the time-energy plane, the same 4 bursts exhibit a low isotropic luminosity (L_{iso}) and a low peak energy (E_p). A strong correlation between the remaining bursts in the time estimator-isotropic energy plane was observed, the correlations between t_{50} - Liso and L_{50} - t_p are especially high, which is interpreted as two different physical processes, since t_{50} is a temporal measure of the time intervals when the burst engine is in its most active phase. In the studied sample, 4 bursts could be characterized in the burst frame as long-dim-close bursts. The classification in the rest frame in time-space and energy of bursts allows to restrict more the possible progenitors of longs GRBs, and also demonstrated that the expansion of the Universe modifies all timescales and energy scales in the same way.

Acknowledgments

I would like first to thank the Ministry of Education, Culture, Sports, Science and Technology of Japan (MEXT) to make possible to pursue my studies with the financial support during the last six years. Also I am very grateful with Prof. Kawai, to receive me in his laboratory and specially for his patience and understanding of my Japanese language deficiency, as well as, his scientific support. I have to thank also WAM-Suzaku team, to provide me data, support and scientific advice, specially Dr. Yamaoka and Dr. Ohno. The laboratory members Yatsu, Toizumi, Usui, Nakajima, Sugimori, Enomoto and the younger students also need to be mention for their support with translations, explanations and friendship that help me to adapt to the laboratory life. Finally I thank the rest of teachers and friends I met during my stay in Japan.

Contents

Chapter 1

Introduction

The atmosphere of the Earth absorbs most of the gamma radiation coming from the space, so gamma-ray astronomy began to develop when detectors could reach altitude levels above the atmosphere using spacecrafts and balloons. Being a relative new branch of astronomy, there are still many unanswered questions among the gamma sources.

Gamma-ray astronomy processes included cosmic rays interactions with interstellar gas, supernova explosions, and interactions of energetic electrons with magnetic fields. Among one of the most enigmatic gamma sources in the Universe we have Gamma-Ray Bursts (GRBs), that were first detected in the early 1970s. These extremely bright objects with a duration in the order of seconds boosted the development of spacecraft technology and is continuously challenging the investigation of new high energy detectors. Nowadays, several satellites are detecting GRBs in a broad energy range given new challenges to the gamma-ray science.

It have passed almost 40 years since the discovery of GRBs and the understanding of their origin, physical process is still incomplete. Although it is well established the cosmological origin of GRBs, with the measure of high redshifts over 8 [35] and isotropically distributed, there are lacks of understanding of their progenitors, radiation mechanism and classification.

To contribute in study of GRBs, this work is centered in one of the canonical types of burst. Long GRBs emit the 90% of their fluence in more than 2 seconds [15] and is believed that have a different progenitor than the other canonical type known as short GRBs. In this purpose a sample of 15 burst with known redshift was selected with the peculiarity that those burst were detected by Swift and Suzaku satellite simultaneouslys. Swift launched in 2004 and Suzaku in 2005 carry detectors that combined offers the unique opportunity to observe GRBs from 15 to 5000 keV, as well as the possibility of perform spectral analysis.

The structure of this work start with a brief review of GRBs prompt emission, including the

physical processes, the temporal estimators and the already established relations between energy and spectral properties, as well energy with temporal properties. As a next step we described the instruments on board the two satellites, emphasizing in the specific detectors for GRBs, to continue the description of the analysis methodology used to extract spectra and time estimator of the selected bursts. The core of the study is centered in the analysis and interpretation of the extracted information which is divided in temporal estimators and spectral properties. Three temporal estimators were used, and after determining the relation among them, the possibility of reclassification of long GRBs is discussed. Following the idea of a bimodality of long GRBs, the spectral counter part is explored, without passing over the standard test for long GRBs given by the Amati-Yonetoku relations [1]. Finally we combined temporal, energy and distance information of GRBs to demonstrated that the classification of GRBs in their rest frame, reveals more hints about their origins that was hidden by the cosmological effects.

Chapter 2

Long Gamma-Ray Bursts

2.1 The prompt emission of Gamma-ray Burst

The cosmological origin of Gamma-Ray Bursts (GRBs) is widely accepted and introduced new challenges in the understanding of its origin, radiation mechanism and progenitors. Considered as the second more powerful explosive events after the Big Bang, many attempts have been done to use them as standard candles of the Universe[19].
GRBs emit radiation from radio band to GeV band and the emission is composed by a prompt emission and an afterglow. The prompt emission radiates in the high energy range of the electromagnetic spectrum and the afterglow radiates from soft X-ray until radio frequencies. In this work we are concentrated in the prompt emission of the GRBs, one of the main reasons is because almost the whole energy is released during this phase. Another challenging reason to center the study in the prompt emission is the lack of understanding of the radiative process, progenitors and classification. We will start a brief description of the prompt emission of GRBs starting with the observations history, the energetics and time properties, continuing with physical processes involved and finally the possible scenarios for the birth of GRBs.

2.1.1 Observations

Gamma-ray bursts observations started with Vela satellites in 1973, which was designed to monitor energetic gamma-ray transient events produced by nuclear weapons. The detected events were unlike nuclear, thus the cosmic origin of the signals gave born to the GRBs era. Only in 1992 with the launch of Compton Gamma-ray Observatory (CGRO); the onborad instrument Burst and Transient Source Experiment (BATSE) could demonstrate the isotropically distribution of bursts in position irrespective of flux (Fig. 2.1). The

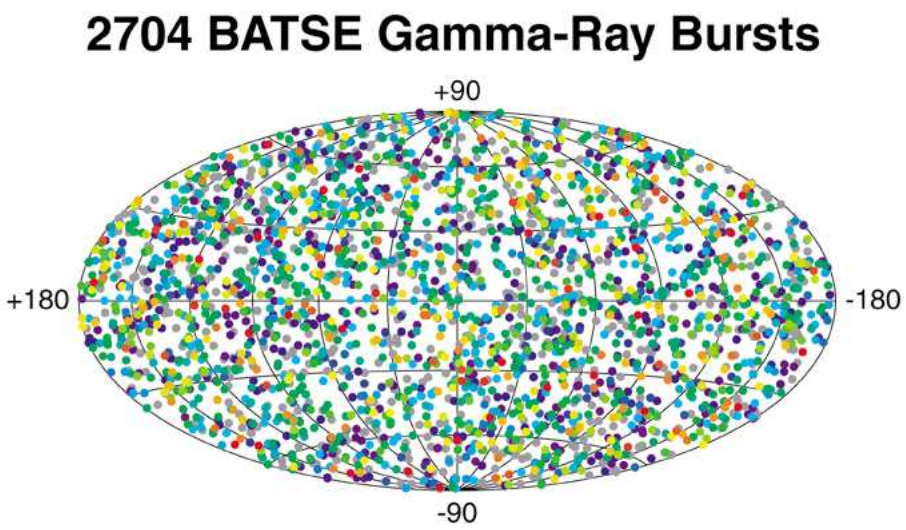

Figure 2.1: Isotropic distribution of GRBs from BASTE

Beppo-SAX satellite introduced measurements of redshifts of GRBs in 1997, suggesting the cosmological origin of bursts. In the present there are several missions detecting GRBs with a approximately rate of 1 event per day. The main characteristic of GRBs is its brightness, substantially bigger than the Milky Way and the rest energy of the sun.

2.1.2 Temporal properties and energetics

A GRBs is an intense emission of X-ray, gamma and GeV radiation that last from a fraction of a second to hundred seconds. The cosmological origin of GRBs is well established, their redshift is distributed from 0.01 to 8 approximately. The occurence of burst is isotropically distributed in the Universe and the common range of the isotropic luminosity is 10^{51}-10^{52} ergs/sec [38].

The spectrum of GRBs is nonthermal with an energy flux that peaks at a few hundred keV. Although there is any theoretical spectral model that satisfied most of GRBs, a phenomenological model introduced by Band *et al* (1993[13]) fits satisfactorily the majority of the observed spectra. Band model used two power laws joined smoothly at a break energy $(\alpha - \beta)E = 0$, the model is desbribed by the following equation.

$$N(\nu) = N_0 \times \begin{cases} (h\nu)^{\alpha} e^{\frac{-h\nu}{E_0}} & \text{for} \quad h\nu < (\alpha - \beta)E_0 \\ ((\alpha - \beta)E_0)^{\alpha-\beta}(h\nu)^{\beta} e^{\beta-\alpha} & \text{for} \quad h\nu > (\alpha - \beta)E_0 \end{cases} \tag{2.1}$$

In the equation describing Band model, α and β denote the spectral indices of the two power laws. When β is more negative than -2, νF_ν peaks at $E_p=(\alpha+2)E_0$. When the hard component of the model is not present, the spetra is characterized by a large negative value of β.

The temporal structure of a GRB is very complex, it is composed by pulses with different shapes that sometimes overlap. The canonical shape is described with a fast-rise and exponential decay. The time estructure is sensitive with energy, the burst becomes narrow with the increase of energy. There were made some attempts to measure the variability of the burst which is defined by the width of the peaks compared to the whole GRB duration [33] an it was found a correlation with the luminosity. A feature between the light curves of GRBs at different energies, is the delay between low energy photons with respect to high energy photons, this phenomenom is known as the spectral lag.

2.2 Physical process

The observed spectrum of a GRBs is nonthermal with a significant high-energy tail. Since the energy involved is around 10×10^{52} erg in a relative small time, the GRB physical process involves a compact object [38]. The main ingredients involved in the generation of a GRBs are particle acceleration, magnetic field amplification, synchrotron emission and inverse compton mechanism. The prompt emission is generated by high energy particles that have been accelerated within collisionless shocks. In this section we discuss the most important known mechanisms and models to convert the kinetic energy of the initial high energy particles into radiation.

2.2.1 Fireball model

A mechanism of generation of GRBs involves a central engine that liberates a relativistic plasma composed by electrons, positrons, photons and a possible baryon contamination component. A plasma with this characteristics is called a fireball. Inside the fireball internal and external shocks of particles with different Lorentz factor convert kinetic energy into random energy. The energy acquired by leptons is radiated by synchrotron process in the local magnetic field or inverse Compton radiation with photons from the fireball. The presence of baryons makes the plasma optically thick, allowing the emitted photons to revert the energy and momentum back to the fluid. The fluid becomes optically thin due to its relativistic velocity and high energy photons escapes producing a non thermal spectrum characteristic of a GRB.

During the fireball expansion, the radiated gamma-emission cools down the plasma and

external shock are produce with the interstellar medium (ISM). This is the beginning of the afterglow where the radiation will continuously be released in an increasing wavelength . During the afterglows, reverse shocks are able to generate bright optical emissions, but the properties of the reverse shocks are determined by the ISM density and the bulk Lorentz factor of the fireball.
The efficiency of all the involved process and the nature of the radiation depend on the magnetic field intensity and the distribution of velocities of electrons of the shock fronts. A possible mechanism is the synchrotron emission, with a power law energy distribution N(E) $\propto$ E^{-p} [36] for electron's velocities.

2.2.2 Blandford-Zaneck model

It is possible to picture a GRBs event using the models involving rotating black holes surrounded by an accretion disk . This mechanism was introduced by Blandford and Znajek (1977 [5]). Here we discuss briefly the process which involves relativistic magnetohydrodynamics and a full reference could be found in [5]. When the magnetic field and angular momentum of a rotating black hole is large enough, the vacuum surrounding the hole becomes unstable, any stray charged particles could be accelerated and radiate producing electron-positron pairs. The electromagnetic field in the vicinity of the event horizon will become approximately force-free. Using perturbation techniques approximate solutions are obtained. This mechanism extracts the rotational energy from the black hole-accretion disk system via the magnetic field.

2.2.3 Synchrotron radiation

As we mentioned before synchrotron radiation is a strong candidate for radiation mechanism of GRBs. The observations of GRBs events are also consistent with synchrotron spectra. We also established as fundamental parameters the intensity of magnetic field B and the energy distribution of electrons which is a function of a minimum Lorentz factor $\gamma_{e,min}$ and the index of electron distribution p. The determination of such parameters is very complicated [38] and two dimensionless parameters are widely use to deal with the emission process: ϵ_B and ϵ_e.
ϵ_B is defined as the ratio of the magnetic energy density U_B and the total internal energy e (Ec.2.2).

$$\epsilon_B = \frac{B^2}{8\pi e} \tag{2.2}$$

Similarly ϵ_e is defined as the fraction of total internal energy which is converted into random energy of electrons as we can see in the following equation.

$$\epsilon_e = \frac{U_e}{e} \tag{2.3}$$

It is assumed that ϵ_B and ϵ_e stayed constant during the burst evolution, also a power law distribution for electrons which could be expressed as a function of the Lorentz factor as is shown in the next formula.

$$N(\gamma_e) \sim \gamma_e^{-p} \quad \text{for} \quad \gamma_e > \gamma_{e,min} \tag{2.4}$$

In order to avoid electron-positron pair generation caused by high γ values, we consider a boundary condition of $p > 2$. The relation between p and $\gamma_{e,min}$ is

$$\gamma_{e,min} = \frac{p-2}{p-1} < \gamma_e > \tag{2.5}$$

where γ_e denotes the mean Lorentz factor of the distribution that writes as

$$< \gamma_e > = \frac{m_p}{m_e} \epsilon_e \gamma_{sh} \tag{2.6}$$

where γ_{sh} corresponds to the Lorentz factor of the shock front into the ISM. $< \gamma_e >$ also depends on the ration between baryons and electrons but the amount of baryons should be small since the fluid has to move relativistically. In the laboratory frame, the whole fluid has a Lorentz bulk factor γ_E, then the observed photons, blue shifted, have a characteristic energy of

$$h\nu_{sync} = \frac{\hbar q_e B}{m_e c} \gamma_e^2 \gamma_E \tag{2.7}$$

The associated cooling time for synchrotron radiation (t_{sync}) , defined as the ratio between the rest energy of the electron and the energy lost by synchrotron emission is written as

$$t_{sync}(\gamma_e) = \frac{3 m_e c}{4 \sigma_T U_B \gamma_e \gamma_E} \tag{2.8}$$

where σ_T is the Thompson cross section. Combining the last two equations we can express the cooling time as a function of energy as shown in the following formula

$$t_{sync} = \frac{3}{\sigma_T} \sqrt{\frac{2\pi q_e \hbar m_e c}{B^3 \gamma_E \nu}} \tag{2.9}$$

The cooling time limits the low boundary value of the time variability of the GRB, the spikes in a burst cannot be shorter than the cooling time. The width of a pulse is a direct measurement of the cooling by synchrotron emission.

2.2.4 Compton radiation

The inverse Compton scattering (IC) of synchrotron emitted photons affects the spectral profiles of the radiation. Low energy photons could be scattered many times until their energy become larger than the electron rest mass, and the probability of dispersion is reduced to the Klein-Nishina limit. The effect of IC is determined by the comptonization parameter Y, usually in lower case the IC scattering becomes important when $Y > 1$. At this regime a considerable fraction of synchrotron photons are dispersed and IC emission becomes important. The emission is detected at high energies (X-rays, γ -rays) which makes it difficult to recognize the IC effect. Nevertheless, the IC energy losses produce a significant cooling of the electrons of the plasma and the cooling time should be shorter than synchrotron cooling time. The energy density of the electrons constitutes the disposable radiation energy, which needs to be radiated by synchrotron and IC processes. The total emitted energy U_e is

$$U_e = U_{sync} + U_{IC} \tag{2.10}$$

IC photons are generated by scattered synchrotron photons, then the Y parameter could be expressed as the ratio of IC emission and synchrotron emission looses, in other words as the ration of synchrotron energy looses energy and the density of magnetic field.

$$Y = \frac{U_{IC}}{U_{sync}} = \frac{U_{sync}}{U_B} \tag{2.11}$$

In the last section we introduced two dimensionless parameters, U_B=$e\epsilon_B$ and U_e=$e\epsilon_e$ that allow us to write the comptonization parameter as follows.

$$Y \equiv \frac{\epsilon_e}{\epsilon_B} \quad \text{for} \quad \epsilon_e \ll \epsilon_B \tag{2.12}$$

$$Y \equiv \sqrt{\frac{\epsilon_e}{\epsilon_B}} \quad \text{for} \quad \epsilon_e \gg \epsilon_B \tag{2.13}$$

The condition for IC scattering depends on the Y value, the contribution is low when $Y < 1$ corresponding to $\epsilon_e < \epsilon_B$ and the radiation process is synchrotron. If $\epsilon_e > \epsilon_B$ most of the radiated energy should have an IC origin. For a formal discussion of the synchrotron and IC processes, see reference [34].

2.2.5 Possible progenitors

Progenitors of GRBs need to generate relativistic jets and they should involve compact objects, those basic ingredients were discussed in last paragraphs. A possible scenario involves a rotating black hole surrounded by an accretion disk is the Blandford-Znajek process. The physical processes and origins necessary to accelerate a fireball are quite speculative. Compact object as rotating powered pulsars, collapse of a massive stars (Collapsars), supernovae (SN) explosions constitute the possible progenitors for long GRBs. Short GRBs have as a possible progenitor compact star in coalescence [29]. In the past several years evidence of GRB/SN connections have been observed, therefore we will emphasize in the collapsar model [31]. Very special conditions are required for a star to evolve all the way to a GRB under the collapsar model. The star must be very massive, at least 40 solar masses [41], to form a central black hole in the first place, the star must be rapidly rotating to develop an accretion disk capable of launching jets, the star must have low metallicity not to lose its angular momentum by mass loss and the star must be able wipe out its hydrogen envelope so the jets can reach the surface. As a result, GRBs are far rarer than ordinary core-collapse supernovae, which require that the star be massive enough to fuse all the way to iron, a deeper discussion could be found in Piran 2005 [38, 29].

2.3 GRBs time estimators

The durations of GRBs is been discussed since their discovery, including the classification between the long and the short bursts. Calculating the duration of the time interval starting when 5% has been detected and ending when 95% of the total fluence gave this canonical classification and the definition of the T_{90} estimator. Long bursts are which T_{90} last longer than two seconds.The bimodality of GRBs started with Kouvelitou in 1993[15] when the logarithms of the duration were studied. Nevertheless, some other durations have been introduced to measure how the prompt emission time history evolves. In this chapter we discuss three time estimators and the results of their use to characterize long GRBs. The measures of time we choose are the autocorrelation function (ACF) at full-width at half maximun (FWHM), the 50 percent of the accumulated fluence and the time of emission of 50 percent of the total fluence. To clarify the explanation of the time estimators, we show GRB070508 as an example for the definition and calculation of the temporal parameters.

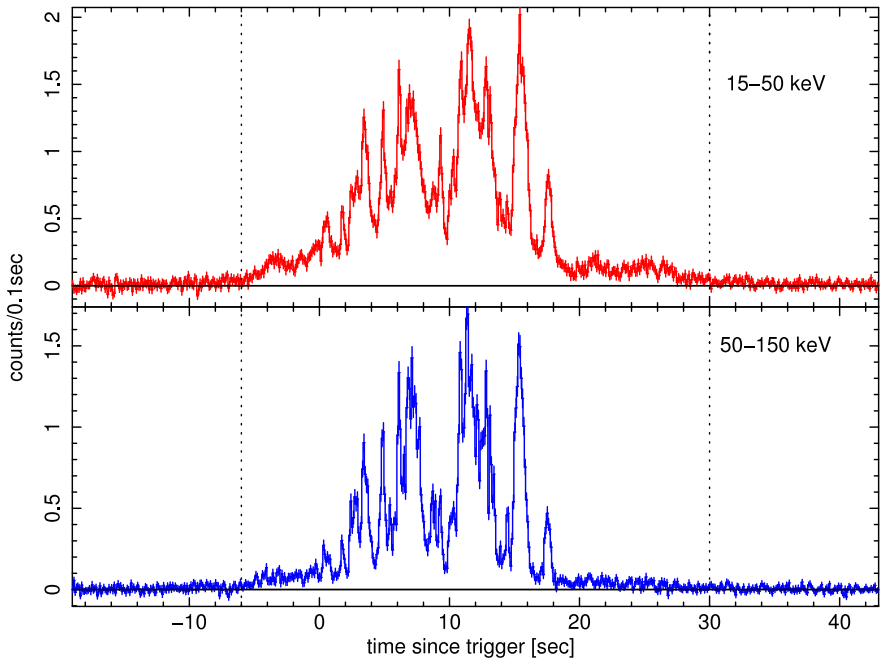

Figure 2.2: Lights curves of GRB070508 in two energy bands (Swift-BAT detector), z=0.82

2.3.1 Auto-correlation function

The autocorrelation function (ACF) is considered a powerful tool in time series analysis because ACF is the Fourier transform of the power density spectra [7, 6]. This fact comes from the Wiener-Khinchin theorem which states that the power spectral density of a random process is the Fourier transform of the corresponding autocorrelation function. ACFs were first introduced into the GRB study by Link et al.(1993)[27] and Fenimore et al.(1995) [17]. The ACF of the light curves gives information about the internal structure of a burst. It is established that the ACF of a light curve in a given band becomes narrow when the energy band of the light curve increase. The narrowing of the ACF with the increase of energy follows a power law considering that the ACF is self similar at different energy bands [17].

The definition of the discrete ACF for a uniformly sampled count history with ΔT time resolution, N time bins and m_i total observed counts at bin i with a corresponding background b_i is shown in the following equation. Where C_i are the net counts defined as C_i=m_i-b_i, δ is the Kronecker function and A_0 is the normalization.

$$A(\tau = k\Delta T) = \sum_{i=0}^{N-1} \frac{C_i C_{i+k} - m_i \delta_{0k}}{A_0} \quad k = 1, ..., N-1 \tag{2.14}$$

Asumming the periodic boundary condition C_i=C_{i+N}, the normalization condition

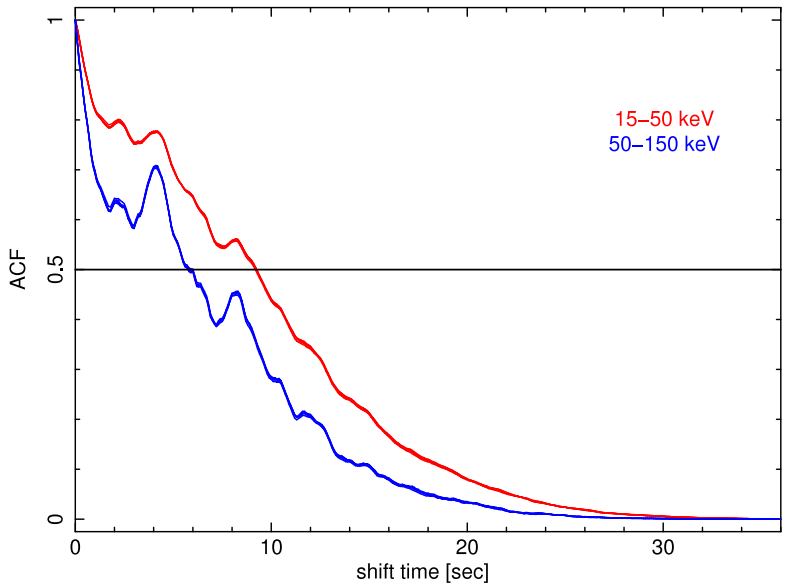

Figure 2.3: Determination of ACF-FWHM for GRB070508 in two energy bands

holds A_0=1 for k=0. The normalization condition is shown in equation 2.15 where the m_i term subtracts the contribution of the uncorrelated noise considering that it obeys the Poisson statistics. In figure 2.3 it is possible to visualize the ACFs of GRB070805 which light curves are in figure 2.2.

$$A_0 = \sum_{i=0}^{N-1} C_i^2 - m_i \tag{2.15}$$

Among the properties of the ACFs of GRBs, we have that they are not self-similar to the GRB time profile which converts it into a count rate independent tool to study the prompt emissions of GRBs at different energies without introducing mathematical assumptions in the model of the light curve[44]. In the last few years, Borgonovo et al.[6] demonstrated a bimodal distribution of long GRBs when the ACF is corrected for cosmic time dilation. Furthermore, signatures of cosmological time dilation have been studied using similar techniques [9], nevertheless the cosmological time dilation seems to be mixed with intrinsic effects. Correlation among bursts are believed to come from the combination of cosmological and intrinsic effects while correlations among pulses in a single GRB give a measure only of intrinsic effects[8].

Time profiles of GRBs generally are complex and energy dependent, and the presence of pulse structure reflects the temporal behavior of the inner engine [33]. It is believe that each pulse is closely related to the collision of two consecutive shells in a Fireball model [38]. The analysis of pulses from the prompt emission of GRBs has been studied with time

resolved spectral analysis[39]. The investigation of the spectral lag of individual pulses performed by Hakkila et al.[22] demonstrated that spectral lag is a pulse property rather than a entire prompt emission characteristic. The intrinsic properties of GRBs continue to be an mystery since the high variability.Comparing to pulse fitting techniques to describe a GRB light curve, ACFs do not need to introduce any mathematical assumptions that could introduce non phenomenological or instrumental errors. The pulse fitting technique is powerful to characterize the pulse parameters [3].

2.3.2 Duration times

The measure of the T_{50} is based on the same principle of T_{90} value (Kouvelitou [15]). This measure is sensitive to the pulses and internal structure of the prompt emission. This kind of time estimators give the canonical classification of GRBs in long and shorts [Kouvelitou [15]]. T_{50} measures the duration of the time interval starting when 25% has been detected and ending 75% of the total fluence. T_{50} is not sensitive to precursors and soft structures in the beginning or end of a burst. In figure 2.4 the T_{50} region of GRB070508 is shown, the T_{50} values is given by the difference of the time where the integrated fluence equals 75% of the total fluence and the time when the fluence equals 25% of the total fluence.

Using a large sample of bursts GRBs and their T_{90} duration, Horvath et al.[25] demonstrated that a third class of GRBs produce better statistics than the canonical bimodal classification. In posterior works using Swift data the classification of GRBs into short, intermediate and longs was confirmed [26, 24].

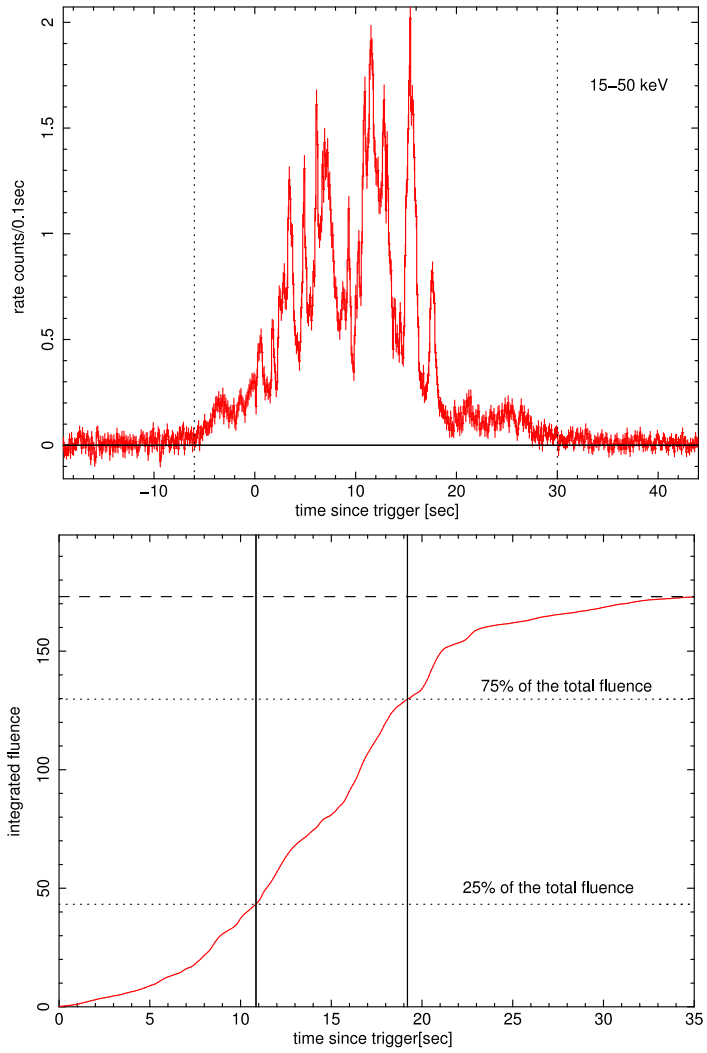

Figure 2.4: T_{50} determination for GRB070508 (15-50 keV band), T_{50}=8.80 sec The light curve in 15-50 keV band is shown in the top panel and in the bottom panel the corresponding integrated fluence in time

2.3.3 Emission time of 50 percent of the total fluence

Another method to estimate the lenght time of a burst was introduced by Mitrofanov in 1999[16]. This method is defined as the time of emission of the half of the total fluence (t_{50}), detected from the highest flux level. This measure excludes all the low emission intervals of a burst, and characterizes the states corresponding to high power emission. This time estimator gives information about the time intervals where the GRB engine is its more active phase. Mitrofanov‘s time measure method usually is shorter than the already mentioned T_{50} [16]. In figure 2.5 the method to determine t_{50} is explained. With the original light curve a decreasing order light curve is generated. Using the new reordered light curve, we calculate the integrated fluence and the t_{50} time corresponds to the summation of all the

bins which rate is larger than rate corresponding to the 50% of the total fluence.

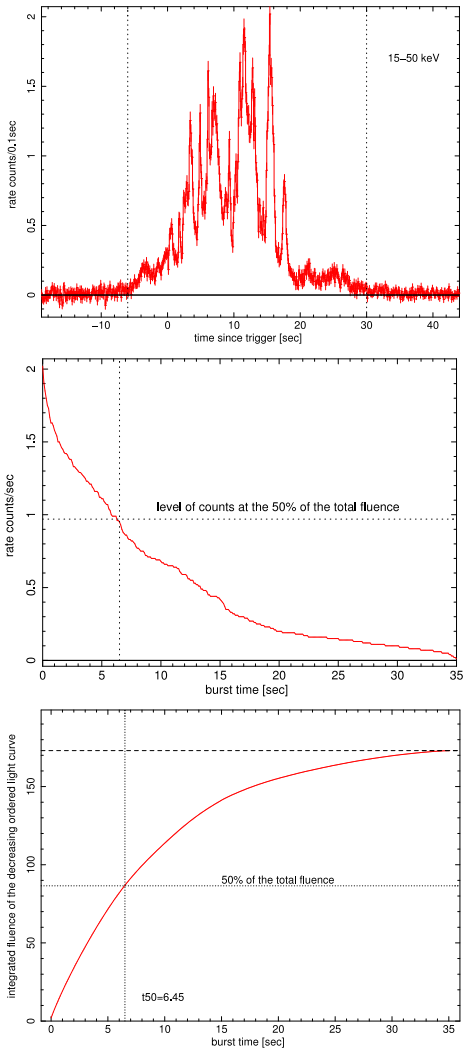

Figure 2.5: Mitrofanov t_{50} estimator determination for GRB070508 (15-50 keV band) The top panel shows the original light curve of the burst, the middle panel corresponds to the decreasing reordered light curve and the botton panel shows the integrated rate in time of the reordered light curve.

2.4 Luminosity relations

The detection of afterglows and redshift estimates of GRBs since the BeppoSAX satellite era introduced intriguing properties of GRBs in their cosmological frame. Correlations between spectral parameters and energy, as well as time histories with energy, at GRBs rest frame proved the cosmological origin of bursts. In this section we explore these two kind of properties of bursts that are intrinsic of the cosmological frame.

2.4.1 Intrinsic spectral and energy relations

The discovery of the correlation between the cosmological rest-frame νF_ν spectrum peak energy and the isotropic radiated energy E_{iso} in Amati work [2] gave born to a series of enigmatic properties of GRBs. The so called Amati relation is continuously been extended after the post-BeppoSAX mission era, demonstrating that their origin is rather physical than caused by instrumental selection effects [1]. A direct interpretation is the optically thin synchrotron shock model [2] for an electron distribution with a power law shape. This kind of results help to restrict the physical model of GRBs. Figure 2.6 shows the first Amati relation for 12 long GRBs.

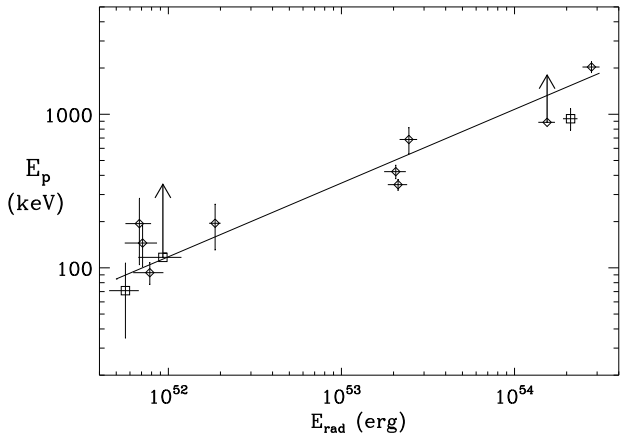

Figure 2.6: Amati relation for 12 GRBs Amati[2002[2]]

Among the spectral and energy relations we find Ghirlanda relation, peak energy-collimated corrected energy [20] and Yonetoku [43] which offers a tighter correlation. A similar relation between the peak energy and Luminosity is discussed by Schaefer [37]. Recently, Goldstein et al. [21]demonstrated that the peak energy fluence ratio leads to the canonical classification of GRBs in short and long bursts, avoiding a time estimation. [4]

2.4.2 Temporal and energy relations

Light curves of GRBs present a broad morphology, depending on the intrinsic GRB time history and energy band. To clarify the physics hidden inside the time profiles of GRBs, the study of various temporal parameters and energy were done. The relation between temporal properties, such as duration and spectral lags, and energy are widely studied. An Spectral lag is the time difference between low energy photons and high energy photons. The spectral evolution timescale of pulse structures is anticorrelated with peak luminosity[30, 3] and

it has been demonstrated that spectral lags are pulse rather than burst properties holding a negative correlation between peak lag and peak luminosity in GRBs[22]. In figure 2.7 we can see that the anticorrelation is not held by short bursts neither GRB/SN bursts.

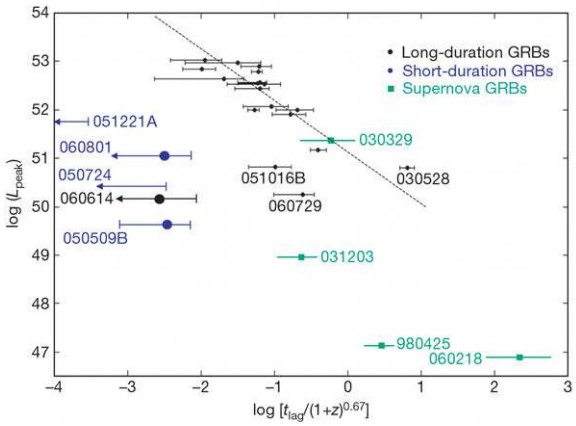

Figure 2.7: Anticorrelation between specral-lag and peak luminosity Gehrels[2006[18]]

The duration of the prompt emission has several interpretations, defining the transition time for the prompt component (Tp) a relation with the X-ray luminosity is established (Qi and Lu 2010[32].

Chapter 3

Instrumentation

In this study we used a set of GRBs detected simultaneously by Swift and Suzaku satellites. The high energy detectors on board those missions cover a broad range of energy. Both missions are the complementarity and permit to detect emission from soft X-rays until γ radiation. In this chapter a description of both observatories is presented, with special emphasis in the detectors designed to observe the prompt emission of bursts.

3.1 Swift satellite

Swift satellite was launched into a low-Earth orbit on a Delta 7320 rocket on November 20, 2004. This multi-wavelength observatory specially dedicated to observe GRBs in the gamma-ray, X-ray, ultraviolet and optical waveband. Among the main achievements, Swift detected GRB090423, the most distant known spectroscopically object in the Universe at z=8.3 and currently localizes approximately 100 GRBs per year. The Swift telescope payload is comprised of three instruments which work in tandem to provide rapid identification and follow-up of GRBs and their afterglows. The Burst alert Telescope (BAT), the X-ray telescope and The UV/Optical telescope (UVOT) composed this mission (Fig. 3.1). The spacecraft autonomously slews within 20 to 75 seconds of detecting a GRB so that the fields of view (FoVs) of the three instruments overlap the location of the burst.

3.1.1 Instruments

The three detectors of Swift are co aligned and permit to observe GRBs from the prompt emission until the afterglow times. The BAT is a wide-field, coded-mask gamma-ray detector that is sensitive to energies of 15-150 keV. It detects GRBs, computes their positions to 1-3 arcminutes, and triggers autonomous slews of the spacecraft to point towards the

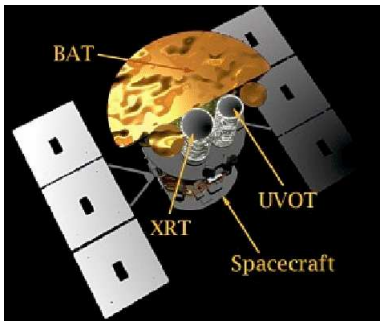

Figure 3.1: Swift satellite and it instruments on board

bursts.
The XRT is a narrow-field X-ray telescope that localizes a GRB to approximately 2-3 arc-seconds, and performs imaging and spectroscopy in the 0.2-10 keV band.
The UVOTis a narrow-field UV/optical telescope with a 30 cm aperture mirror that operates at wavelengths between 1600 $\mathring{A}$ and 6000 $\mathring{A}$. It provides burst positions to 0.5 arcseconds relative to the stars in its field of views (FoV), a finding chart, and performs broad-band imaging on GRB afterglows.

3.1.2 Burst Alert Telescope

BAT with its large field of view (FoV) is designed to provide critical GRB triggers and 4-arcmin positions, in figure 3.2 the BAT instrument is shown. It is a coded aperture imaging instrument with a 1.4 steradians field-of-view half coded . The energy range is 15-150 keV for imaging with a non-coded response up to 500 keV. BAT coded aperture FoV always includes the XRT and UVOT FoVs, long duration gamma-ray emission from a burst can be studied simultaneously in the X-ray and UV/optical regimes. The BAT is composed by 32768 pieces of CdZnTe that form a 1.2×0.6 m sensitive area detector. Groups of 128 detector elements are assembled into 8×6 arrays, each connected to 128-channel readout Application Specific Integrated Circuits.

The BAT has a D-shaped coded aperture mask, made of approximately 54000 lead tiles with an area of 2.7 m^2 (Fig 3.3). The coded-aperture mask uses a completely random, 50% open-50% closed pattern. A detailed description of the instruments is available in[14].

BAT data

There are two types of data produced by the BAT, standard survey data and standard burst model data. The standard survey mode data products are sky images, a catalog listing of all detected sources, light curves for all detected sources, spectra and response matrices for all

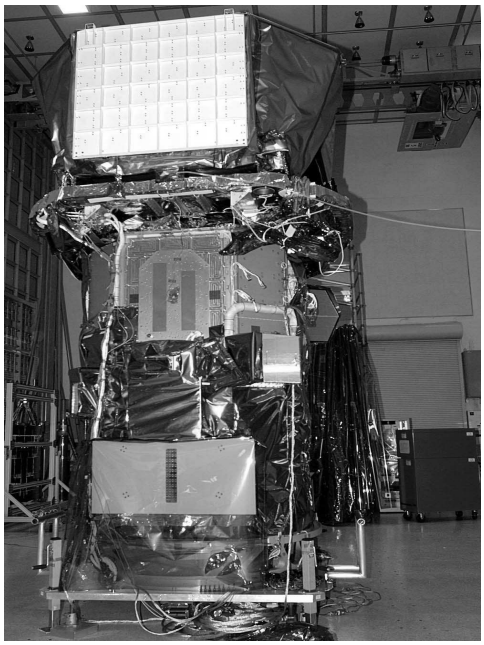

Figure 3.2: BAT instrument

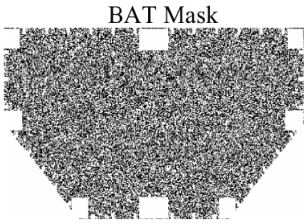

Figure 3.3: BAT mask

detected sources, and pointing maps. In survey mode the instrument collects count-rate data in five-minute time bins for 80 energy intervals. The standard Burst Mode data products are burst spectra on various time scales, response matrices, light curves, and images. When a burst occurs it switches into a photon-by-photon mode and pre-burst information is also saved. BAT event data is the most relevant data, it allows background removal using mask weighting technique.

3.2 Suzaku satellite

Suzasu was successfully launched on July 10, 2005 from the Uchinoura Space Center (USC) in Japan. The principal achievement of this mission was to carry the first X-ray

micro-calorimeter to the space. Suzaku is placed in a near-circular orbit with an apogee of 568km, an inclination of 31.9degrees, and an orbital period of about 96minutes. The maximum slew rate of the spacecraft is degrees/min.

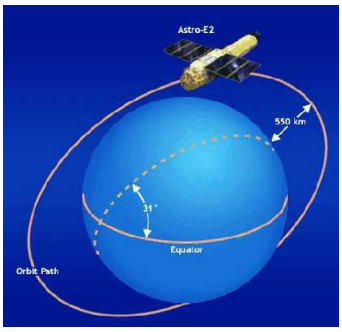

Figure 3.4: Suzaku satellite orbit

3.2.1 Instruments

Suzaku is composed by five nested conical thin-foil grazing incidence telescopes (XRT) four with focal lenght of 4.75 m and one with 4.5m. At the focus of each telescope there are distributed one X-ray Spectrometer (XRS) and 4 X-ray imaging Spectrometer (XIS). XRS works in the energy range from 0.3 to12 keV with an effective area of 190 cm^2, an energy resolution of 6.5 eV at 6 keV and a FoV of 2.9‘×2.9‘. Each unit of XIS is a 1024×1024 pixel CCD detecting in the energy range of 0.2 to 12 keV. Three CCDs are front illuminated and one back illuminated. The effective area is 340 cm^2 for the front illuminated and 390 cm^2 for the back illuminated. The energy resolution of XIS is 130 eV at 6 keV with a FoV of 18‘×18‘.
The other instrument is the Hard X-ray Detector (HXD) which is made of GSO crystals and silicon PN diodes. The HXD operates between 10 to 600 keV, GSO scintillator in energies over 30 keV and silicon PIN diodes in energies below 60 keV. The effective area is 145 cm^2 at 15 keV (PIN) and 315 cm^2 at 100 keV (GSO). The correspondent FoV is 34‘×34‘ below 100 keV and $4.5^o \times 4.5^o$.
The last detector is the Wide-band All-sky Monitor which is the lateral BGO aniti-coincidende shield of the HXD.

3.2.2 Wide-band All-sky Monitor

The WAM is a large and thick anticoincidence shield of the Hard X-ray Detector onboard Suzaku. WAM detector is composed by 4 identical walls, each one has 4 anti-counter

units (Fig.3.2). The main role of the WAM is the background rejection for the HXD main detectors, i.e. PIN diodes and GSO. It also has a wide field of view and a large geometrical area of 800 cm^2 per one face, which can be utilized as an all-sky monitor aiming for GRBs, solar flares, and bright X-ray transients. The sensitive energy range for the WAM is from 50 keV to 5000 keV in gamma-rays [42]. The excellent feature of the WAM is its large effective area of 400 cm2 even at 1 MeV (Fig.2), which enables us to study the high energy radiation of the GRBs at MeV range (Gonzalez et al. 2003) and determine a peak energy above 300 keV of the synchrotron emissions. Two types of data are produced by WAM, gamma burst data (BST) transient (TRN) data. BST data is available when a trigger occurs, the time history data (TH) has a fine resolution of 1/64 s in 4 energy ranges and 55 channel pulse height (PH) histogram data with coarse time resolution of 1 s. TRN data covers all the time with 1-second time resolution for monitoring the background. In table 3.1 the characteristics of WAM data are shown.

Data	Energy	Time resolution	Time coverage
BST	4ch	1/64 s (TH)	64 s
BST	55 ch	0.5 s(PH)	64 s
TRN	55 ch	1 s (PH)	telemetry each 1 s

Table 3.1: Characteristics of the WAM data

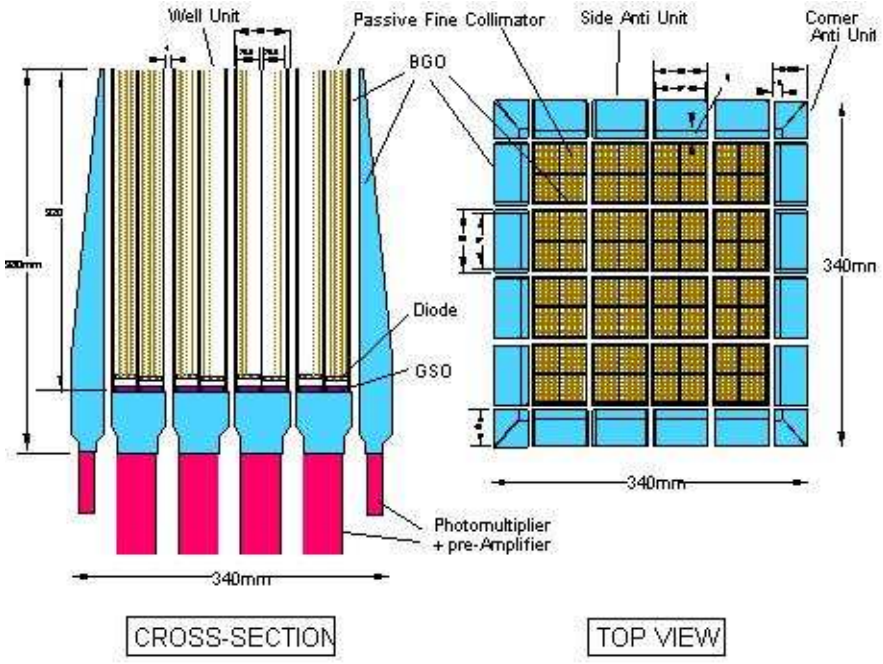

Figure 3.5: Views of the HXD scintillation counters, WAm consists of the surrounding 20 BGO scintillion counters

Chapter 4

Gamma-Ray Bursts analysis

4.1 Data reduction

The sample of GRBs used in this study is composed by 15 bursts with known redshift detected by Swift and Suzaku satellites. The following table shows the sample with the time since mission corresponding to both satellites and the GRB duration used for the spectral and temporal analysis. For Swift the time is expressed in seconds since 2001.0 UTC (decimal) and for Suzaku in seconds since 2000.0 UTC (decimal).

GRB	Swift (T0)	Suzaku (T0)	Tstart	Tstop
GRB060814	177289340.42	208911740.04	T0-7	T0+165
GRB060908	179398643.78	211021043.35	T0-13	T0+18
GRB061007	181908490.3	213530889.81	T0-10	T0+100
GRB070508	200290699.78	231913098.84	T0-6	T0+30
GRB070612A	203308728	234931126.98	T0-8	T0+300
GRB071003	213090057.28	244712456.01	T0-10	T0+50
GRB071010B	213741950.27	245364348.99	T0-2	T0+30
GRB080319C	227622359.62	259244757.96	T0-1	T0+40
GRB080413A	229748062.02	261370460.3	T0	TO+35
GRB080916A	243251123.71	274873521.61	T0-3	T0+60
GRB090424	262275134.02	293897531.33	T0-1	T0+30
GRB090618	267006514.69	298628911.85	T0-8	T0+160
GRB090812	271749733.89	303372130.9	T0-7	T0+80
GRB091127	281057151.1	312679547.81	T0-1	T0+15
GRB100413A	292872814.08	324495210.38	T0-2	T0+230

Table 4.1: GRBs sample and triggert time expressed in mission elapsed time [sec]

4.1.1 Swift-BAT data

In the spectral analysis of Swift, we use BAT event files to extract spectra and light curves. The equivalent energy of the used channels are 15-150 keV, and two light curves were extracted in 15-50 keV and 50-150 keV band. The definition of counts for a light curve from BAT detector is a background subtracted counts per fully illuminated detector for an equivalent on-axis source. The area of a single BAT detector is 0.16 cm^2 . Thus, the conversion between per unit area for fully illuminated detector is counts.cm-2 = counts.fully illuminated detector.0.16cm^{-2}

The spectra were corrected by the standard tools, mask-weighting and systematic errors. The software for BAT analysis is distributed by HEAsoft as well as the latest calibration files CALB(2009).

4.1.2 Suzaku-WAM data

Suzaku-WAM detector, is composed by four units as we mentioned in chapter 3. Each of the WAM units detect a GRB independently, and the sometimes the detection is to noisy or is not detected at all. As an example, in figure 4.1 GRB070508 has been detected in a better way by WAM1. Taking this fact into account, we only extracted data from the unit with the better signal.

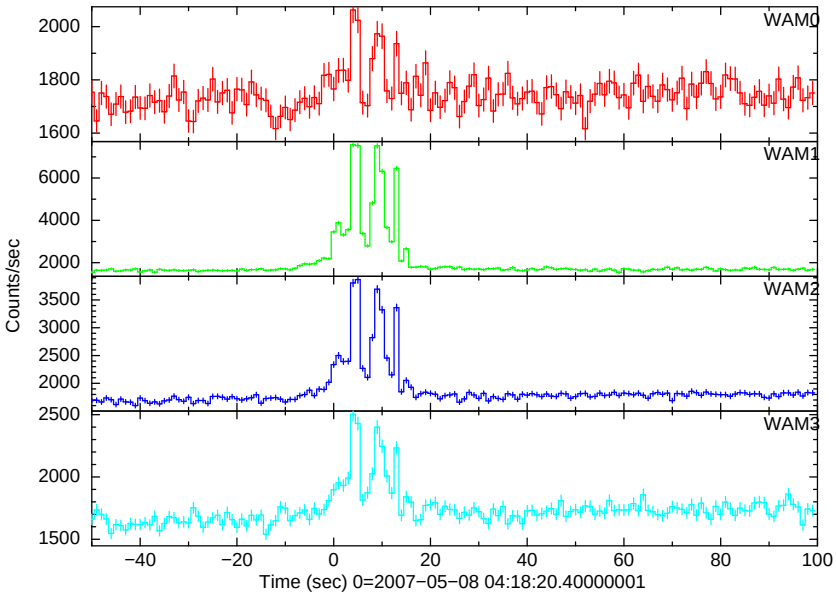

Figure 4.1: GRB070508 light curves for each WAM unit in channels 2-16

From each WAM unit it is possible to extract spectra and light curves. The software for this purpose has not yet been made public, then the analysis was done inside the WAM team

and with they collaboration. The structure of the response files are complicated then they were generated by a WAM-team specialist. There are standard tools to create spectra, but only for transient data. To generate spectra we use transient data (1 sec time resolution), we ignore channel 0-4 since the response files have systematic uncertainties in low energies. When count level is to high, it is necessary to introduce a systematic error of 10% in channels 0-10. Light curves could be generated using both kinds of WAM data (BST, TRN), if the burst triggered the detector BST data is available. Light curves were generated in four bands as described in table 4.2. The energy correspondence depends on gain drift of the detector and is taken into account in the response files.

Band	channels
TH0	2-3
TH1	4-7
TH2	8-16
TH3	17-54

Table 4.2: Energy bands channels correspondence

4.2 Spectral models

The spectral analysis was performed using XSPEC 12.6 software package. Suzaku and Swift spectra were fitted together using a GRB model or cut-off-power law model. Only GRB091127 was fitted using a sinple power low, the other two spectral models gave poor statistics and GRB091127 is associated with a supernova. The GRB model inside is XSPEC corresponds to a Band function (Ec. 2.1) . The cut-off power model has the following formula:

$$N(E) = \frac{E^{-\alpha}}{100keV} E^{-\frac{E(2-\alpha)}{E_p}} \tag{4.1}$$

where α is the power law index and E_p is the peak energy. The advantage of this definition of power law comes from the direct calculation of value of the peak energy. The combined spectra from Suzaku and Swift of the selected bursts are shown in appendix A.

4.3 Temporal estimators analysis

A complementary analysis was performed in order to investigate the duration of the bursts. With the extracted light curves we proceed to determine three different time estimators. Bellow we explain the methodology to determine the temporal parameters. The light curves of the 15 bursts in 15-50 keV and 50-150 keV bands are available in appendix A. Suzaku light curves in TH0, TH1, TH2 and TH3 are shown, with their energy equivalence.

4.3.1 Autocorrelation function methodology

Autocorrelation functions, considered powerful tools in the study of time series, introduce statistical fluctuations [6]. To reduce the uncertainties, we generated Monte Carlo simulations of the light curves (100) and we proceeded to calculate the ACF of each one of the simulated light curves, following the definition of chapter 2. In order to take into account the uncorrelated noise, we assumed that the noise of each simulated light curve obeys a Poisson distribution. We measure the ACF broad values at the Full Width Half Maximum (FWHM) and we take the value with a confidence level of 90%. ACF is a symmetric function, then it is enough to determine the half of the function and the measured values only need to multiply by 2.

In figure 4.2 , it is possible to observe an example of the simulated light curves of GRB070508 in two energy bands. For each light curve we generated the associated ACF, in Figure 4.3 it is possible to observe the amplified region of the ACF around the FWHM. The ACFs corresponds to the light curves in 15-50 keV band, and the ACF-FWHM values lays in the region between the black lines. Within the red lines, the ACF-FWHM value is determined with a 90% of confidence level. To calculate the ACF of the selected GRBs, we used light curves with a bin size of 100 miliseconds for bursts with a high signal to noise ratio. For GRB070612A and GRB100413A the bin size of the light curve was 1 second in order to improve the signal to noise ratio. Nevertheless these two GRBs have a T_{90} longer than 200 seconds enough longer compared to the bin size.

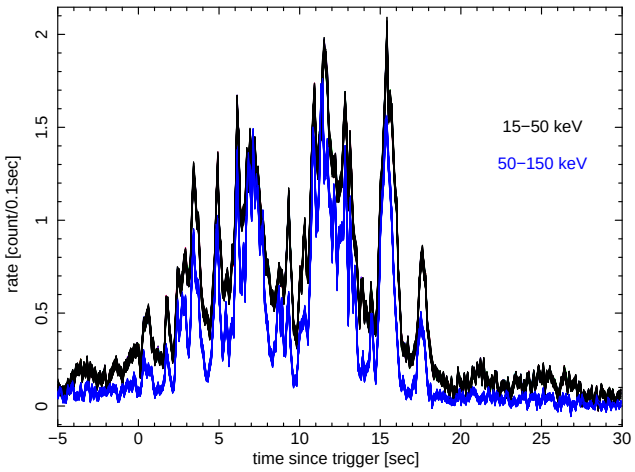

Figure 4.2: Simulated light curves of GRB070508 generated from original Swift light curves. The noise of each of the light curves follows the Poisson statistics

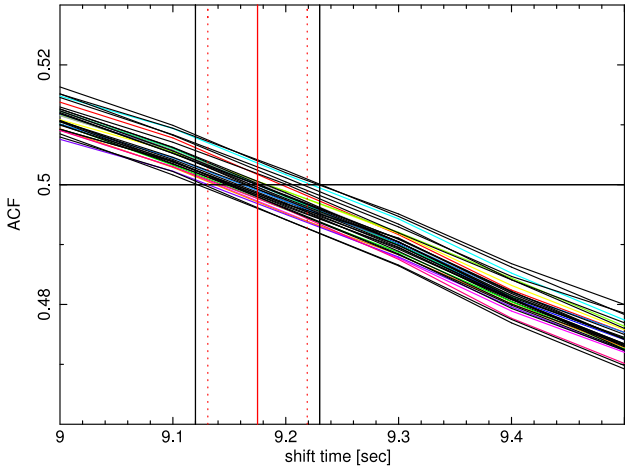

Figure 4.3: ACFs of the simulated light curves of GRB070508 in 15-50 keV band, the region between dashed red lines correspond to 90% confidence level

4.3.2 Duration time T_{50} calculation

For the calculation of T_{50} we used the associated software for each data type. For Swift data we used the **battblocks tool**, which is distributed with HEAsoft software. And for Suzaku data, there is also an available tool to determine the T_{50} value. Nevertheless, Suzaku tool has not been yet released, but it works similarly to **battblocks tool** using Bayesian blocks. In figure 4.4, we show the example of T_{90} and T_{50} for unit WAM1 in all the channels.

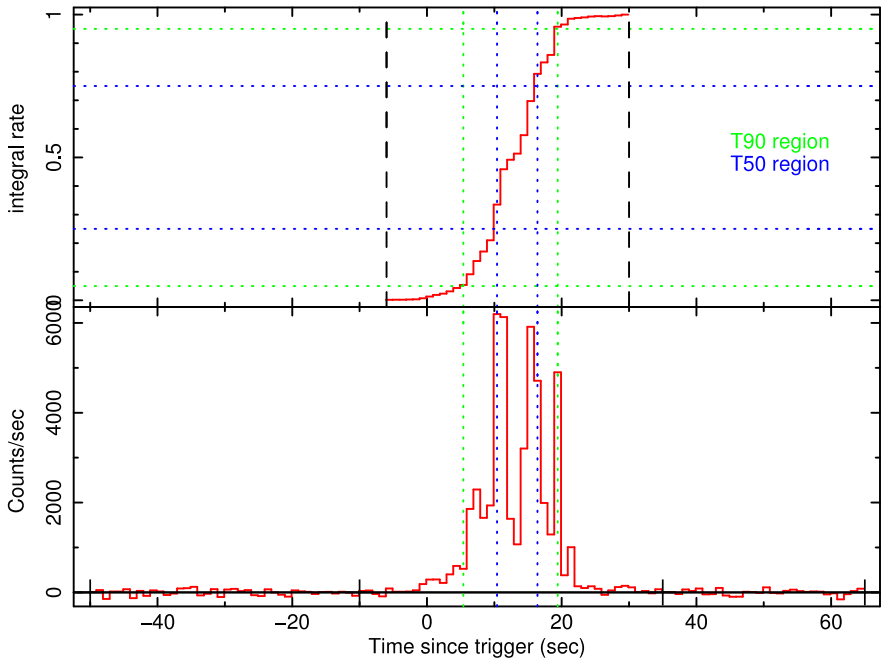

Figure 4.4: T_{50} and T_{90} regions of GRB080705 from WAM1 unit in channels 0-54

4.3.3 Time of emission of the 50 percent of the fluence t_{50}

The estimation of the t_{50} parameter was done following the established method mentioned already in Chapter 2. Using the original light curve in a given band, we reordered it into a new light curve in decreasing order of counts. With this new light curve we determine the integral rate, and example of the procedure is plotted in figure 2.5 . We repeated the same process using the simulated light curves to obtain an error estimation, measured also in a 90% of confidence level of counts at the 50. In Figure 4.5, and example of the obtained region of emission times for GRB070508 in the 15-50 keV band is shown.The plot corresponds to the reordered simulated light curves and the duration time is determined in function of the count level at 50% of the total fluence. The values inside the red lines correspond to the 90% confidence level of the emission time. Differently as T_{50} which is determined by a time difference, t_{50} is determined by the line which crosses the value of the half of the total integrated fluence in the original light curve.

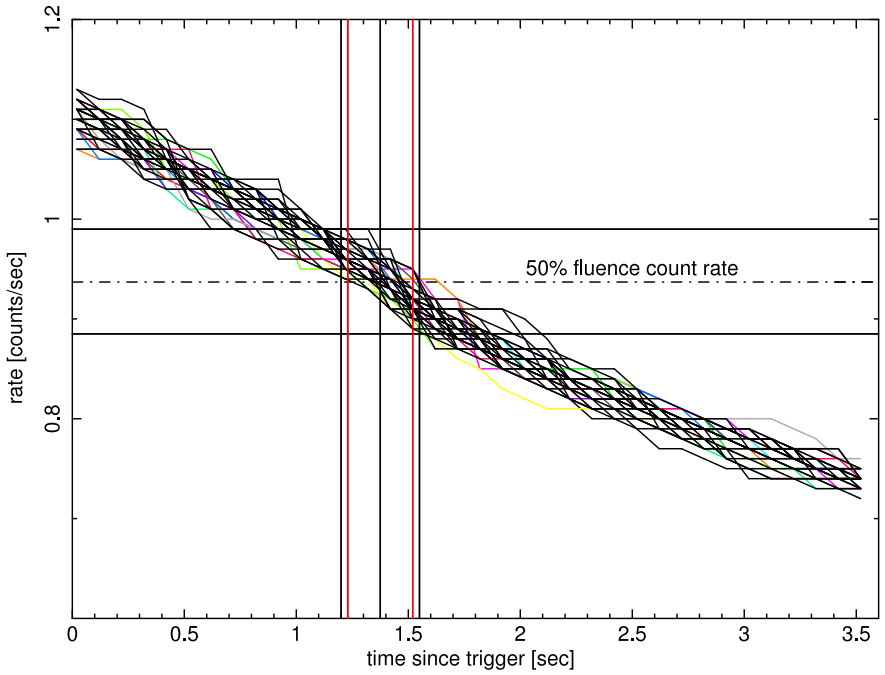

Figure 4.5: Determination of the emission time (t_{50}) of GRB080705 in 15-50 keV band, red lines correspond to the 90% confidence level region. The plot shows the decreasing ordered light curves and the emission time is determined by the equivalented count rate at the 50% total fluence

4.4 Statistical analysis

Several relations between GRBs have been establishes since their discovery, but there is no clear theoretical models to justify the origin of these relations. In order to look for new relations between the observed parameters, the usual methodology is to determine how strong and probable is that two different parameters are related without assuming any mathematical equation. Calculating the correlations between two variables is one of methods, but the Spearman rank correlation permits us to know the strength of the link between two sets of parameters. Spearman's rank correlation coefficient (ρ) is a non-parametric measure of how possible is to describe the relation between two variables using a monotinic. The definition of ρ [28] for a set of n pairs of two varaibles X_i, Y_i with no tied values is expressed in function of a new converted ranked x_i, y_i, and the differences d_i = x_i - y_i between the ranks of each observation. The rank assigns 1 to the bigger values, 2 the second big and consecutevely un the lower values and ρ is given by:

$$\rho = 1 - \frac{6\Sigma d_i^2}{n^3 - n} \tag{4.2}$$

A perfect Spearman correlation of +1 or 1 occurs when each of the variables is a perfect monotone function of the other. Nevertheless, it is quite rare that the taken observations

obey perfectly the Spearman correlation. There is a method to measure the significance of the obtained value of correlation and associates degrees of freedom to the sample, defined as the number of pairs in your sample minus 2. Applying a Fisher transformation to the distribution of ρ, it is possible to establish a likehood of the correlation occuring by chance. Usually, it is acceptable when ρ is above 5%, but below 1%, meaning a confidence level of 95%. In figure 4.6 a graphical explanation of a determined value of ρ and its associated chance probability is shown.

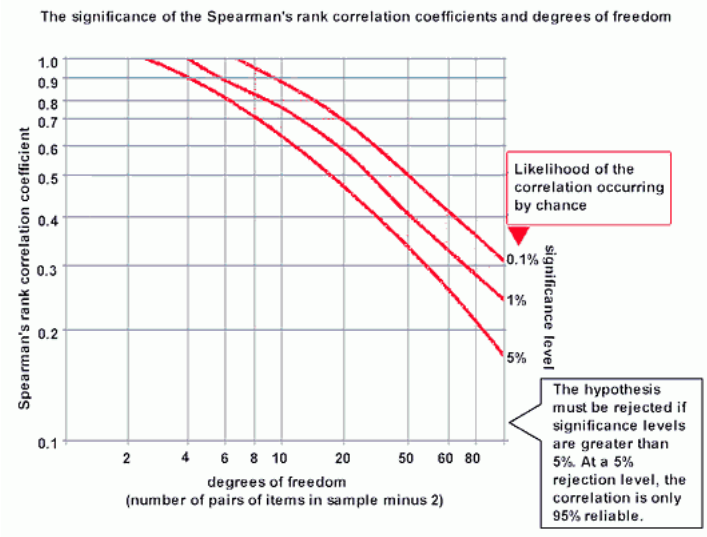

Figure 4.6: Significance graphic of the Spearman's rank correlation [Barcelona Field Study Center]

Chapter 5

Temporal classification of GRBs

5.1 Data sample and characteristics

In this study a set of 15 GRBs simultaneously detected by Suzaku and Swift satellites were studied. The selected bursts are long GRBs, T_{90} values are longer than 2 seconds, and all the bursts have a measured redshift. They have been detected between August 2006 and April 2010. Another condition imposed to the bursts is related with their fluence. We defined bright bursts, as the ones that have BAT fluences in 15-150 keV band higher than 30×10^{-7} erg/cm^2. Among the selected GRBs, only one has been associated with a supernova event. GRB091127 with z=0.49 (Cucchiara et al GCN10202) is associated with SN 2009nz[10]. The rest of the bursts could be qualified as standard long GRBs. The redshift distribution has a maximum value of 3.9 and a minimum value of 0.49, and there is no evidence of a clustering in the sample. In this section we study three types of time estimators in order to quantify the duration of the bursts. Since each of the time estimators have a physical meaning, we proceed to investigate the relations between them in the observer frame and in the burst frame. Finally, we aim to look for subclasses of long GRBs, just by looking its temporal behaviour at different bands and using the three estimators.

5.2 Time estimation in GRBs

The classification of GRBs, is generally related with its duration. Temporal properties of bursts permit to define two or three categories[24]. We defined three possible time estimators of GRBs , the duration of the time for the 50% of the fluence (T_{50}), the ACF at FWHM (ACF) and the emission time of the 50% of the total fluence (t_{50}). These three estimators measures the half-time of the total emission in different ways. We proceed to

investigate the relation between each others. We chose the temporal values at 50% level, since there is some tendency of miss-classifications due to extended emission in soft X-rays bands when T_{90} is used [12]. For example GRB090424, has a T_{90} duration of 52.7 in the 15-50 keV band and T_{90} of 8.1 s in the 50-150 keV band. Looking at the light curves in appendix A, it is possible to recognize the long soft X-ray tail. A similar behavior is observable in GRB080319C, only in 15-50 keV band an extra pulse was detected. On the other hand, the values measured at the half maximum are statistically more robust[6].
A well know property of light curves of GRBs is that time histories become shorter at high energies. We aim to study the dependence of the the estimator also with energy, so we have determined the values of each one of the time estimators in 2 bands, 15-50 keV and 50-150 keV (observer frame). In Appendix C the light curves from Suzaku are shown in 4 bands:TH0, TH1, TH2 and TH3. The energy equivalence of the bands is different for each one of burst, because of the gain variation of the multipliers tubes; in table C.1 the enery range for each burst is shown. In the other hand, the limitation of the binning size and the small signal to noise ratio it was not possible to determine three time estimators at high energies. Nevertheless, in some cases the value of T_{50} is shown below the respective light curve.

Burst	z	T_{50} [15-50 keV]	ACF [15-50 keV]	t_{50} [15-50 keV]
GRB060814	0.84	62.00 ± 1.41	20.06 ± 0.16	27.50 ± 0.56
GRB060908	2.43	7.75 ± 3.29	10.40 ± 0.45	6.38 ± 0.75
GRB061007	1.26	23.50 ± 0.42	48.70 ± 0.30	19.30 ± 0.34
GRB070508	0.82	8.80 ± 0.22	18.47 ± 0.13	6.45 ± 0.48
GRB070612A	0.62	173.00 ± 28.43	70.80 ± 11.40	74.00 ± 8
GRB071003	1.10	23.60 ± 5.39	27.80 ± 0.80	16.50 ± 1.32
GRB071010B	0.95	6.00 ± 0.25	10.94 ± 0.16	4.76 ± 0.4
GRB080319C	1.95	7.90 ± 1.03	11.35 ± 0.15	5.73 ± 0.32
GRB080413A	2.43	16.50 ± 1.00	5.44 ± 0.18	6.88 ± 0.52
GRB080916A	0.69	22.75 ± 0.90	36.31 ± 0.19	15.90 ± 0.60
GRB090424	0.54	3.70 ± 0.10	4.50 ± 0.12	2.75 ± 0.18
GRB090618	0.54	32.10 ± 0.32	56.40 ± 0.40	27.20 ± 0.36
GRB090812	2.45	31.60 ± 8.08	20.60 ± 2.00	20.50 ± 1.24
GRB091127	0.49	6.00 ± 0.14	2.86 ± 0.41	1.85 ± 0.42
GRB100413A	3.90	101.40 ± 16.58	103.50 ± 11.10	151.50 ± 7.6

Table 5.1: Redshift and values of the three time estimators, T_{50}, ACF-FWHM (90% confidence level), and t_{50} in 15-50 keV band. All the Values are expressed in seconds (observer frame).

Each of the chosen time estimators measure a specific temporal characteristic of the same physical process, then we expect some relation between each of the parameters. The list of the calculated values are in tables 5.1 an 5.2. In table 5.1 the redshift, T_{50}, ACF,

Burst	T_{50} [50-150 keV]	ACF [50-150 keV]	t_{50} [50-150 keV]
GRB060814	61.30 ± 1.20	18.52 ± 0.18	23.50± 0.31
GRB060908	6.50 ± 0.56	7.55 ± 0.40	5.10± 0.84
GRB061007	22.30 ± 0.36	34.20 ± 0.60	17.00± 0.75
GRB070508	6.90 ± 0.10	11.77 ± 0.33	4.55± 0.12
GRB070612A	172.00 ± 10.12	23.00 ± 12.60	43.01± 8.80
GRB071003	11.60 ± 2.04	17.50 ± 1.90	11.80± 2.2
GRB071010B	4.60 ± 0.36	8.16 ± 0.20	1.26± 0.35
GRB080319C	6.80 ± 0.36	9.80 ± 0.20	4.88± 0.40
GRB080413A	14.75 ± 0.35	3.84 ± 0.12	4.27± 0.90
GRB080916A	20.60 ± 2.02	9.49 ± 0.31	8.70± 0.72
GRB090424	3.00 ± 0.14	2.28 ± 0.08	1.75± 0.30
GRB090618	23.70 ± 0.22	41.70 ± 0.30	21.10± 0.36
GRB090812	20.90 ± 0.89	14.65 ± 0.95	15.10± 1.14
GRB091127	2.70 ± 0.91	1.64 ± 0.64	0.98± 0.14
GRB100413A	100.40 ± 11.92	89.10 ± 16.90	58.50±8.80

Table 5.2: Values of the three time estimators, T_{50}, ACF-FWHM (90% confidence level), and t_{50} in 50-150 keV band. All the Values are expressed in seconds (observer frame).

and t_{50} in 15-50 keV band are shown, and in table 5.2 the same time estimators but in the 50-150 keV band are shown, in both tables the measured time correspond to the observer frame. In order to study the relation between the time estimators, we determine the linear correlation coefficient, the Spearman correlation (r) and the chance probability P. The analysis was perfomed in the observed frame and in the burst frame and the obtained values are shown in table 5.3. Looking at table 5.3 we conclude that the three time estimators are strongly correlated in the observer frame, as well as, in the burst frame. The different correlations could be observed in Figures 5.1, 5.2 and 5.3 in the observer frame, in the following order. Figure 5.1 shows the correlation in 15-50 keV band of ACF and t_{50} as a function of T_{50}, figure 5.2 shows the same correlation but in the 50-150 keV band and figure 5.3 shows the correlation of ACF and t_{50} in both energy bands. The following figures 5.4, 5.6 and 5.7 correspond to the correlations in the burst frame in the same order order that was mentioned.

The Spearman correlation is always high and the chance probability is below 5% in both reference frames, so the correlation between the three estimators clear. Nevertheless, the relation between the duration time and the ACF is not linear, and the effect becomes more obvious at high energies. Although the physical process is the same, and ACF are mesuring different aspects of the emission process. T_{50} gives information about the duration of the whole burst activity and the ACF gives information more related with the internal structure of the burst, in other words how the pulses are emitted, their separation and their intensity.

Correlation (Band keV)	lin	r	P	z-lin	z-r	z-P
T_{50}-t_{50} (15-50)	0.76	0.98	2×10^{-4}	0.89	0.94	4×10^{-4}
T_{50}-ACF (15-50)	0.75	0.86	1.2×10^{-3}	0.76	0.81	2.3×10^{-3}
ACF-t_{50} (15-50)	0.90	0.86	1×10^{-4}	0.84	0.89	8×10^{-4}
T_{50} -t_{50} (50-150)	0.86	0.94	4×10^{-4}	0.92	0.90	8×10^{-4}
T_{50}-ACF (50-150)	0.52	0.86	1.2×10^{-3}	0.40	0.83	1.8×10^{-3}
ACF-t_{50} (50-150)	0.86	0.91	6×10^{-4}	0.72	0.89	8×10^{-4}

Table 5.3: Linear correlation coefficients linear (lin), Spearman correlation (r) and chance probability (P) between the 3 estimators in observer and GRB frame (z-lin, z-r and z-P)

The linear relation between ACF and t_{50} reflects the similarities of both estimators. t_{50} is sensitive to the time intervals where the engine is in the most active phase, corresponding somehow to the regions of the time history where the emission reach a threshold level and depends on the internal structure of the burst as ACF does. The linearity between t_{50} and ACF is conseved also in the high energy band. The correlation observed between T_{50} and t_{50} also seems to be linear in low energies (15-50 keV) and hard energies (50-150keV). The linearity of the correlation could arise from the fact that T_{50} measures the duration of the activity without taking into account the soft long tails and soft pulses in the beginning of the burst. This time should coincide with the regions of the time histories where the engine is its more active phase, represented by internal structures caracterized by high amplitudes.

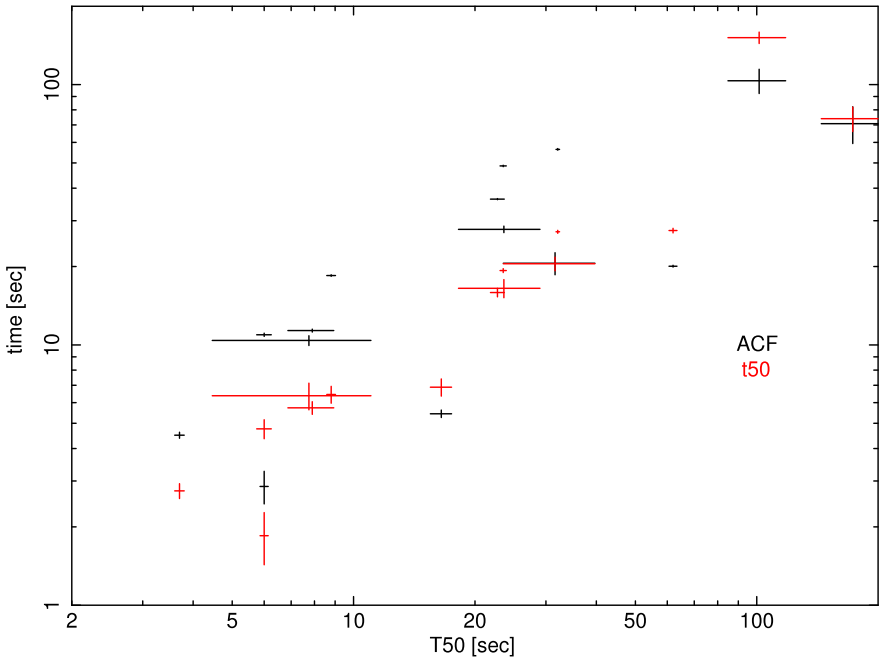

Figure 5.1: Correlation of ACF and t_{50} as a function of T_{50} in the observer frame in the soft band (15-50keV)

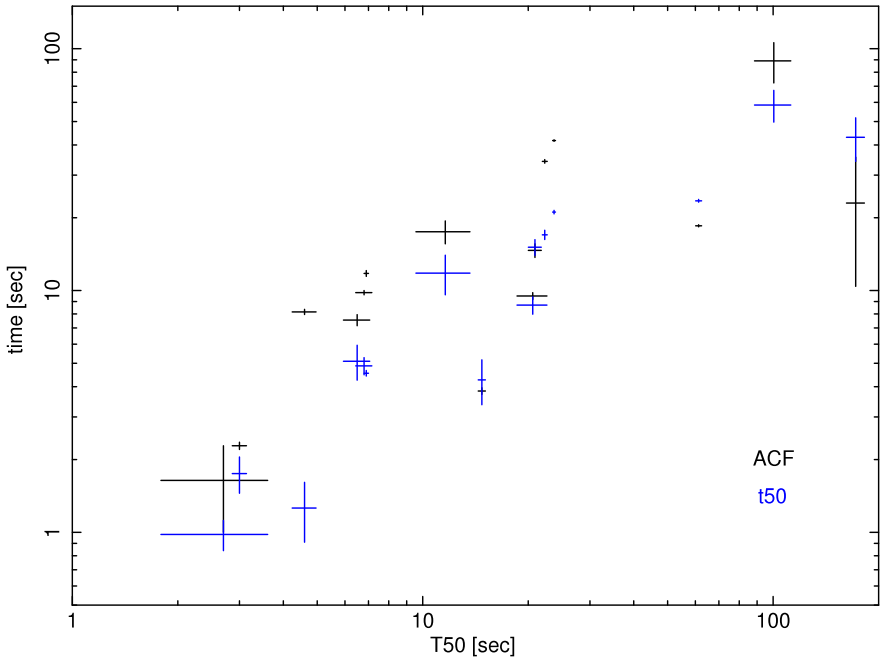

Figure 5.2: Correlation of ACF and t_{50} as a function of T_{50} in the observer frame in the hard band (50-150keV)

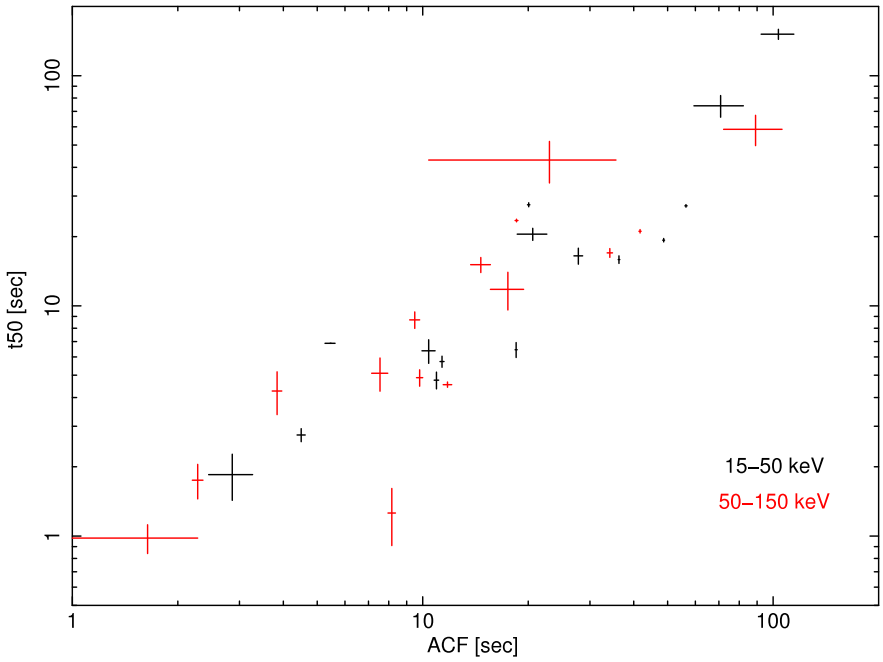

Figure 5.3: Correlation between ACF and t_{50} in soft and hard bands in the observer frame. In this case the correlation is linear

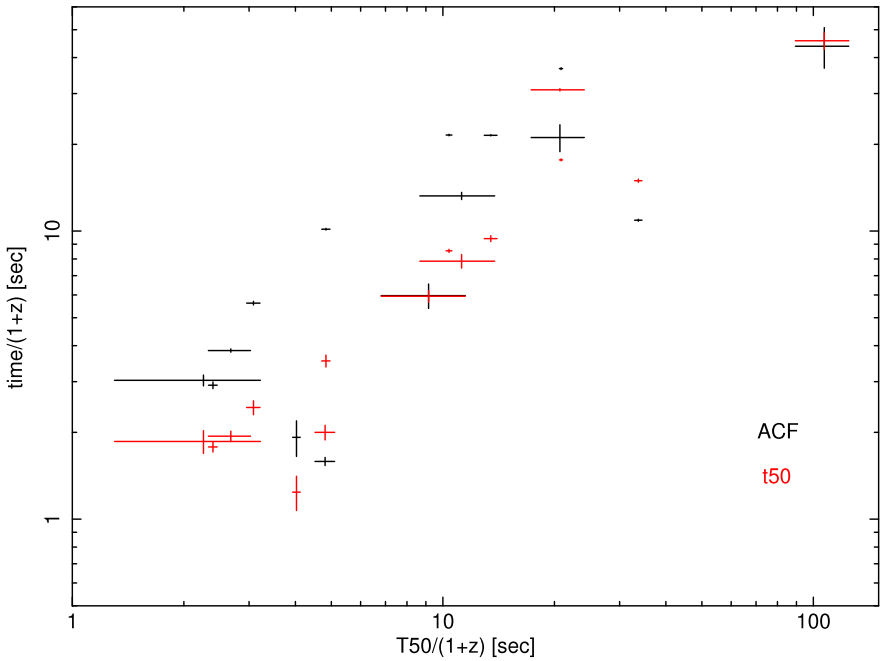

Figure 5.4: Correlation of ACF and t_{50} as a function of T_{50} in the burst frame in the soft band (15-50keV)

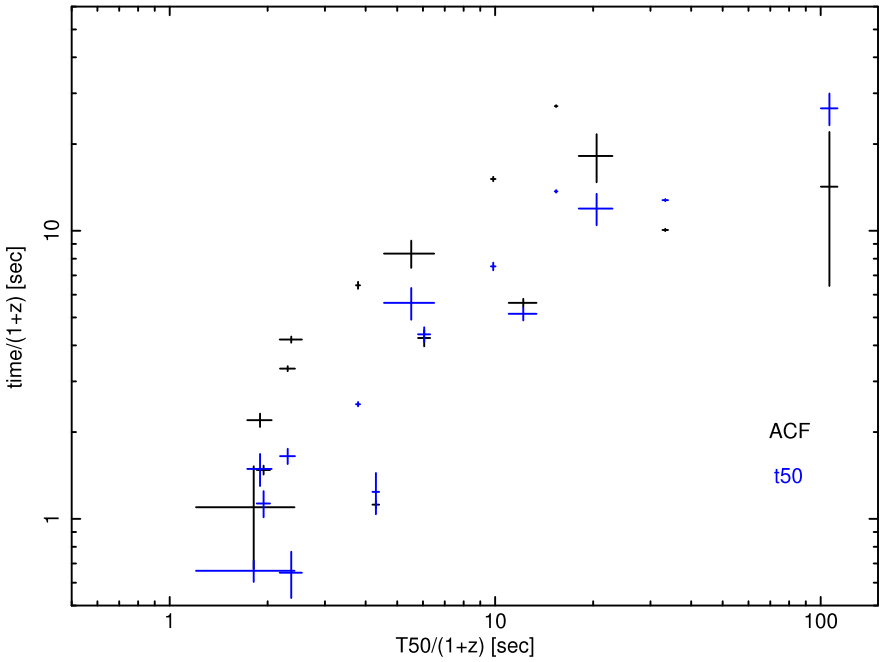

Figure 5.5: Correlation of ACF and t_{50} as a function of T_{50} in the burst frame in the hard band (50-150keV)

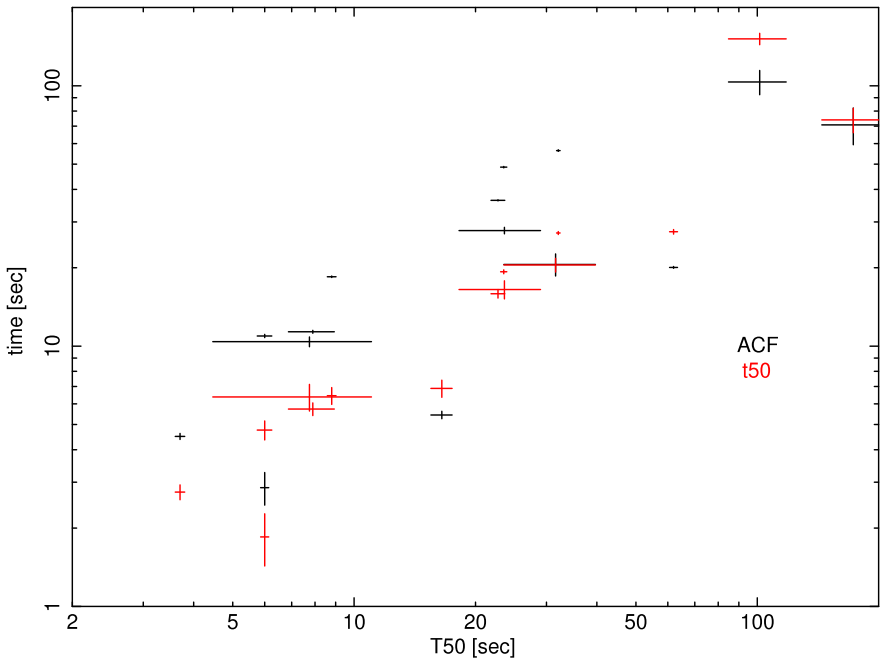

Figure 5.6: Correlation between ACF and t_{50} in soft and hard bands in the burst frame. In this case the correlation is linear

5.3 Temporal bimodality

The cosmologically corrected ACF of long GRBs presents a bimodal distribution. It was first observed in a BATSE-KONUS wind sample of GRBs with known redshifts. In figure 5.5, it is possible to appreciate the two classes of bursts only when the ACF is plotted in the GRB frame[6], this plot correspond to the work of Borgonovo using 16 long bursts from BATSE and Konus Wind. There is no clear explanation of the observed bimodality, so we also did a similar analysis with our sample of GRBs. We produced two sets of ACFs, one using light curves in 15-50 kev band and another one using light curves in 50-150 keV band.

In figure 5.6 we can observe the ACFs of the 15 long GRBs, there in no evidence of special bursts that have a broader ACF or a narrower ACF since the ACFs are in the observer frame. For each burst we plotted 5 ACFs produced by 5 Monte Carlo simulated light curves.

In Figure 5.7 we have plotted the ACF corrected by the factor 1/(1+z) and there are 4 GRBs that seems to have a broad ACF, also found in the study of Borgonovo [6, 7]. A first comment, we can say that the bimodality is not the result of some selection effects intrinsic to the detector. In a previous work using a small sample of GRBs from BATSE, Konus wind and BeppoSAX in total 22 GRBs, Borgonovo[7] also found the bimodality. The bursts that have a broad ACF should be closer and also longer in order to be a subclass of GRBs.

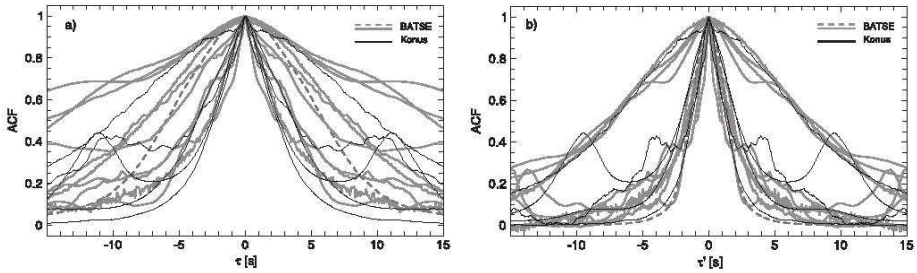

Figure 5.7: Bimodality distribution of the ACF cosmologically corrected, Borgonovo 2004[6]

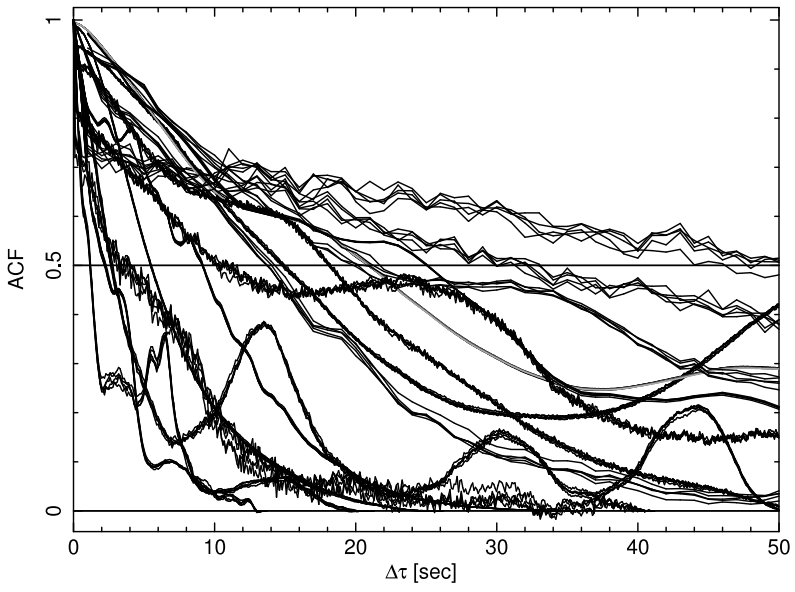

Figure 5.8: ACFs of the 15 GRBs in the observer frame, using the light curves in 15-50 keV band

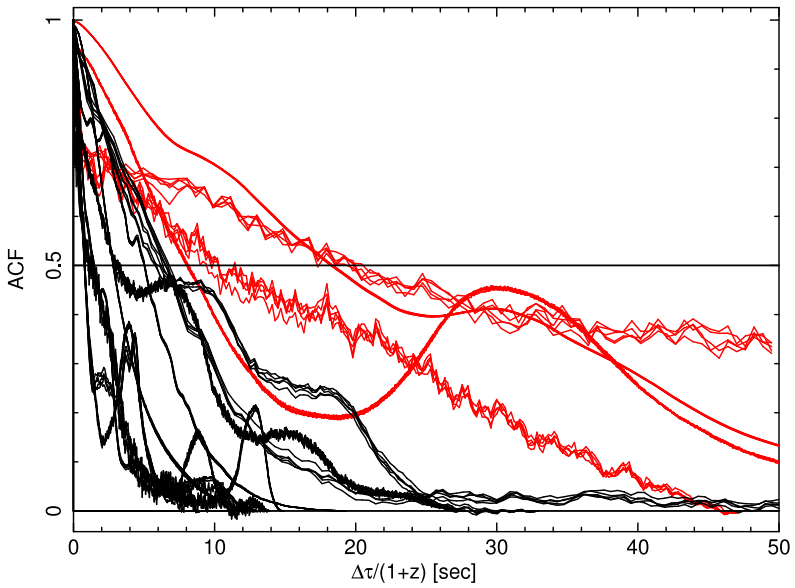

Figure 5.9: Cosmologically corrected ACF the sample of GRBs, red possible ACF of candidates of a subclass of long GRBs

GRB060814, GRB070612A, GRB080916A and GRB090618 have common characteristics. The 4 GRBs have a redshift less than 1 and the value of their ACFs are larger in the rest frame. This two characteristic could be a hint that unveil the origin of the bimodality. Compared to the rest of the bursts the time dilation effect due to cosmological expansion is weaker than for GRBs with high redshifts. Since the ACF reflects the power density spectra (PDS) of the burst, the value of its FWHM is related to the mean period of activity of the engine that produce the radiation. Borgonovo [7] also found that the PDS shape is different for the broad-long ACF bursts and narrow-long ACF bursts, to confirm if those 4 bursts are a subclass of long GRBs, we also look at the value of the other time estimators in the burst frame. In a previous work Vasquez[40], we also shown that there was already an ACF bimodality and in the present work we extended to the other temporal estimators.

The cosmological effect should work in the same way in all the temporal parameters. To confirm this trend, we applied the cosmological correction to the other time estimators, T_{50} and t_{50}. To investage if they behave similarly to ACF, in figures 5.10 and 5.11 we plot the temporal estimator and the distance in two energy bands. The three time estimators have a similar position in the plots, the values of each of the time estimator is longer compared to the distance. We define a region of long-closer bursts, a close burst should have a redshift smaller than 1. To define a long temporal interval we suggest that the three temporal estimators should have similarly large values compared to the rest of the sample. GRB060814, GRB070612A, GRB080916A and GRB090618 have the values of their three time estimators in these regions. GRB061007 has only T_{50} in the long temporal region,

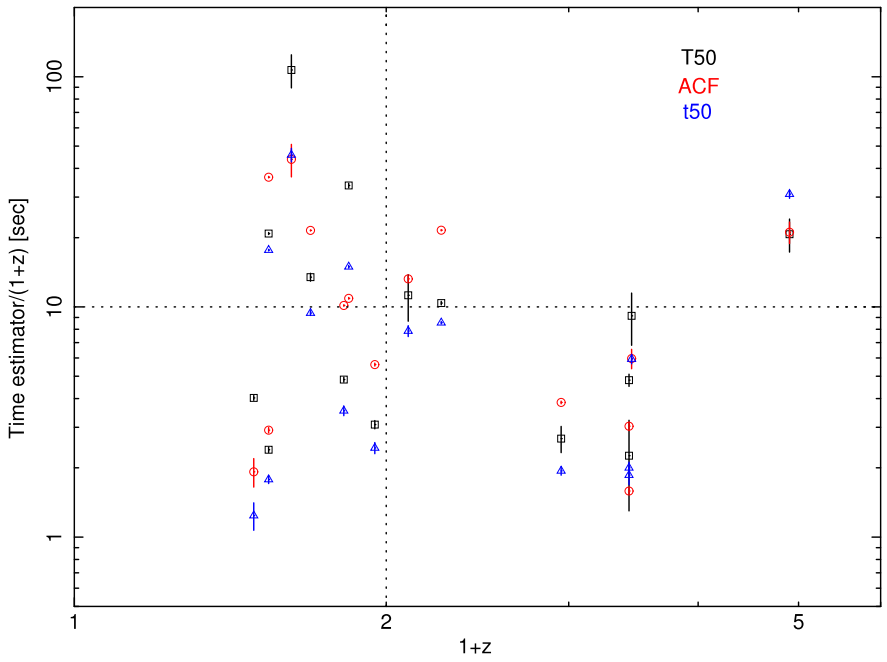

Figure 5.10: Time estimators at 15-50 keV band and distance for long GRBs

and looking at the light curves, it is possible to observe that the burst structure is composed by emission and quiescent episodes. The large values of T_{50} would have origin during the integration of the fluence in the quiescent episodes. Each of the time estimators reflect a specific temporal characteristic, then the 4 bursts have in common the same time of engine activity and same duration time. Using T_{50} instead of T_{90} is an advantage since the values of T_{90} could be enlarged by extended emission specially in X-ray band [12].

5.4 Long-closer bursts

In this chapter we established strong dependence between the three time estimators, and we suggest that even there are measuring in different manner a time interval, the measures should be dilated in the same way by the Universe expansion. The relation between T_{50}-t_{50} and ACF-t_{50} seems to be linear and energy independent. On the other hand the relation T_{50}-ACF is not linear and varies with energy, but the Spearman correlation is strong in both studied bands, so the relation should be exponential like. The use of the half values of fluence and ACF avoided to miss-estimated the regions that could corresponds to soft X-ray excess and the obtained values mainly reflect the most active phase of the prompt emission that could be underlying the physical process to convert the kinetic energy into radiation. We established that the bimodal distribution of the cosmologically corrected ACF is also present in the Swift GRBs with known redshift. We found 4 GRBs that behave like a

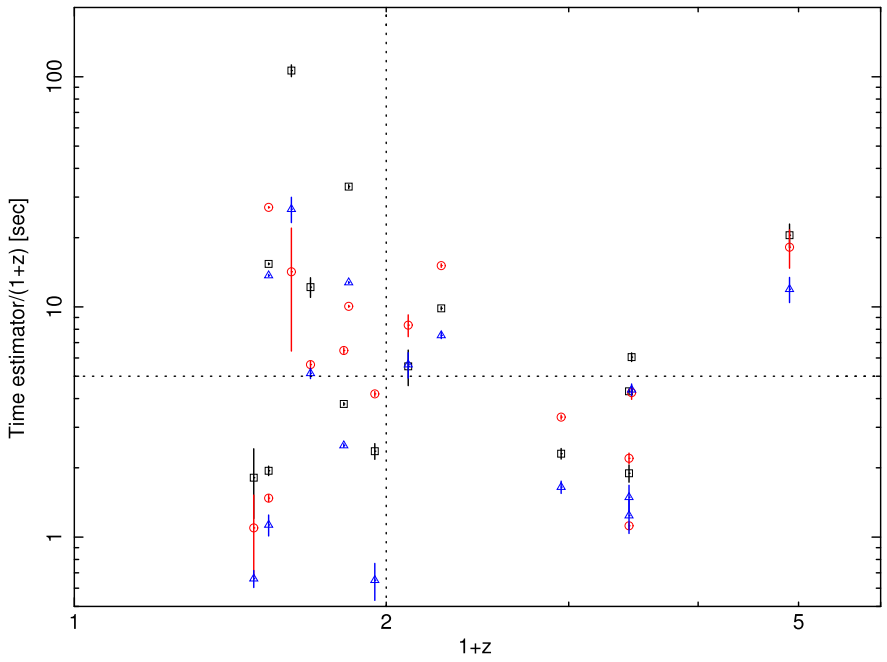

Figure 5.11: Time estimators at 50-150 keV band and distance for long GRBs

different sub-group. GRB060814 (T_{90}=147s), GRB070612A (T_{90}=361s), GRB080916A (T_{90}=61) and GRB090618 (T_{90}=114s) have a broader ACF, are closer and longer. We also confirmed that T_{50} and t_{50} behave as ACF when the values are cosmologically corrected in the two energy bands, giving more support to the subclass of long-closer bursts. At high energy band the values are shorter but correlates similarly than in low energy, that is also another observation of the Universe expansion that equally works not only in time but also in energy. The bimodality of long GRBs is also present in the afterglow light curves, Dainotti 2010[11] establishes using 77 bursts from Swift, a subgroup of long bursts. The canonical plateau breaking (exponential to power law) in the light curves correlates between X-ray luminosity differently for two kind of afterglows, inferring possible different explosion mechanisms between both types of long bursts. The bimodality during in the afterglow phase, could be originated in the promp emission phase since in our work the evidence of two different types of long GRBs was put in evidence.

Chapter 6

Spectral properties of the Suzake-Swift GRBs

In Chapter 5, we already found similarities between the temporal characteristics in the candidates for a subclass of long GRBs. Those burst are longer and are closer than the rest of long bursts. In this chapter we aim to find an spectral and energy counterpart for the proposed classification. We start showing the spectral parameters of burst sample and we look for any anomalies of the long burst in the peak energy and isotropic luminosity L_{iso} plane as well as testing the sample with the Amati relation.

6.1 Spectral properties of Swift-Suzaku bursts

Swift-BAT instrument have detected more than 300 GRBs since it was launched. The rapid slew of this satellite permitted to measure the redshifts of many bursts, but the energy range covered by the satellite is narrow, 15-150 keV. On the other hand, Suzaku-WAM instruments, have a broad range energy of operation (50-5000 keV) but no ability to determine positions, therefore no redshift measurements. The observations of both satellites are complementary, they gave the chance to work in a broad energy band and also with redshift information. The high energy region of bursts are detected by Suzaku and the soft counterpart by Swift, which permit to determine the spectral shape of the burst in a energy range between 15 to 5000 keV, revealing parameters such peak energy that were no properly determined using only one of these instruments. Nevertheless, the simultaneous observations of burst by Suzaku and Swift are quite rare. As we already mention, the present study has a sample of 15 long GRBs with known z.

GRB	z	α	Epeak [keV]	β	red.χ^2/DOF
GRB060814	0.84	$1.45^{+0.05}_{-0.05}$	$292.9^{+56.8}_{-40.7}$	-	0.85/105
GRB060908	2.43	$1.01^{+0.17}_{-0.22}$	$144.5^{+56.3}_{-32.3}$	-	1.0/75
GRB061007	1.26	$0.83^{+0.03}_{-0.03}$	$506.5^{+1.4}_{-1.3}$	$-3.73^{+0}_{-0.53}$	1.21/97
GRB070508	0.82	$1.18^{+0.05}_{-0.05}$	$247.1^{+25.7}_{-22.6}$	-	0.81/90
GRB070612A	0.617	$1.59^{+0.14}_{-0.16}$	$328.35^{+2791.6}_{-151.3}$	-	0.83/78
GRB071003	1.10	$1.24^{+0.06}_{-0.06}$	$2355.1^{+2244.3}_{-786.7}$	-	1.05/89
GRB071010B	0.947	$1.66^{+0.13}_{-0.15}$	$44.7 +5.9_{-7.8}$	-	0.80/77
GRB080319C	1.95	$1.26^{+0.08}_{-0.08}$	$575.7^{+201.8}_{-119.1}$	-	1.10/85
GRB080413A	2.43	$1.45^{+0.10}_{-0.12}$	$227.1^{+171.4}_{-69.9}$	-	1.37/76
GRB080916A	0.689	$1.22^{+0.17}_{-0.19}$	$120.9^{+57.7}_{-24.0}$	-	1.03/97
GRB090424	0.544	$0.99^{+0.12}_{-0.13}$	$298.3^{+18.3}_{-13.4}$	$-2.69^{+0.27}_{-1.18}$	1.11/76
GRB090618	0.54	$1.51^{+0.03}_{-0.03}$	$247.9^{+13.1}_{-12.1}$	-	0.44/77
GRB090812	2.452	$1.08^{+0.07}_{-0.07}$	$558.5^{+193.3}_{-125.8}$	-	0.45/69
GRB091127	0.49	$2.14^{+0.05}_{-0.10}$	-	-	0.81/74
GRB100413A	3.90	$0.98^{+0.10}_{-0.11}$	$593.0^{+378.9}_{-182.0}$	-	1.22/94

Table 6.1: Best spectral fitted values for the Suzaku-Swift GRBs, the value of β indicates that the model corresponds to a GRB model. For the rest of the bursts a CPL model was used except for GRB091127 which fit values arise from a single power law. (values at 90%of confidence level)

6.1.1 Spectral Analysis

We perform the spectral analysis described in Chapter 4. The results are tabulated in table 6.1 and in table 6.2. We have computed the isotropic luminosities (L_{iso}) in the 1-10000 keV cosmological rest-frame energy band and we assumed a standard cosmology with Ω_m=0.3, Ω_Λ=0.7 and H_0=70 km s^{-1}Mpc^{-1} [23]. The values have are measured in a confidence level of 90%.

GRB	L_{iso} [10^{52}erg/sec]	+	-	Ld [Gly]
GRB060814	0.072	0.003	0.005	17.66
GRB060908	0.761	0.057	0.187	66.14
GRB061007	1.930	0.152	0.041	29.29
GRB070508	0.446	0.025	0.026	17.13
GRB070612A	0.014	0.002	0.013	12.13
GRB071003	0.817	0.085	0.254	24.72
GRB071010B	0.110	0.004	0.005	20.58
GRB080319C	1.510	0.153	0.203	50.44
GRB080413A	0.724	0.071	0.172	66.14
GRB080916A	0.031	0.001	0.006	13.84
GRB090424	0.141	0.008	0.012	10.24
GRB090618	0.182	0.004	0.004	10.24
GRB090812	1.220	0.141	0.270	66.86
GRB091127	0.148	0.006	0.006	9.11
GRB100413A	1.928	0.281	0.703	117.22

Table 6.2: Isotropic luminosity and luminosity distance (Ld)of Suzaku-Swift GRBs

The tabulated values correspond to the best fit a cut off power law (CPL) normalized to 100 keV (Eq. 4.1) or a Band model (Eq. 2.1), β values indicate for which GRBs Band model was used. Most of the GRBs present better statistics with a CPL model. GRB091127 is an outlier since this burst is in association with a supernova, the best statistics were found using a single power as spectral model. For the rest of bursts the photon index on the low energy power is distributed normally, the values are between the reported in other samples [1]. Peak energies in table 6.1 are computed in observer frame

6.2 Amati relation test

A well established relation for GRBs with known redshift is the correlation between the cosmological rest-frame νF_ν spectrum peak energy and the isotropic-equivalent radiated energy, known as Amati relation. This relation only holds for long GRBs but the interpretation of this relation is still in discussion. The isotropic energy depends on the energy spectral shape of the burst, but there is no yet a defined model for GRBs. The relation establishes that E_{iso} dependence on E_{peak} follows a power law, with index 2[2]. In order to verify the Amati relation we used a set of 39 long GRBs from Amati work 2006[1]. The chosen data corresponds to observations between 1997 until 2005, and the data we used corresponds to observations between years 2006 until 2010. The whole sample covers 13 years of observations done by 5 different satellites. In figure 6.1 the Amati relation is plot-

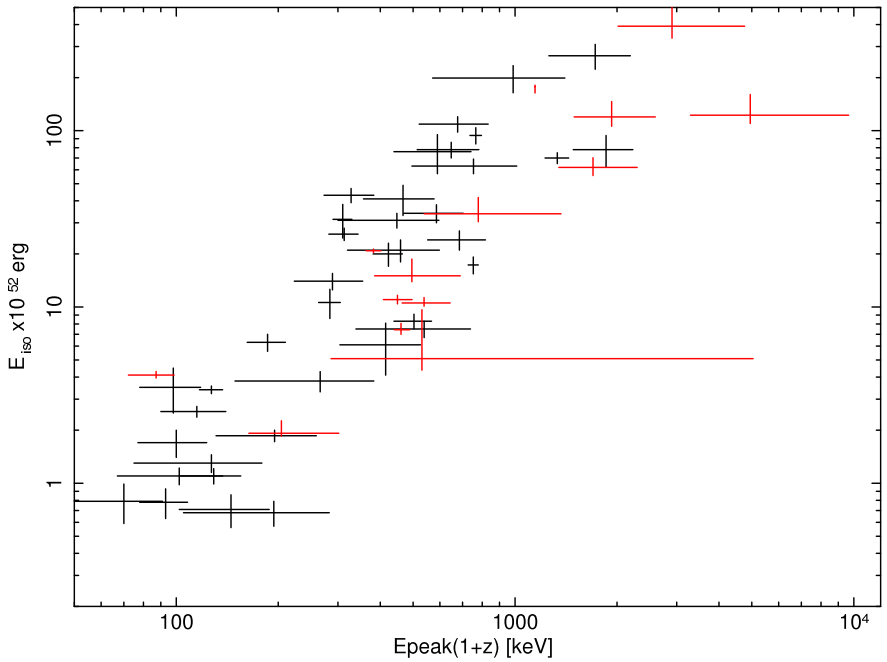

Figure 6.1: Amati relation for Swift-Suzaku bursts (red), in black 39 GRBs from Amati 2000[1]

ted, the bursts from this work are shown in red and in black the set of 39 bursts from Amati previous work [1]. There is no evident outliers, which suggests thet the analysis is correct and inside the standard values. Amati relation mathematical expression is expressed as follows.

$$E_{iso} = C \times E_{peak}^{m} \tag{6.1}$$

Amati reported a power index value m=0.570 $\pm$ 0.02 for the 39 long GRBs, the sample of 15 GRBs we used gave a power index m=0.523 $\pm$ 0.02. Although both power index valeus are not the same, the difference is not too significative, which susuggests that there no miss-computations of the spectral values. The Spearman rank correlation value of the studied sample is 0.84 with a chance probability of 2.6×10^{-3}, the obtained value of probability is above 5%, but below 1, we can say we are 95% confident about our analysis.

Chapter 7

Combining time, energy and distance

All timescales of GRB variability are expected to show the effect of time dilatation, a consequence of this cosmological effect is that distant bursts should be brighter and short compared with close burst that should dimmer and long. The Amati-Yonetoku like relations, already confirm that distant burst are brighter[1]. We have estimated the duration time of the emission of GRBs (T_{50}), the time intervals where the burst engine is in a high state of activity (t_{50}) and the ACF-FWHM (ACF) of GRB which give an estimation of the power of the emission in a given band and characterize the internal structure of the bursts. Now, we aim to investigate how the cosmological dilatation affects the different kind of time estimators and energy.

7.1 Time, energy and distance of long GRBs

The time estimators measured in the laboratory frame are dilated and redshifted in energy [8]. It is necessary to apply the cosmological correction in time and energy to determine how distance, time and energy are modified. We compared the three time estimators in the GRB frame with their isotropic luminosity. Assuming that all the timescales are modified in the same way by the Universe expansion; if they have a same kind of origin all the properties will be altered in the same way. Looking for anomalies that could be cosmological effects, different types of phenomena or intrinsic effects we compared the time corrected estimator with the isotropic luminosity. The bimodal distribution of long GRBs established by Borgonovo[6, 7], and confirmed previously, is a hint of the existence of an subclass of long burst. To elucidate the nature of this bimodality we combined the time estimators in the rest frame with their corresponding isotropic luminosity. In table 6.1 as a first attempt we compare the distance which is given by the redshift, one time estimator (t_{50}) and the isotropic luminosity (L_{iso}). In the sample of studied bursts, the subclass of long GRBs

could by hidden in GRBs with a small z, they are longer or have low luminosities. If the origin of the anomaly is non cosmological the time stretching should be different, then we first look for longer bursts which are labeled (+) in table 7.1. We expect to detect a similar time stretching and energy redshifting in three estimators we calculate in both energy bands. Just looking at the values of table 1, the 4 marked GRBs have small z and the active engine last longer and the energy is low.

GRB	z	t_{50}(50-150 keV) sec	L_{iso} 10^{52}ergs
GRB060814(+)	0.84	23.50	0.072
GRB060908	2.43	5.10	0.761
GRB061007	1.26	17.00	1.930
GRB070508	0.82	4.55	0.446
GRB070612A(+)	0.62	43.01	0.014
GRB071003	1.1	11.80	0.817
GRB071010B	0.95	1.26	0.110
GRB080319C	1.95	4.88	1.510
GRB080413A	2.43	4.27	0.724
GRB080916A(+)	0.69	8.70	0.031
GRB090424	0.54	1.75	0.141
GRB090618(+)	0.54	21.10	0.182
GRB090812	2.45	15.10	1.220
GRB091127	0.49	0.98	0.148
GRB100413A	3.9	58.50	1.928

Table 7.1: Comparative values of distance, energy and time for long GRBs

In table 7.2 we explore the correlation between each one of the time estimators in the rest frame with the isotropic luminosity. The values of the sample as a whole do not show any correlation at all, but when the candidates to be outliers are removed a correlation between time and energy is evident. The correlation increases when the energy is higher. The plots of and L_{iso} and T_{50} are shown in figures 7.1 and 7.2, for ACF-E_{iso} and L_{iso} in Fig.7.3, 7.4 and t_{50}-E_{iso} 7.5, 7.6 respectively. The better correlation is observed within the time of emission (t_{50}) and L_{iso}, and becomes stronger in the 50-150 KeV band. The time of emission give us a measure of periods of time where the GRB engine is more active, and is directly connected with the nature of the phenomenon. A such increase in the correlation is an evidence of the intermediate class of GRBs and give us some hints about a possible different origin.

Nevertheless, the light curves of those outliers of the class of long GRBs have a stronger emission at 15-50 keV Band. This fact is another physical characteristic of the third class of GRBs.

Estimator and band(kEV)	r	P	r(+)	P(+)
T_{50} (15-50)	-0.229	0.68	0.682	7.8×10^{-2}
ACF (15-50)	-114	0.76	0.699	5.0×10^{-2}
t_{50} (15-50)	0.146	0.64	0.643	4.0×10^{-2}
T_{50} (50-150)	-0.216	0.73	0.675	3.5×10^{-2}
ACF (50-150)	0.180	0.75	0.730	4.6×10^{-2}
t_{50} (50-150)	-0.05	0.78	0.786	5.8×10^{-3}

Table 7.2: Time estimators-L_{iso} Spearman correlation coefficients (r) and chance probabilities P for the whole sample (15 GRBs), (r+) and (P+) are the correlation coefficients and chance probabilities for sample without the long-dimm the bursts (11 GRBs)

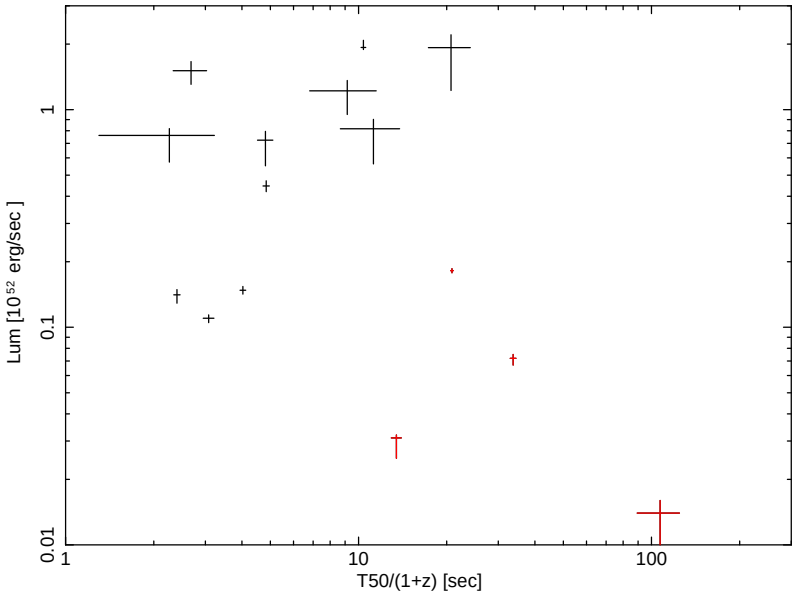

Figure 7.1: Isotropic luminosity as a function of T50 in 15-50 keV band, red crosses represents the long-dim bursts

7.2 Peak energy relation with time parameters

The Amati-Yonetoku relation gives us information about the two parameters that come from spectral analysis. In the previous section we just investigate the temporal properties with the isotropic luminosity. Now we study the possible relations between the peak energy parameters and each of the time estimators. We already have 4 GRBs that behave differently than the rest of the sample, in time and in energy. In this section we verify if GRB060814 ,GRB070612A, GRB080916A and GRB090618 also form a group separate the peak energy in the burst frame is compared with each of the time estimators. We proceed in a similar methodology as for time estimator-L_{iso}. We compute the correlation

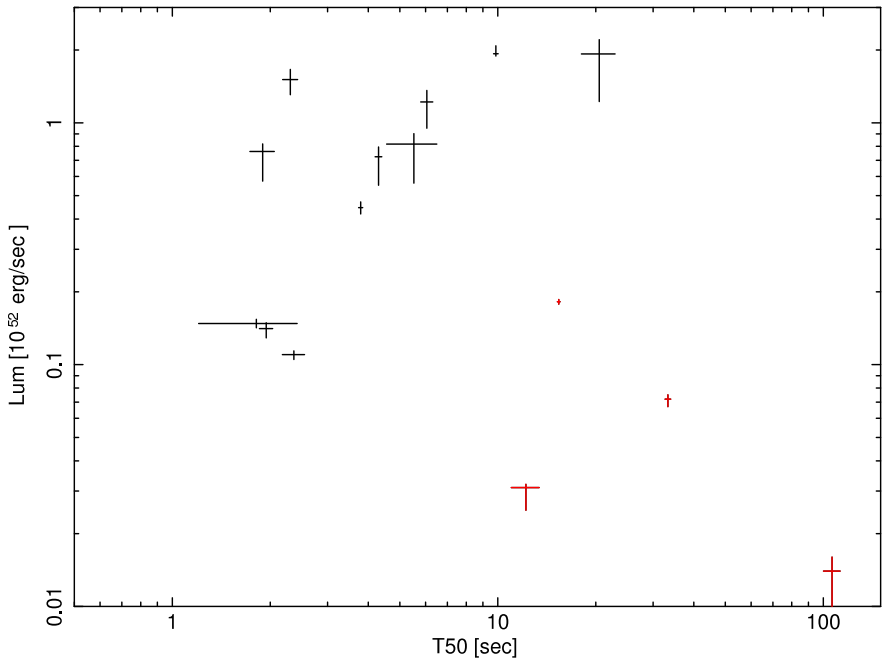

Figure 7.2: Isotropic luminosity as a function of T50 in 50-150 keV band, red crosses represents the long-dim bursts

coefficients for the whole sample and for the sample without the 4 outliers candidates. The values of the correlation coefficients are shown in table 7.3. Epeak energy depends on the distribution of relativistic velocity of leptons, so there should be an other kind of physical process.

In general, the values of the correlations are smaller than for Liso. We should mention that there is no possible correlation between ACF and Epeak, the plots for these two parameters are shown in figures 7.9 and 7.10 where the time estimators correspond to the 50-150 keV Band. Figures 7.7 and 7.8 show the correlation between Epeak and T_{50} in the soft and high energy bands. The time estimator that correlates better with Epeak is t_{50}, and figures 7.10 and 7.11 shows in red the 4 outlier candidate GRBs.

The correlation between t_{50} and Epeak suggest that GRB060814 ,GRB070612A, GRB080916A and GRB090618 form a cluster in the region of longer burst activity with a relative low peak energy. That could be reflecting a different engine that need more time with a less efficient energy conversion. A similar interpretation could be applied to the correlation between T_{50} and Epeak althought but the statistics are still poor to confirm. We could associate the long duration due to the time history composed by broad pulses, which suggest a long interaction of the colliding shells considering a fireball model. In the appendix A, the light curves of all the bursts are shown, and effectively these 4 GRBs have a time history composed by several broad pulses. The lack of correlation of ACF with energy suggest that this time

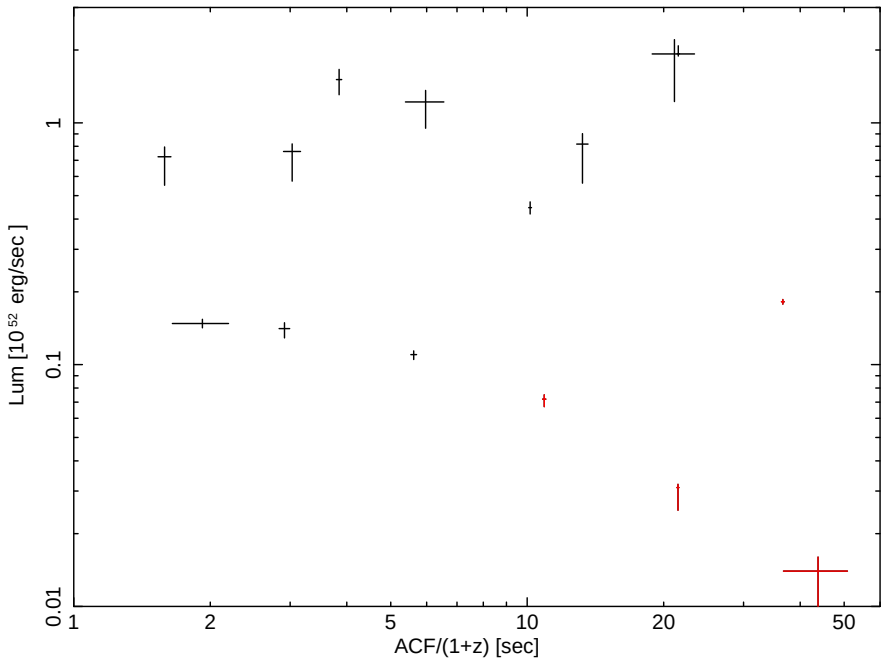

Figure 7.3: Isotropic luminosity dependence with ACF in 50-150 keV band, red crosses represents the long-dim bursts

estimator does not shows the average time of the physical process. The ACF is more related with the intrinsic properties that are accuring during the emission.

Average energy measurements of GRBs shows a strong correlation with the emision and duratio time, and these time estimators are linearly dependent, and put in evidence the presence of a third class of GRBs. In this work we propose to classify GRBs in the rest frame, and we found among the standard long burst a types of GRBs that are less energetic, longer and relatively close.

Estimator and band(kEV)	r	P	r(+)	P(+)
T_{50} (15-50)	0.11	0.68	0.68	5.0×10^{-2}
ACF (15-50)	-0.01	0.97	0.44	0.18
t_{50} (15-50)	0.11	0.69	0.56	8.0×10^{-2}
T_{50} (50-150)	0.15	0.58	0.61	3.5×10^{-2}
ACF (50-150)	0.13	0.62	0.47	0.47
t_{50} (50-150)	0.24	0.38	0.75	2.0×10^{-2}

Table 7.3: Time estimators-E_p Spearman correlation coefficients (r) and chance probabilities P for the whole sample (15 GRBs), (r+) and (P+) are the correlation coefficients and chance probabilities for sample without the long-dimm the bursts (11 GRBs)

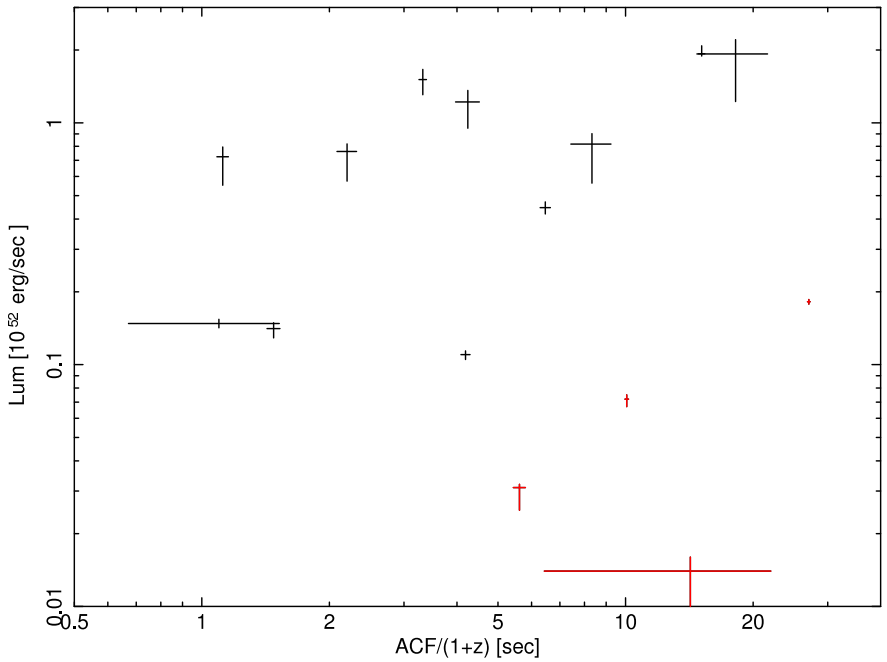

Figure 7.4: Isotropic luminosity dependence with ACF in 50-150 keV band, red crosses represents the long-dim bursts

7.3 Long-near-dim bursts

Except for GRB091127 which is associated with a supernovae, there is a strong evidence of a clustering of bursts with large duration of the outburst activity and large active phase of emission. This burst are outliers in the time estimator-E_{iso} planes and t_{50}-Epeak, T_{50}-Epeak planes. The best correlation are between the time of emission of 50% of the total fluence with Eiso (0.91) and Epeak (0.86) when the 4 burst are removed. The correlation is stronger in the 50-150 keV band, where it is not expected to have some miss-measurements of some soft-X ray extended emission. The value of t_{50} reflects the times intervals where the engine of the GRB is in its more active phase, since there is a clear difference between the 4 outliers and the rest of the sample, we strongly suggest that the engine for the two class of long burst are different, rurthermore the distance is also near, then the progenitors should be also different. The classification of GRBs in the rest frame give us more information about the prompt emission origin, there are two kind of long burst with specific temporal, spatial and energy properties. In the GRB frame, long bursts can be classified in longer-near-dim bursts and long-distant-bright bursts that seem to obey a positive correlation. Normal long burst behaves as is already expected, dim burst are closer and distant burst should be brighter [8].

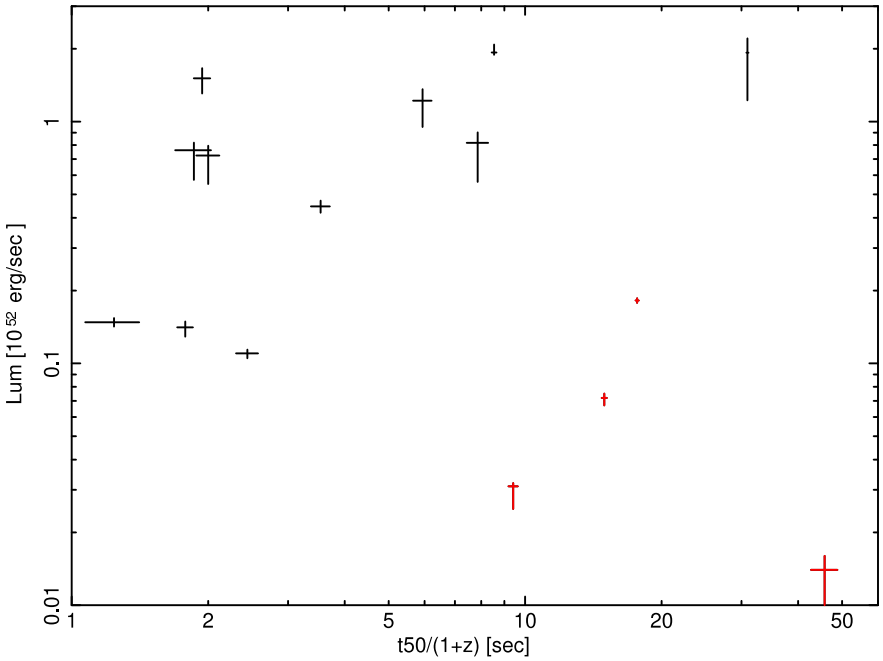

Figure 7.5: Isotropic luminosity as a function of t50 in 50-150 keV band, red crosses represents the long-dim bursts

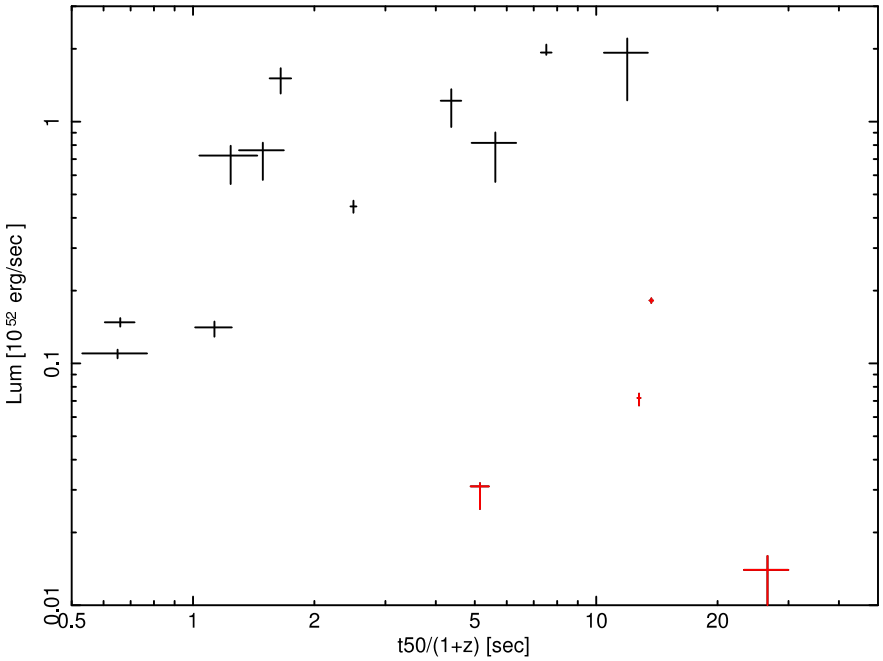

Figure 7.6: Isotropic luminosity as a function of t50 in 50-150 keV band, red crosses represents the long-dim bursts

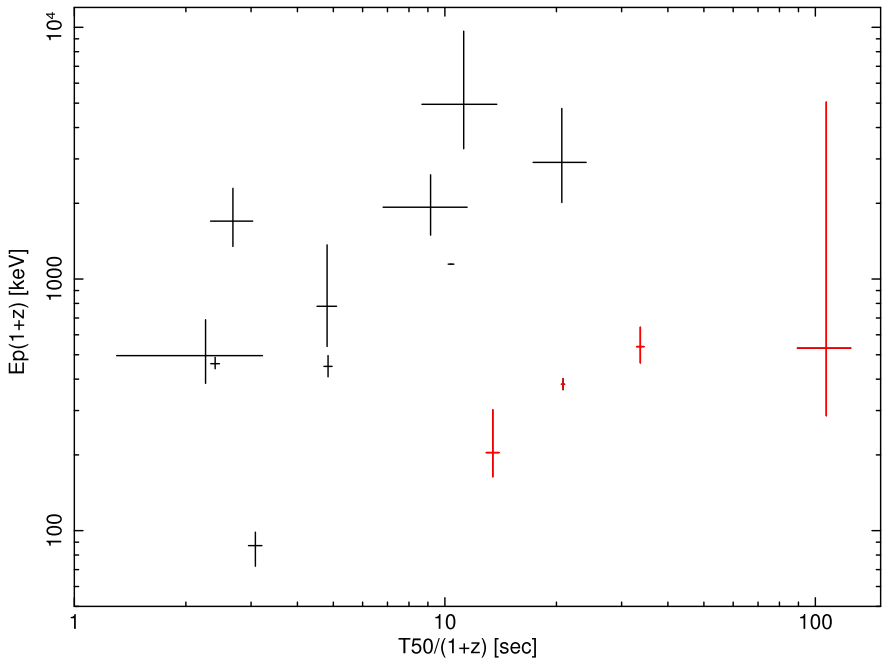

Figure 7.7: Dependence of E_{peak} with T_{50} in 15-50 keV band, long-near-dim burst are represented in red

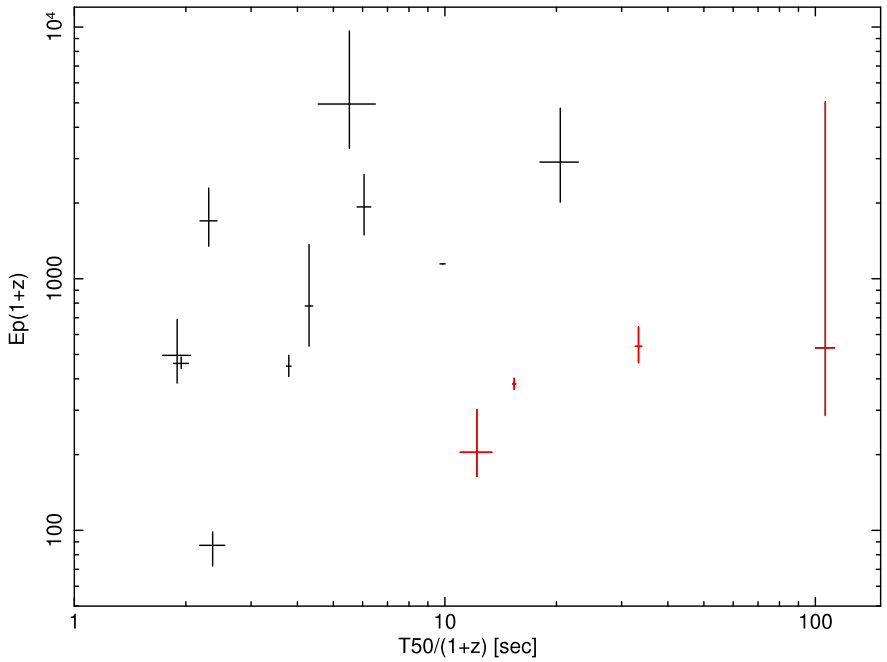

Figure 7.8: Dependence of E_{peak} with T_{50} in 50-50 keV band, long-near-dim burst are represented in red

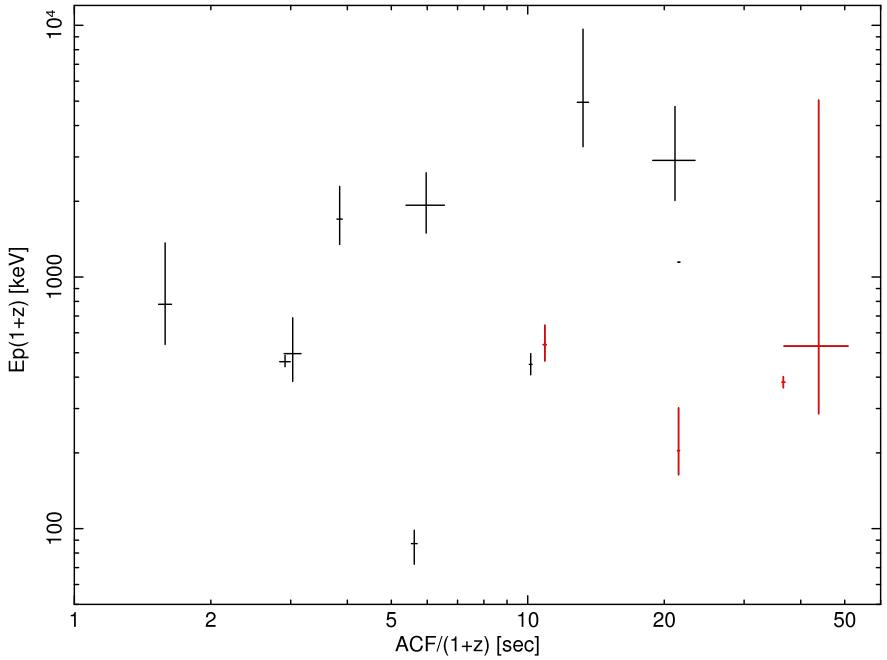

Figure 7.9: Dependence of E_{peak} with T_{50} in 15-50 keV band, long-near-dim burst are represented in red

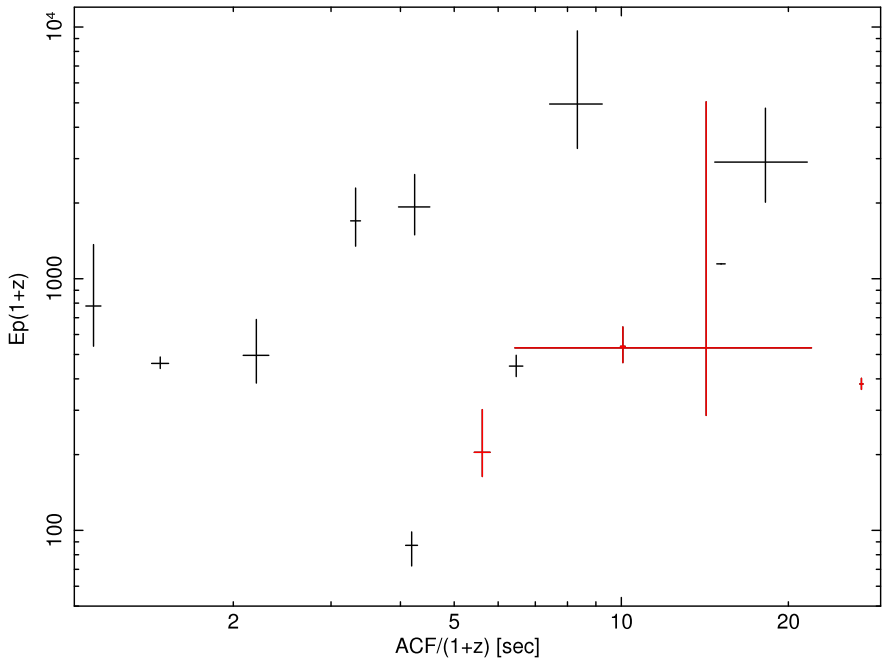

Figure 7.10: Dependence of E_{peak} with ACF in 50-150 keV band, long-near-dim burst are represented in red

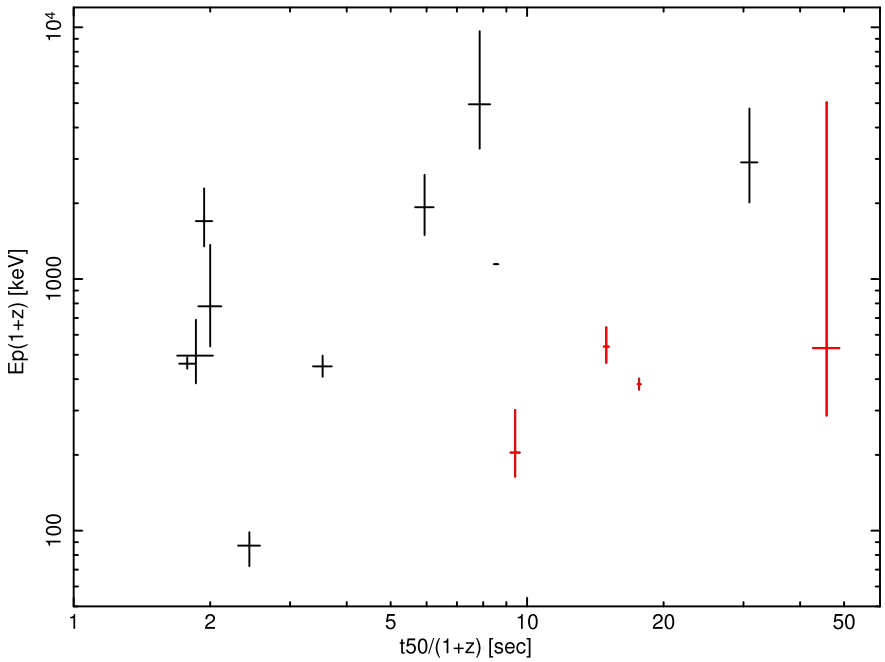

Figure 7.11: Dependence of E_{peak} with t_{50} in 15-50 keV band, long-near-dim burst are represented in red

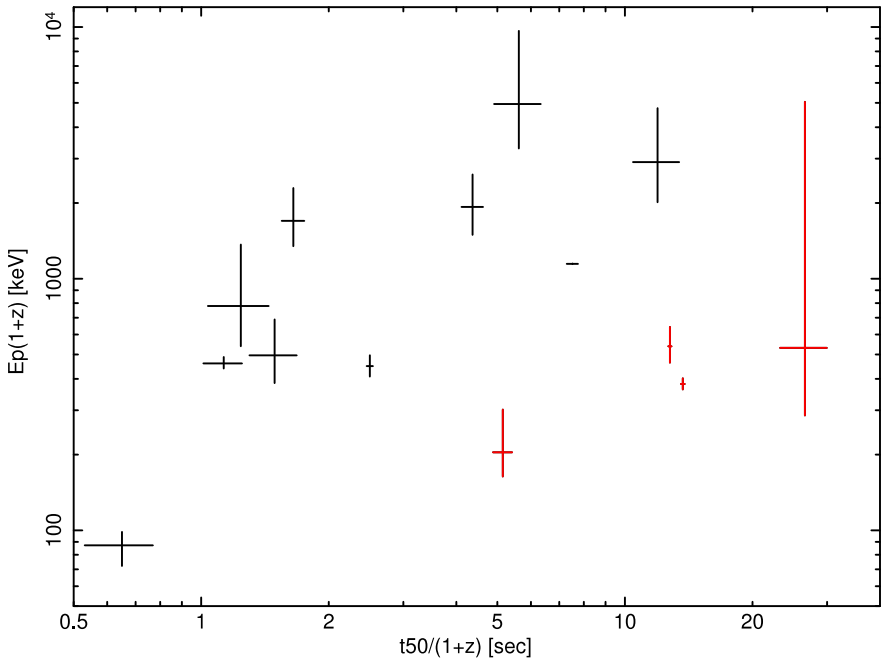

Figure 7.12: Dependence of E_{peak} with t_{50}in 50-150 keV band, long-near-dim burst are represented in red

Chapter 8

Conclusions

8.1 Temporal estimators classification

Classification of GRBs has started since their first detection, the standard method to classify them is to compute the time of emission of the 90% of the total fluence T_{90}. The canonical two classes of burst are long and short [15], nevertheless a division into 3 classes was recently demonstrated by Horvath [24]. The last two mentioned classification were done in the observed frame. One of the most intriguing questions is to know if this classifications are hidden some intrinsic properties due to cosmological effects. In 2007, Borgonovo[7] shown that long GRBs have a bimodal distribution when the ACF is cosmologically corrected, opening the possibility to classify GRBs in the rest frame. Following this idea, we also found a similar bimodal distribution of long GRBs when the ACF is computed in the rest frame. Since we expect that cosmological dilatation effect is the same for all the timescales, we also extend the bimodality for others time estimators: duration times of outburst activity (T_{50}) and the time intervals where the engine is in the most active phase (t_{50}). There are 4 GRBs that in the time-distance plane, form a subgroup. Long-near burst and long-distant burst, seems to have different origin and behavior. One of the most obvious properties is that the redshift is relatively small without supernovae association, that could give a hint of the possible different progenitor, although to produce a fireball the scenarios are quite restricted, specially the collapsar model need some low metallicity environments[**?**]. In the light curves, we also observed that there are some common trends, the time history is composed by broad pulses that underlie a longer active phase.

The three chosen time estimators gave a different type of time intervals measurement, but a relation between them should be expected, we are measuring temporal parameters of the same physical phenomenon. We established that the three estimators are strongly correlated and that there is a linear dependence between the T_{50}-t_{50} as well as ACF-t_{50}. The

linearity of the dependence seems to be independent of the energy, a simililar correlation values were obtained in the high energy band (50-150 keV). The advantage of using T_{50} instead of T_{90} is justified by the fact that T_{90} could lead to a miss-measurement of the duration due to some soft-extended emissions[12], GRB090424 and GRB071010B shows longer values of T_{50} at 15-50 keV band because of the soft tail, as it is possible to appreciate in the respective light curves.
Although we cannot establised a standard trend for the behavior of the light curves in bands higher than 150 keV, due to the gain dependence of WAM-Suzaku instrument degradation, there temporal values are shorter at the high band from BAT-Swift detector.

8.2 Space-time and enegy evidence for a subclass of long bursts

From the temporal analysis of 15 bursts detected simultaneously by Swift and Suzaku with known redshift, we already determine a subgroup of long GRBs. GRBs that are closer and are longer in the rest frame seem to form a different type of long burst. GRB060814 ,GRB070612A, GRB080916A and GRB090618 have similar light curves, showing broad pulses in their time histories. To investigate the counterpart in energy, we performed a spectral analysis using Swift-BAT and Suzaku-WAM instruments, which are complementary, and offer the unique possibility to have spectra from 15 to 5000 keV. The combined spectra from both observatories allows to compute with a reliable statistics spectral parameters such peak energy, isotropic energy and isotropic luminosity.
Universe expansion should redshift objets in energy and dilate in time. We verified that all the timescales we used obey the cosmological principle of expansion. When they are cosmologically corrected, a classification of long GRBs into two groups is possible. ACFs and peak energy are not correlated, but the time intervals of most active phase and the duration emission time of the 50% of the total fluence are strongly correlated with peak energy and the isotropic luminosity when the 4 long-near GRBs are suppressed. The 4 bursts have a longer temporal estimators and have a smaller isotropic luminosities, so we could include another restriction on energy to the long-near burst, they are dimmer and its peak energy also lays in the longer t_{50} and low Epeak quadrant.
The evidence of a subclass of GRBs is also present in the time-energy planes, which reinforce the possibility of different engine or progenitor for GRBs which have longer active phase, they are dim and have a small redshift. Furthermore, as we mentioned in chapter 5 a bimodality of long GRBs in the afterglow phase has been reported which is interpreted as possible difference of explosion mechanism between both types of long bursts

(Dainotti[11]). The classification of GRBs in the rest frame unveils more information about the engine that powers the prompt emission of long bursts. Using a short time estimators in the 50% level, specially t_{50} which represents the time intervals of the most active phase and the counterpart in energy, give strong evidence to suggest that long GRBs could have more than one origin. The correlation between t_{50} with Epeak when the long-dim-close burst are suppressed in the analysis, could reflect the difference in the fermion's velocities distribution, which maybe would be related to a different physical origin of the two suggested class of long GRBs. The classification of GRBs considering the cosmological expansion gives more hints of the origin of burts, and uncover the information hidden in the classification in the observer frame. Nevertheless, the lack of redshift detection is still a restriction to have large burst samples with confident statistical levels. Finally, we found that the spectral analysis reproduce the Amati relation which give to the obtained results reliability. And confirms that the Amati relation is almost independent from the systematics effects.

Appendix A

Light curves and spectra

Swift light curves in 15-50 keV and 50-150 keV bands. The spectrum corresponds to model that fits better Suzaku and Swift data.

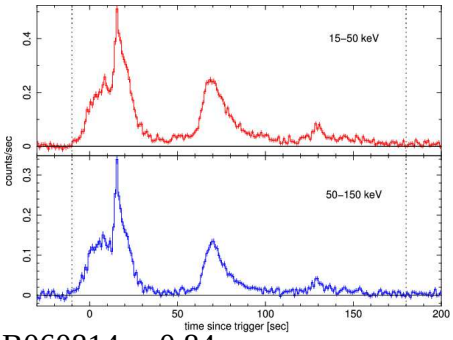

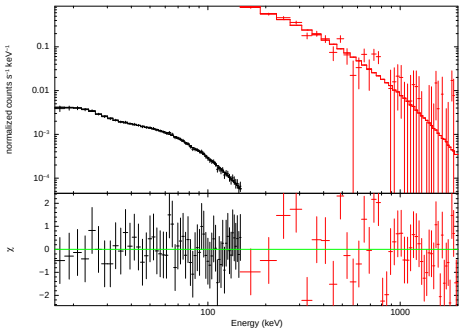

GRB060814 z=0.84

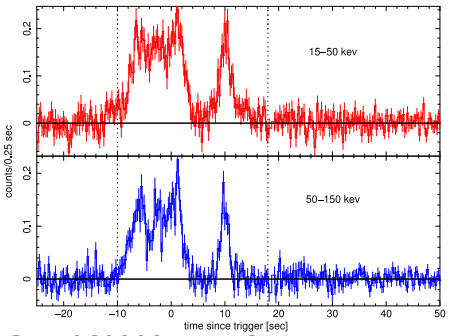

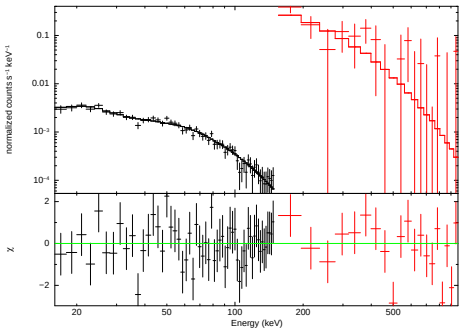

GRB060908 z=2.43

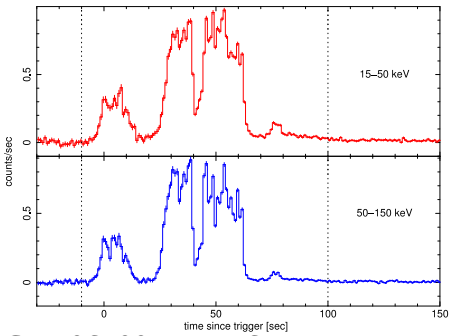

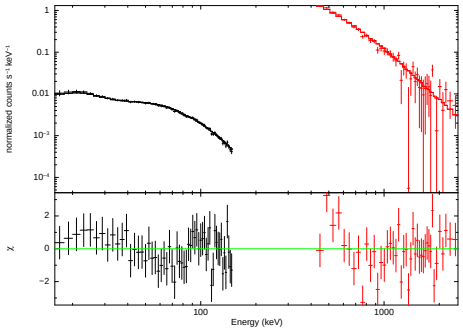

GRB061007 z=1.26

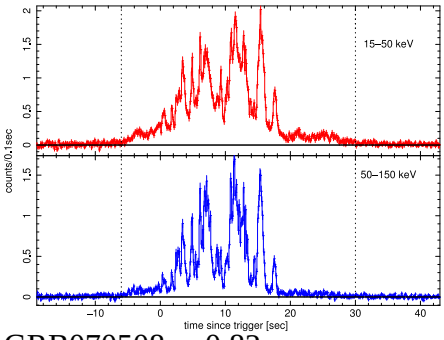

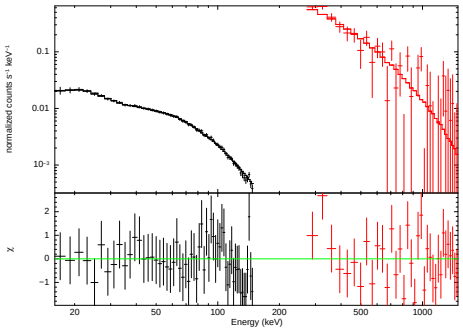

GRB070508 z=0.82

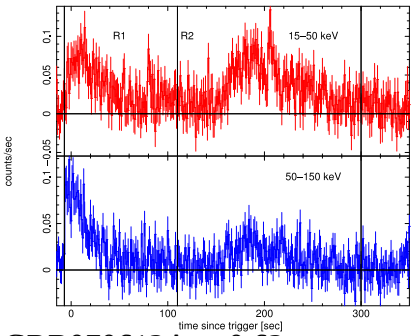

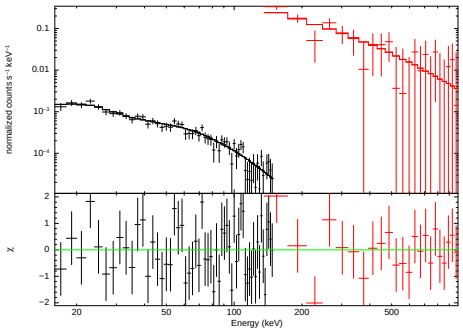

GRB070612A z=0.62

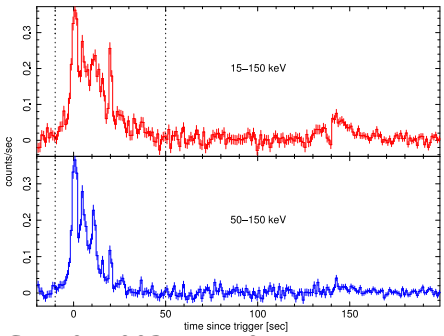

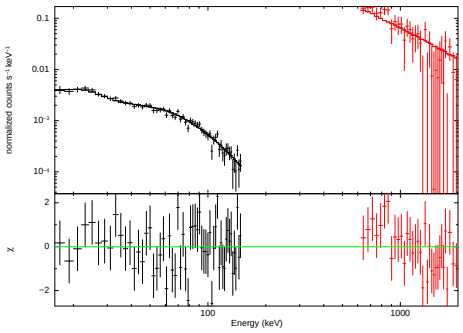

GRB071003 z=1.10

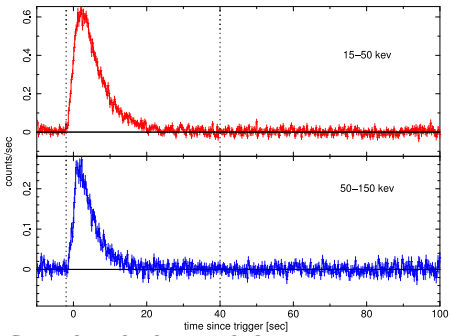

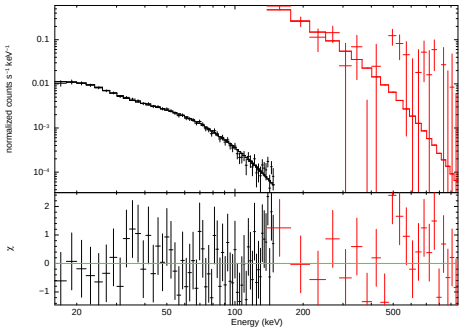

GRB071010B z=0.947

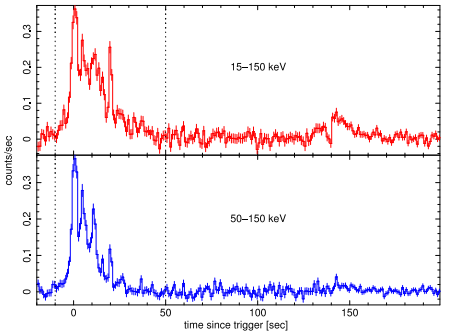

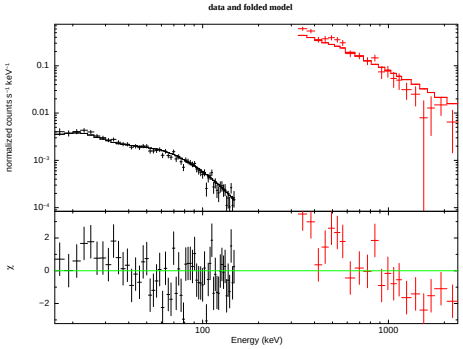

GRB080319C z=1.95

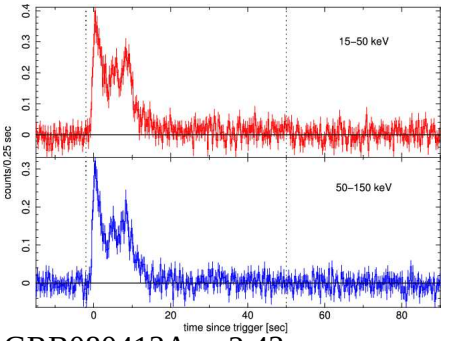

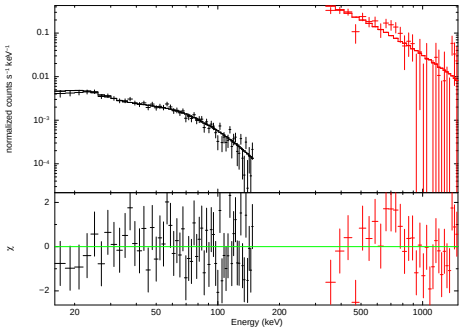

GRB080413A z=2.43

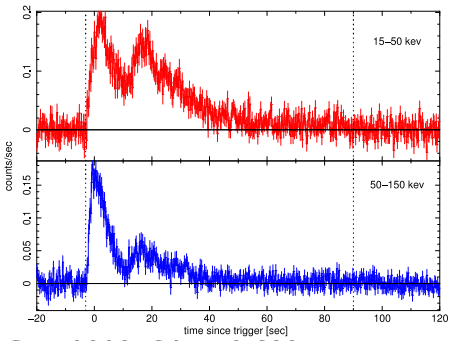

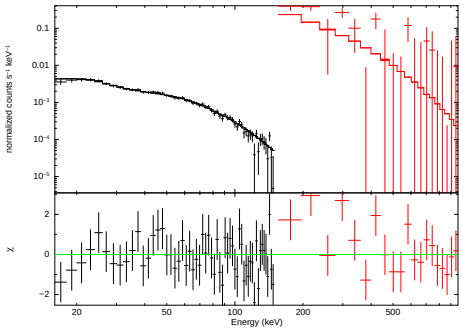

GRB080916A z=0.689

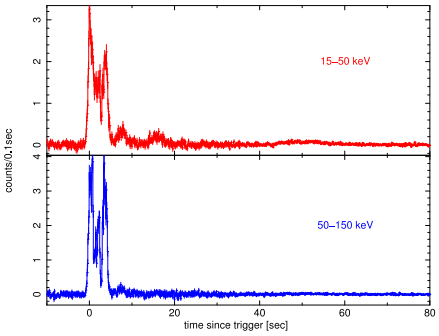

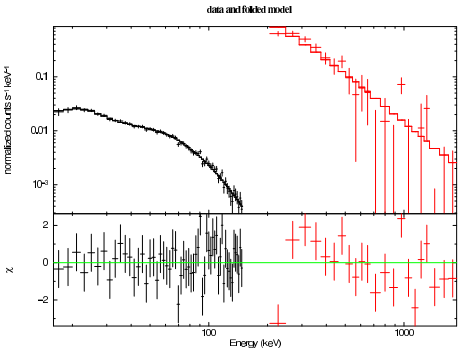

GRB090424 z=0.544

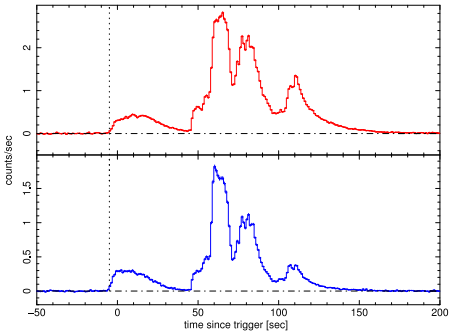

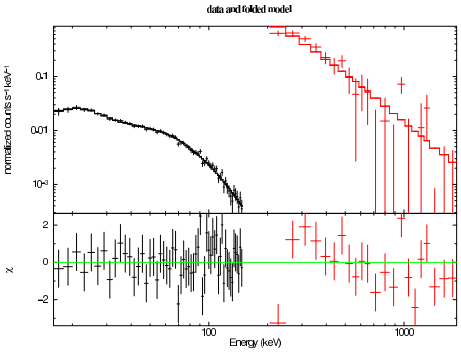

GRB090618 z=0.54

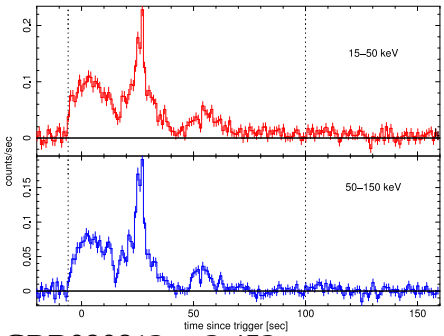

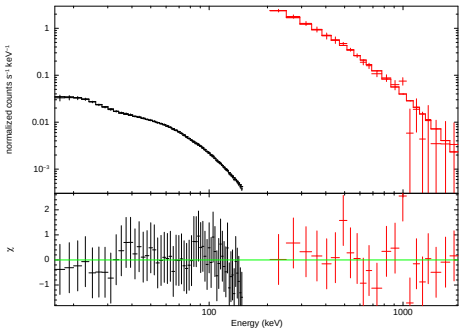

GRB090812 z=2.452

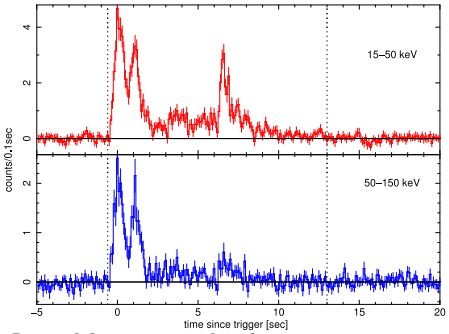

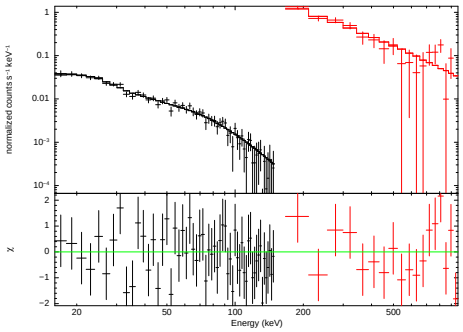

GRB091127 z=0.49

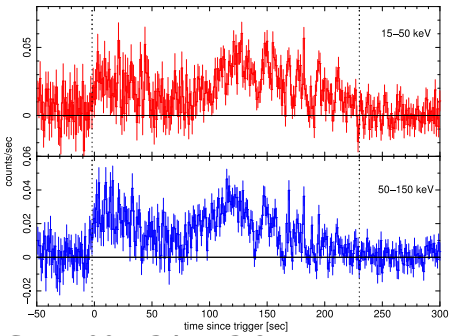

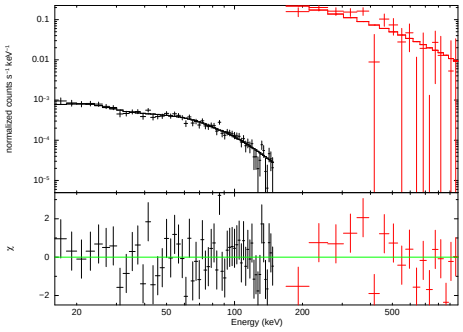

GRB100413A z=3.9

Appendix B

T_{90} values in two Swift energy bands

Burst	T_{90} [15-50 keV]	T_{90} [50-150 keV]
GRB060814	146.1 ± 4.1	143.4 ± 7.1
GRB060908	19.75 ± 2.1	17.8 ± 0.7
GRB061007	92.0 ± 6.0	59.1 ± 2.1
GRB070508	24.7 ± 0.8	17.3 ± 0.6
GRB070612A	361.0 ± 55.6	223.5 ± 17.7
GRB071003	149.9 ± 5.8	137.5 ± 98.5
GRB071010B	37.2 ± 2.8	32.5 ± 3.0
GRB080319C	41.0 ± 10.7	11.5 ± 0.9
GRB080413A	46.6 ± 0.5	44.8 ± 1.6
GRB080916A	61.4 ± 8.3	62.7 ± 19.3
GRB090424	52.7 ± 2.0	8.1 ± 7.3
GRB090618	114.3 ± 0.8	107.8 ± 0.8
GRB090812	98.1 ± 12.8	54.6 ± 2.4
GRB091127	9.3 ± 1.2	7.2 ± 0.9
GRB100413A	203.1 ± 13.1	189 ± 16.9

Table B.1: Values of T_{90} in 2 energy bands , the values are expressed in seconds (observer frame).

Appendix C

Light curves from Suzaku

Suzaku light curves are shown in 4 energy bands TH0, TH1, TH2 and TH3. In table 4.1, the channel equivalence of the bands is available. In the next table, the energy equivalence is described. The energy range usually changes in flight because of the gain variation of the photomultiplier tubes. Not all the burst were detected in higher energy bands. Due to the limitation of the binning size of the light curves to 1 second and the low signal to noise ratio; the temporal parameters could not be determined. When it was possible to determine T_{50}, the value is shown.

GRB	TH0	TH1	TH2	TH3
GRB060814	107 ± 40	227 ± 80	489 ± 181	-
GRB060908	90 ± 19	186 ± 40	-	-
GRB061007	130 ± 20	229 ± 79	486 ± 178	3204 ± 2540
GRB070508	95 ± 36	203 ± 72	436 ± 160	2900 ± 2300
GRB070612A	99 ± 37	210 ± 73	-	-
GRB071003	123 ± 18	216 ± 74	456 ± 166	2810 ± 2190
GRB071010B	120 ± 19	214 ± 75	-	-
GRB080319C	125 ± 25	200 ± 57	432 ± 172	3050 ± 2450
GRB080413A	125 ± 24	225 ± 80	-	-
GRB080916A	115 ± 40	237 ± 81	480 ± 122	-
GRB090424	120 ± 42	248 ± 85	525 ± 190	-
GRB090618	96 ± 22	228 ± 110	536 ± 198	3520 ± 2750
GRB090812	140 ± 22	267 ± 105	535 ± 180	-
GRB091127	123 ± 43	254 ± 87	537 ± 196	-
GRB100413A	147 ± 23	260 ± 90	550 ± 200	-

Table C.1: Energy equivalence for the light curves, the energy is expressed in keV

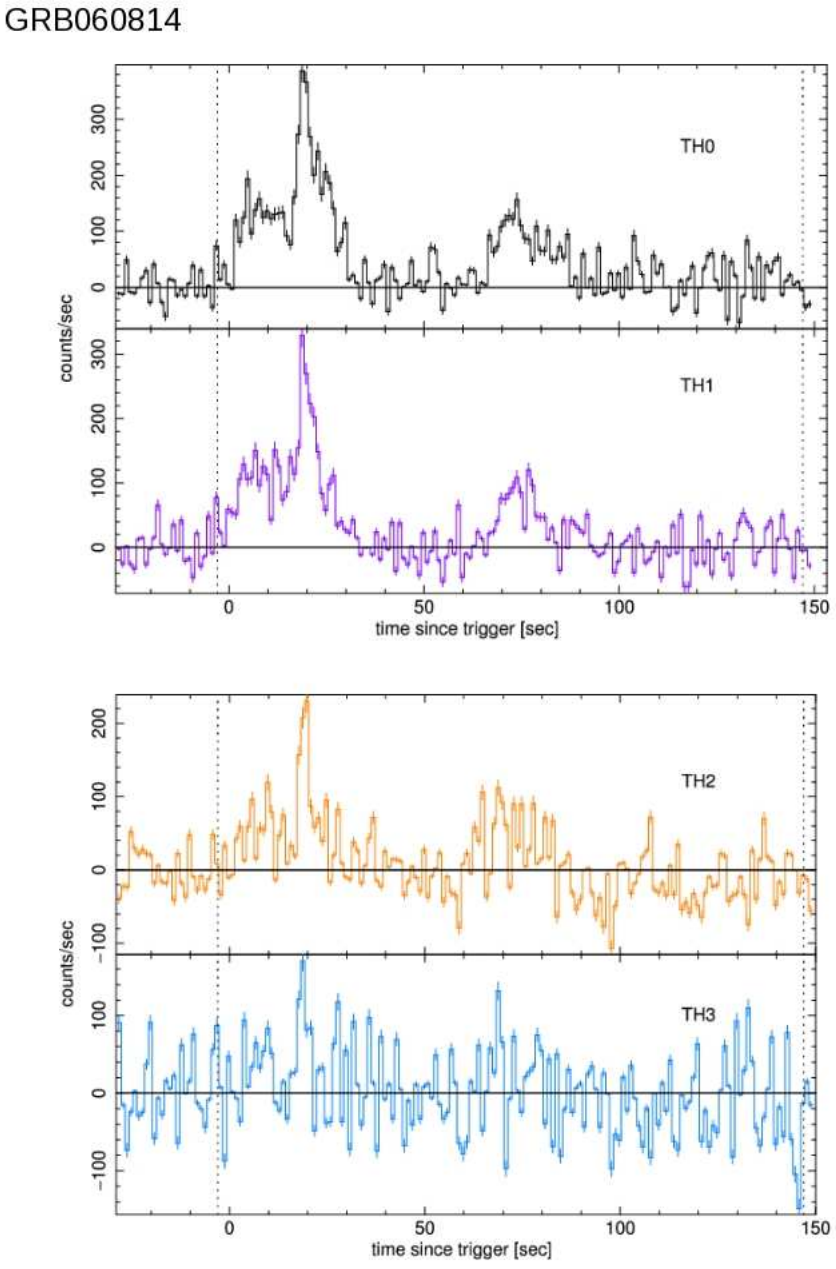

Figure C.1: TH0(T_{50}=58s)

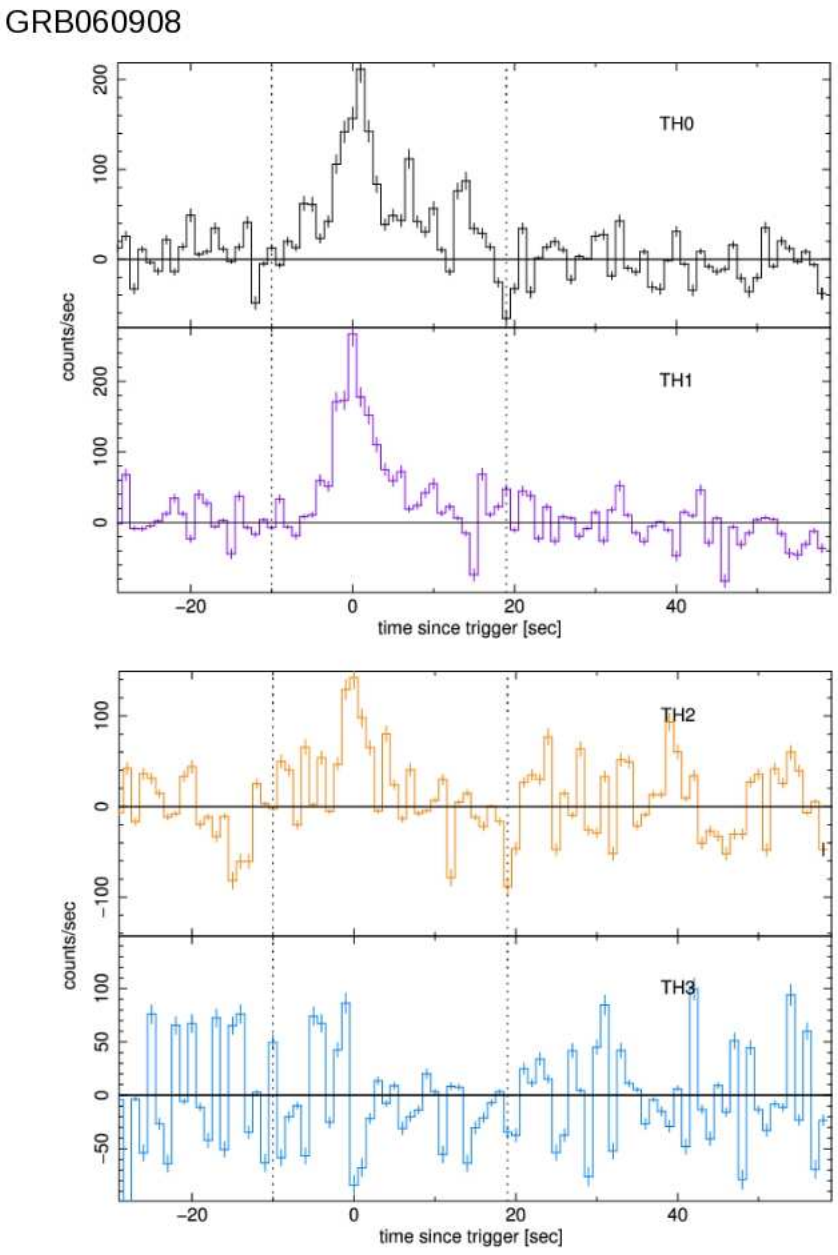

Figure C.2: TH0(T_{50}=8s)

GRB061007

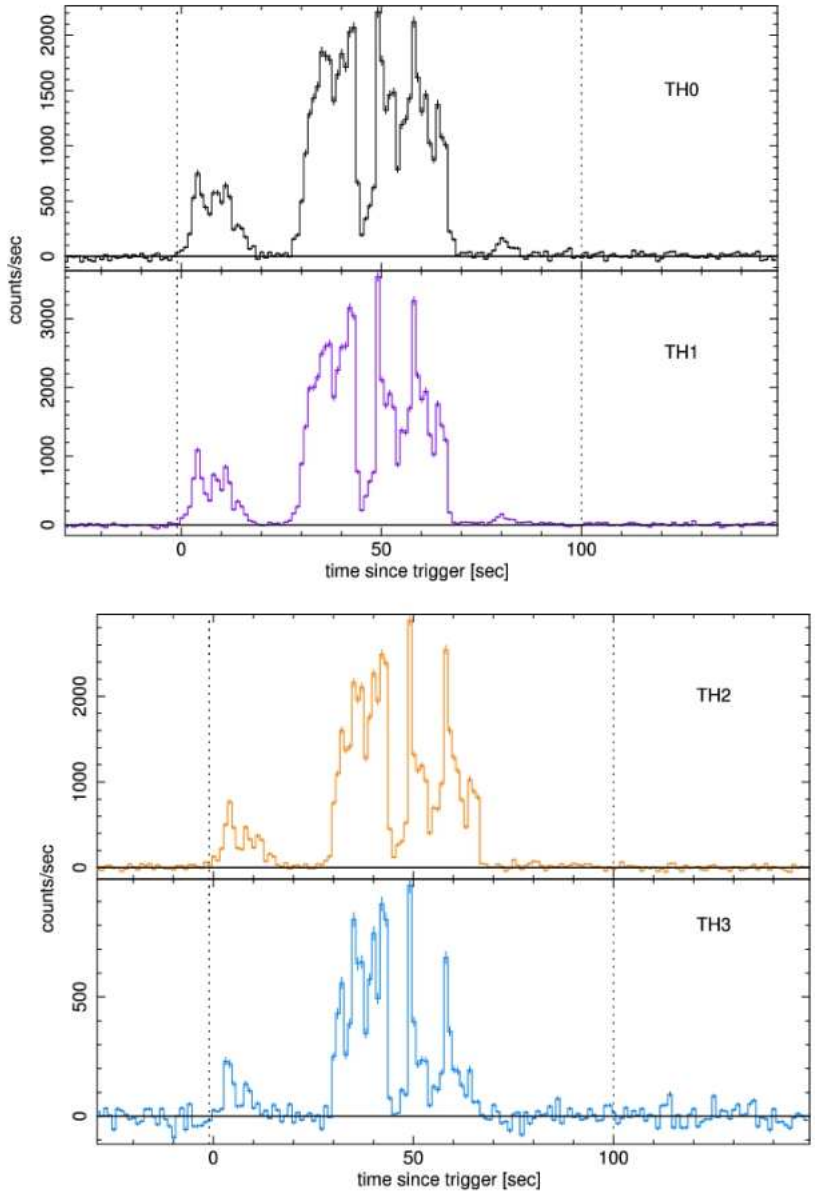

Figure C.3: TH0(T_{50}=22 s), TH1(T_{50}=21 s) TH2(T_{50}=20 s) TH3(T_{50}= 14s)

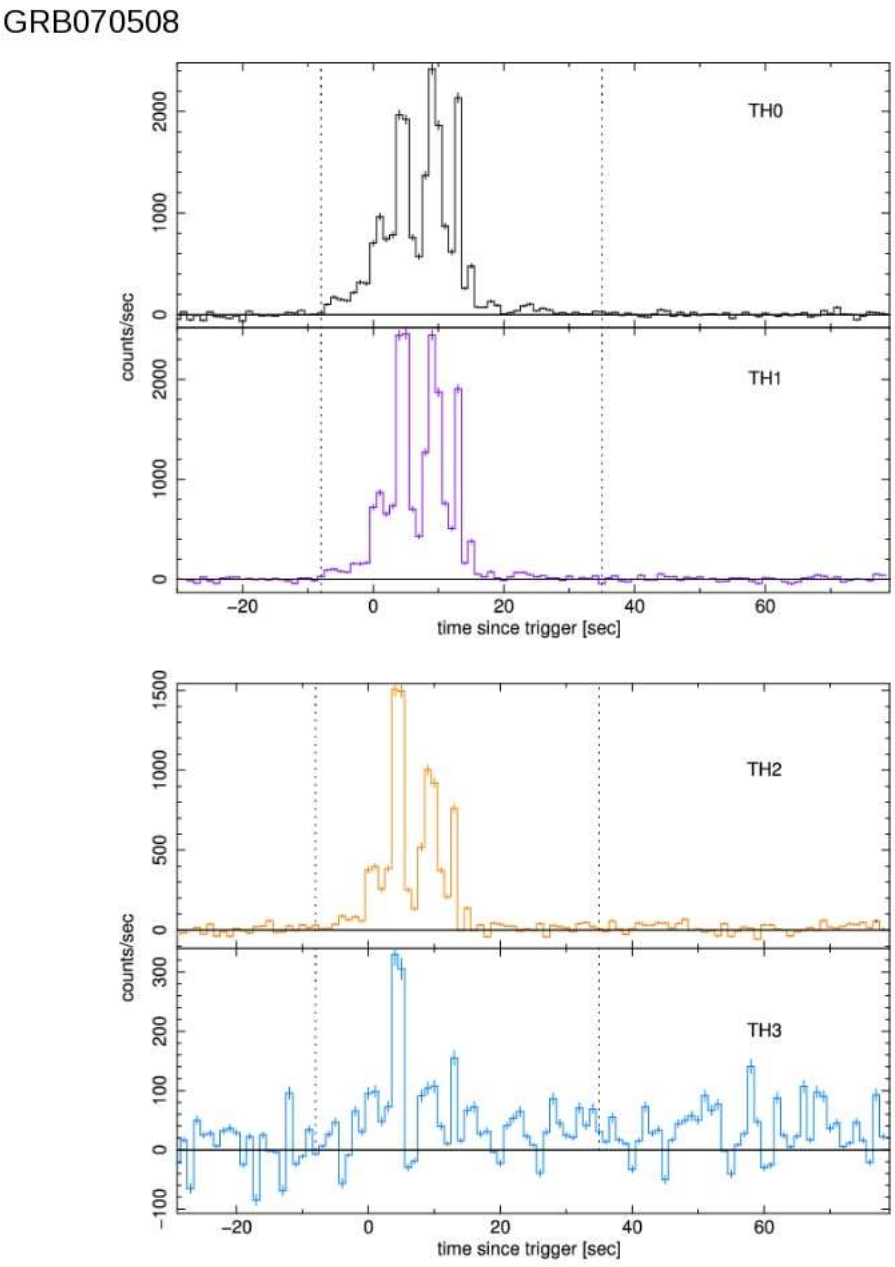

Figure C.4: TH0(T_{50}=6 s), TH1(T_{50}=5.75 s), TH2(T_{50}=5.36 s)

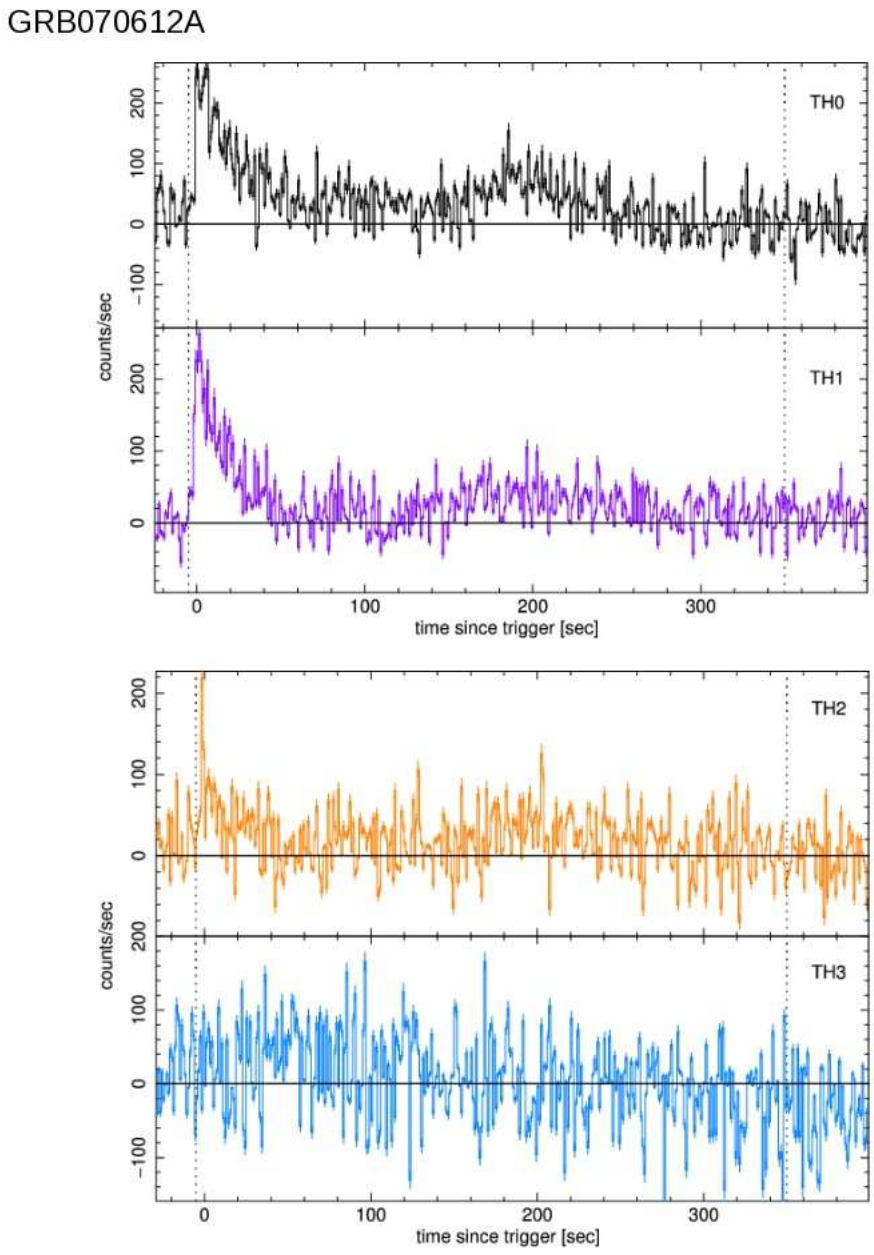

Figure C.5: TH0(T_{50}=162 s),TH1(T_{50}=162 s)

GRB071003

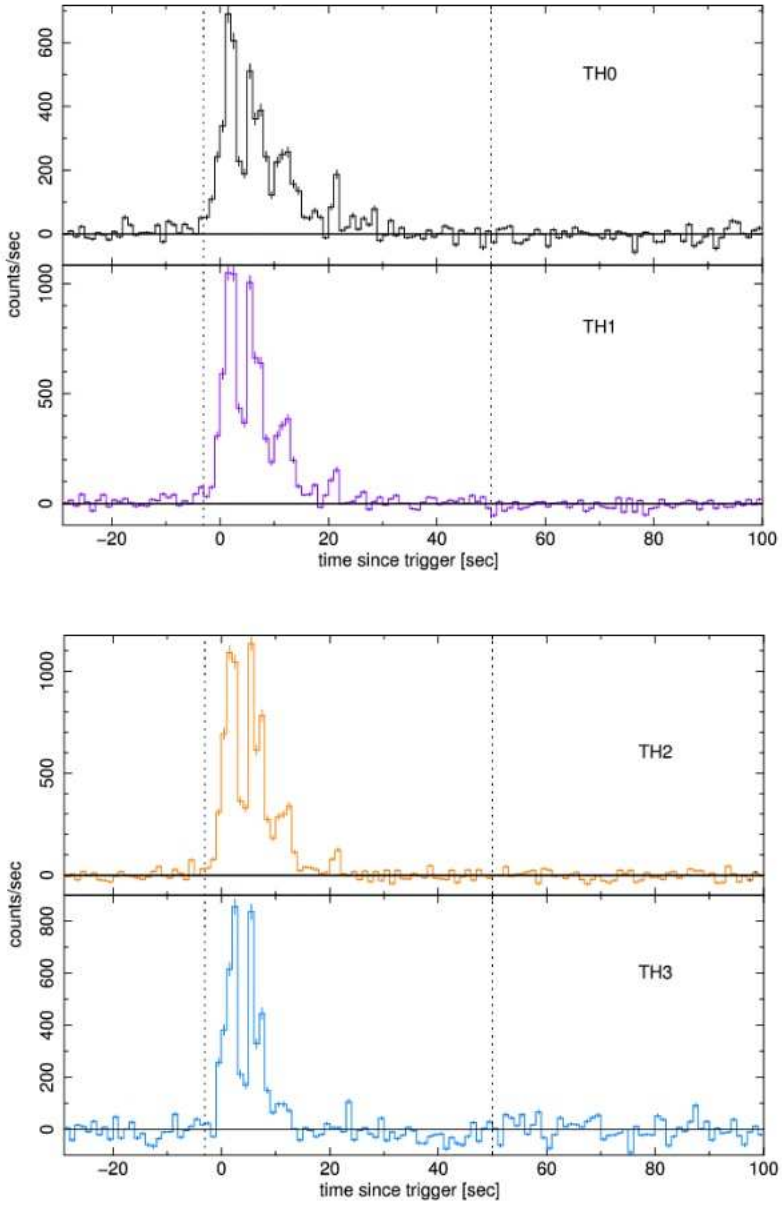

Figure C.6: TH0(T_{50}=9 s), TH1(T_{50}=7 s), TH2(T_{50}=6 s), TH3(T_{50}= 4s)

GRB071010B

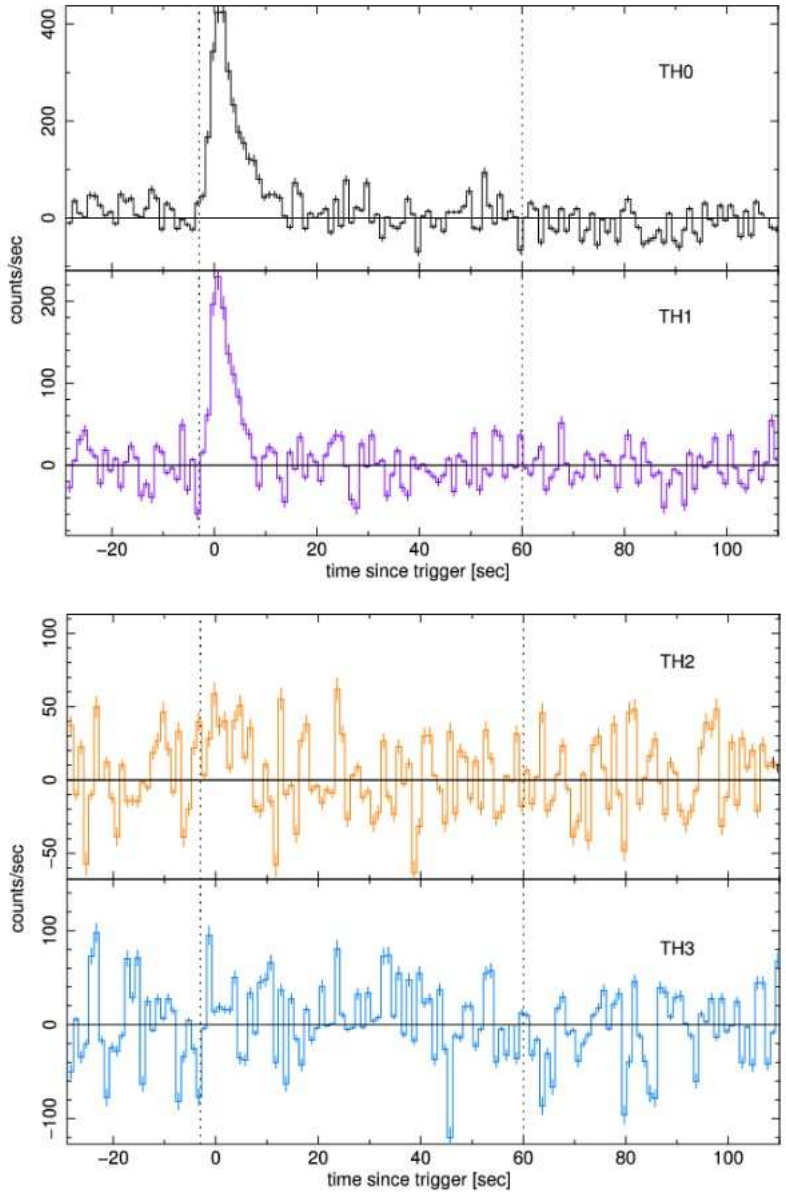

Figure C.7: TH0(T_{50}=5 s), TH1(T_{50}=6 s)

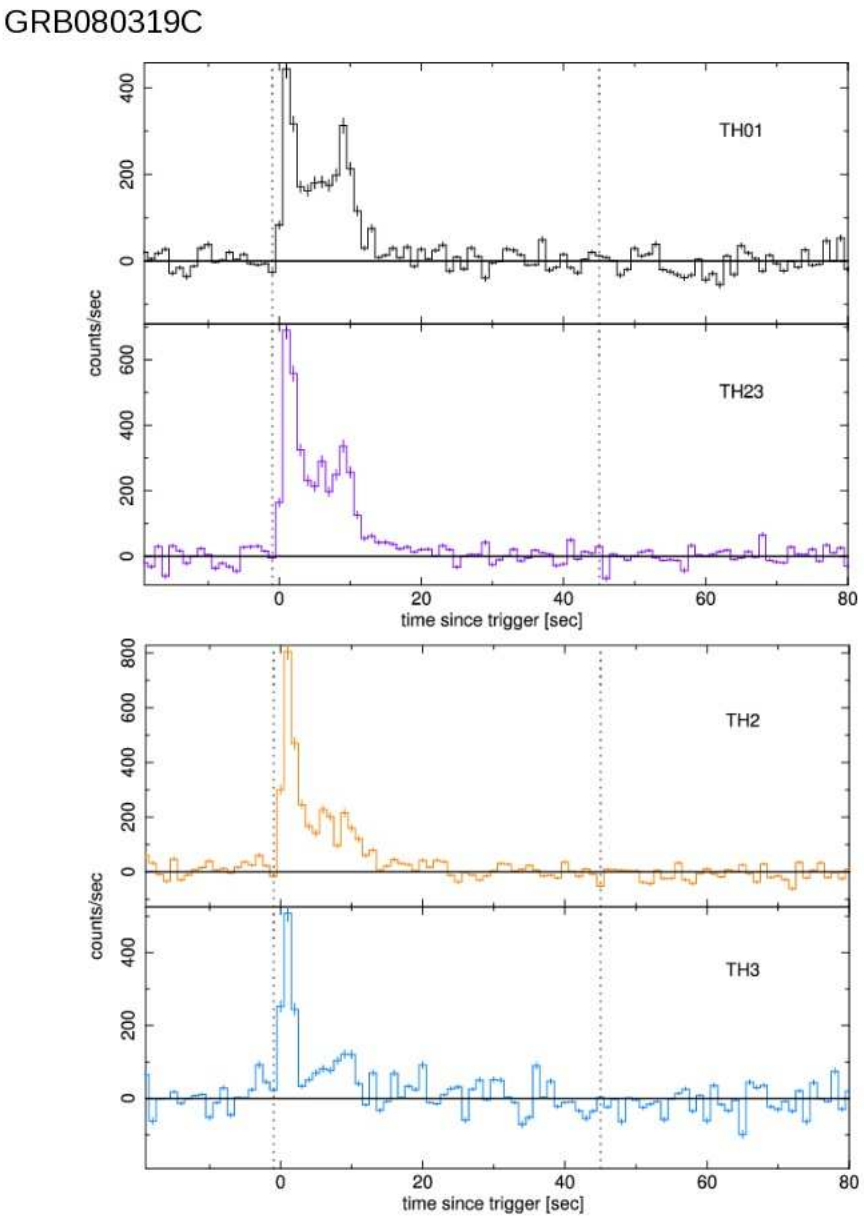

Figure C.8: TH0(T_{50}=7 s), TH1(T_{50}=6 s), TH2(T_{50}=7 s)

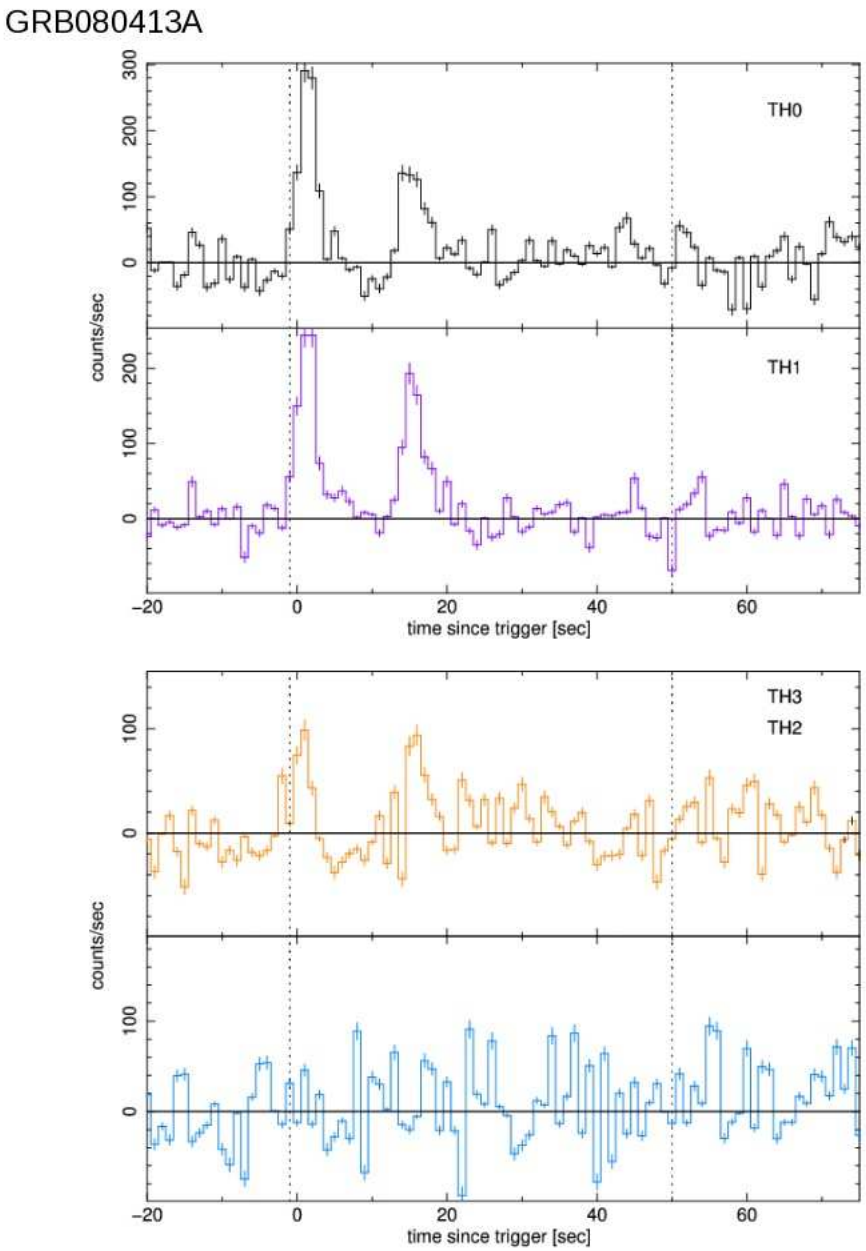

Figure C.9: TH0(T_{50}=14 s), TH1(T_{50}=14 s)

GRB080916A

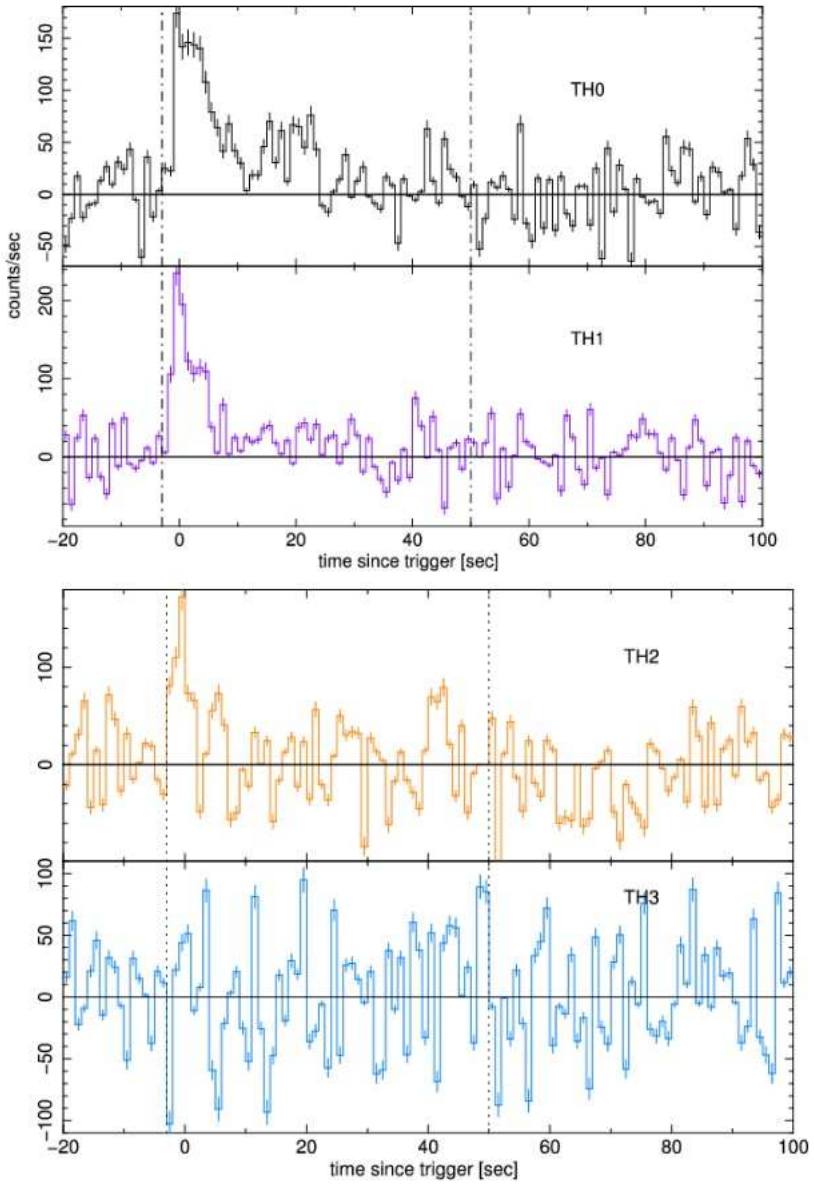

Figure C.10: TH1(T_{50}=2 s)

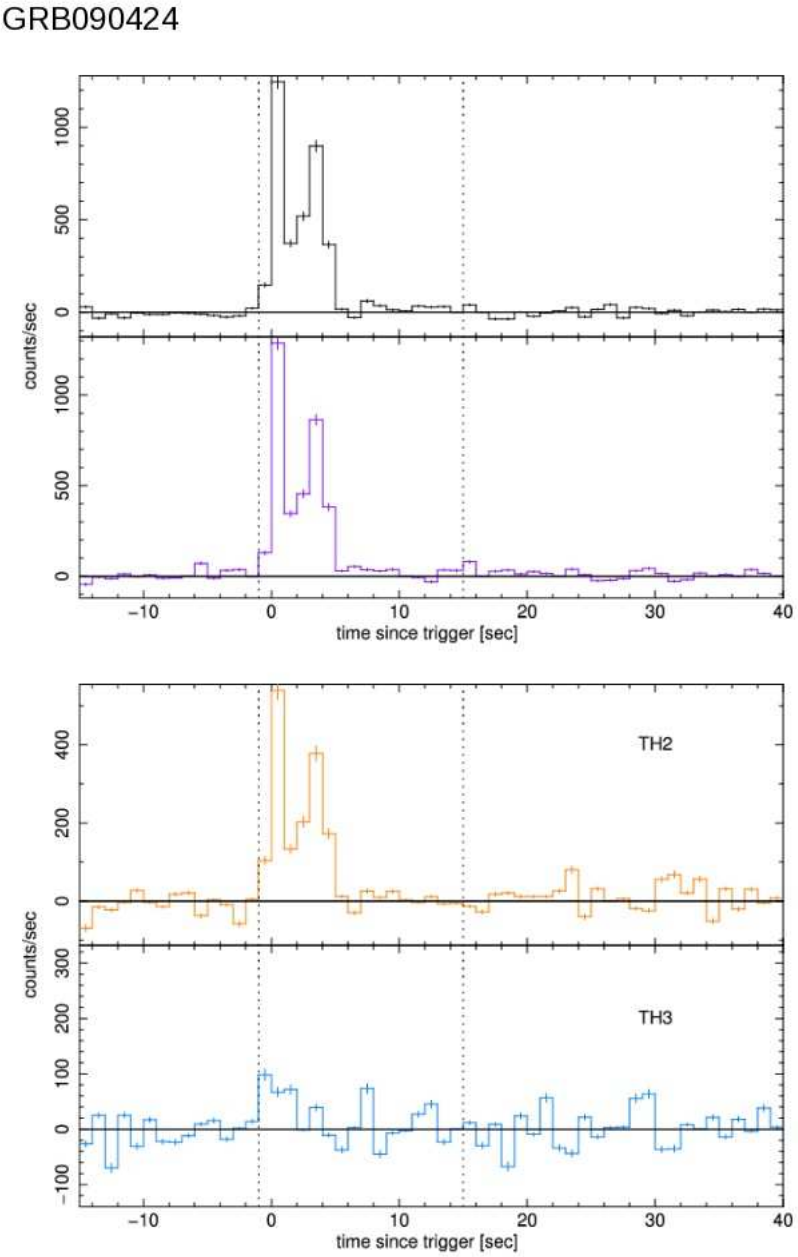

Figure C.11: TH0(T_{50}=2.98 s), TH1(T_{50}=2.88 s), TH2(T_{50}=2.87 s

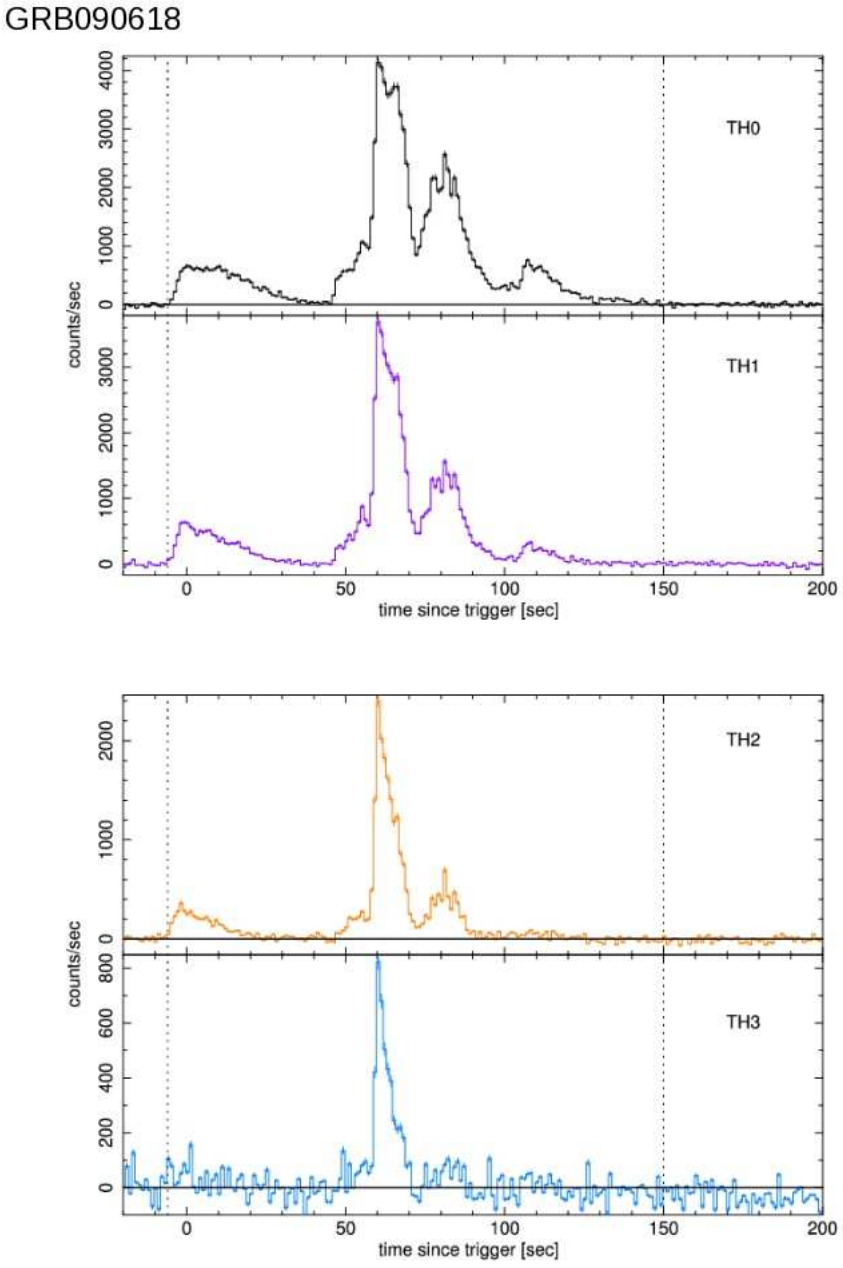

Figure C.12: TH0(T_{50}=22 s), TH1(T_{50}=18 s), TH2(T_{50}=12 s, TH3(T_{50}=6 s

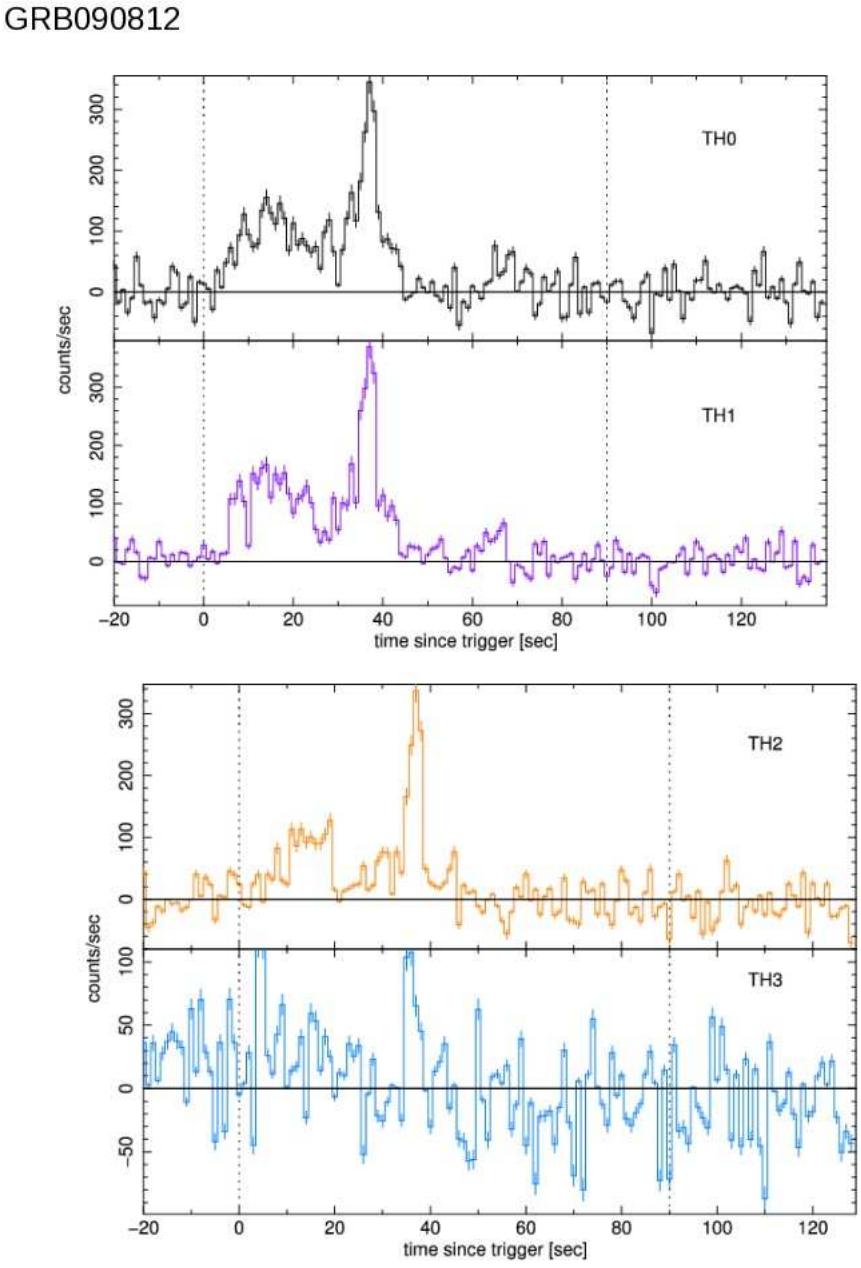

Figure C.13: TH0(T_{50}=22 s), TH1(T_{50}=21 s)

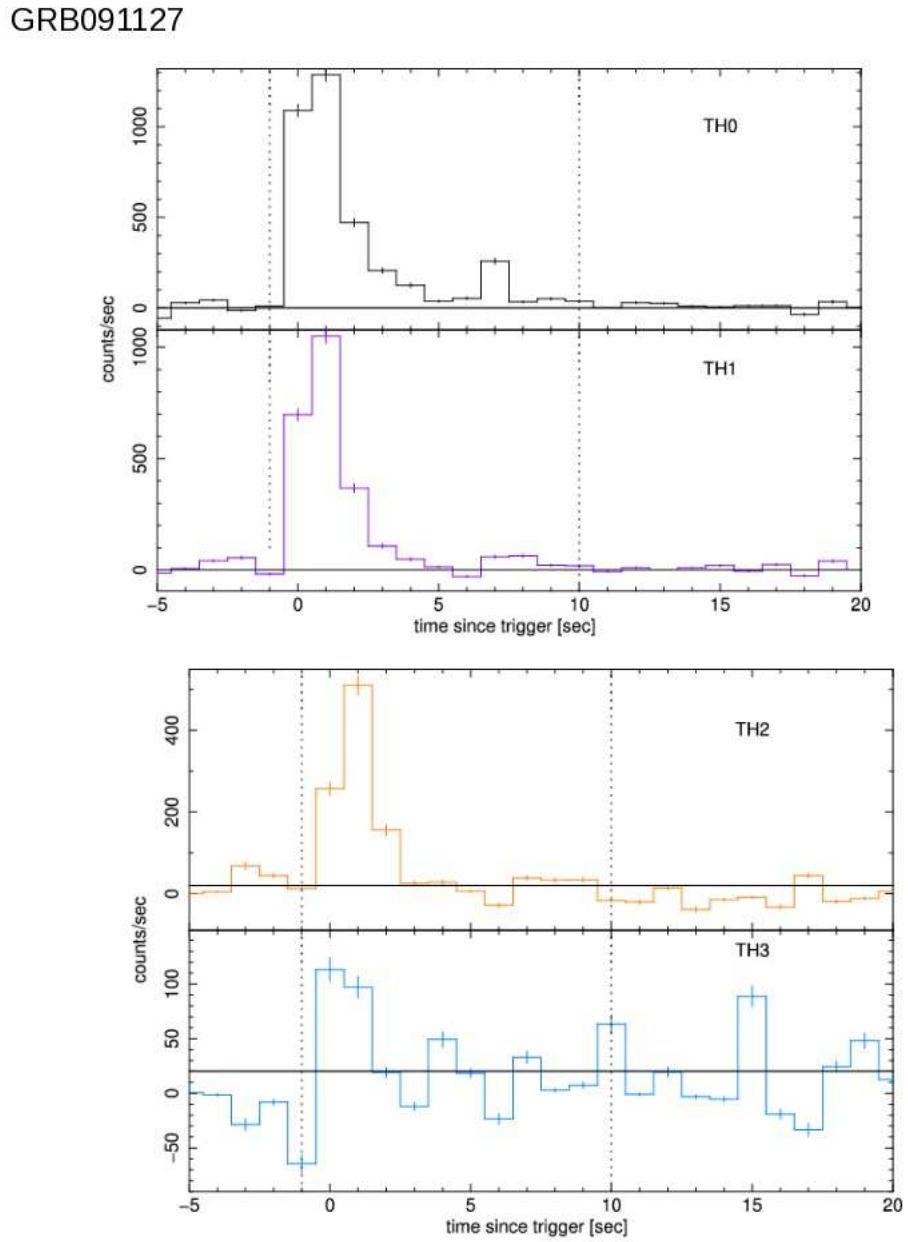

Figure C.14: TH0(T_{50}=2 s), TH1(T_{50}=1 s), TH2(T_{50}=1 s)

GRB100413A

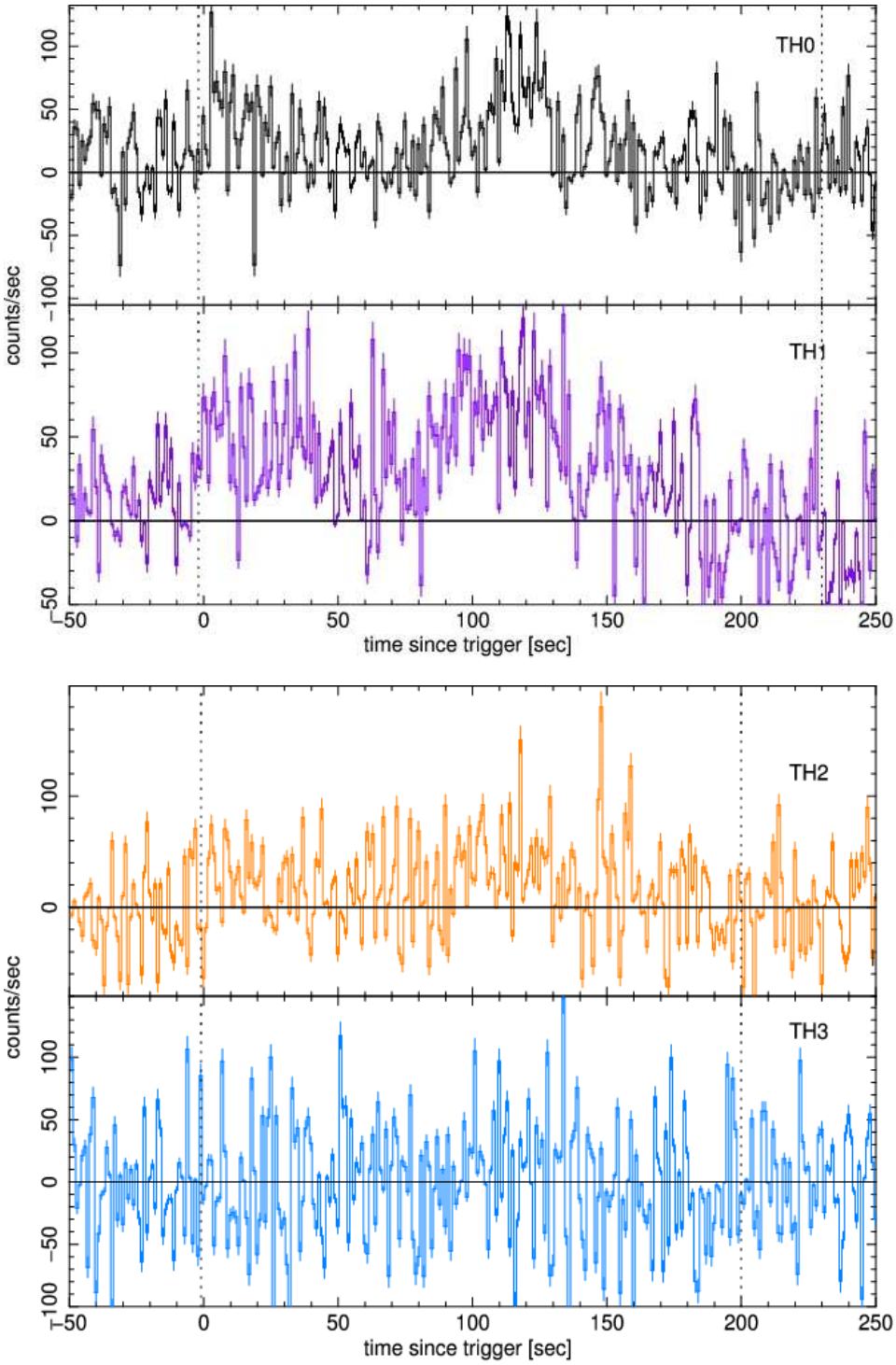

Figure C.15: TH0(T_{50}=22 s)

Appendix D

List of GRBs from Amati 2006

In the following table there is the list of bursts used to compare the validity of the Amati relation, the missions used correspond to BeppoSAX (SAX), HETE-2(HET), KONUS wind (KON) and Swift-BAT (BAT). Figure 11.1 shows the relation established by Amati[1] where the power law $E_{peak}=95\times E_{iso}^{0.49}$ is represented by the solid line.

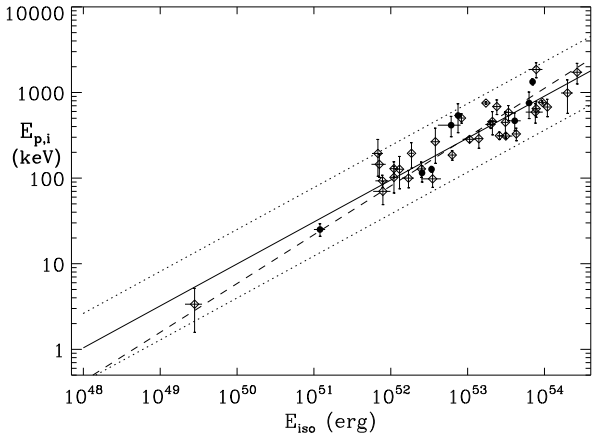

Figure D.1: Amati correlation for 39 long GRBs and 2 XRF from Amati 2006[1]

GRB	Type	z	Epeak[keV]	Eiso[10^{52}erg]	Instruments
970228	LONG	0.695	195±64	1.86±0.14	SAX
970508	LONG	0.835	145±43	0.71±0.15	SAX
970828	LONG	0.958	586±117	34±4	BAT
971214	LONG	3.42	685±133	24±3	SAX
980613	LONG	1.096	194±89	0.68±0.11	SAX
980703	LONG	0.966	503±64	8.3±0.8	BAT
990123	LONG	1.60	1724±466[(b)]	266±43	SAX/BAT/KON
990506	LONG	1.30	677±156[(b)]	109±11	BAT/KON
990510	LONG	1.619	423±42	20±3	SAX
990705	LONG	0.842	459±139[(b)]	21±3	SAX/KON
990712	LONG	0.434	93±15	0.78±0.15	SAX
991208	LONG	0.706	313±31	25.9±2.1	KON
991216	LONG	1.02	648±134[(b)]	78±8	BAT/KON
000131	LONG	4.50	987± 416[(b)]	199±35	BAT/KON
000210	LONG	0.846	753±26	17.3±1.9	KON
000418	LONG	1.12	284±21	10.6±2.0	KON
000911	LONG	1.06	1856±371[(c)]	78±16	KON
000926	LONG	2.07	310±20	31.4±6.8	KON
010222	LONG	1.48	766±30	94±10	KON
010921	LONG	0.450	129±26	1.10±0.11	HET
011211	LONG	2.14	186±24	6.3±0.7	SAX
020124	LONG	3.20	448±148[(b)]	31±3	HET/KON
020813	LONG	1.25	590±151[(b)]	76±19[(b)]	HET/KON
020819b	LONG	0.410	70±21	0.79±0.20	HET
021004	LONG	2.30	266±117	3.8±0.5	HET
021211	LONG	1.01	127±52[(b)]	1.3±0.15	HET/KON
030226	LONG	1.98	289±66	14±1.5	HET
030328	LONG	1.52	328±55	43±4	HET/KON
030329	LONG	0.17	100±23[(b)]	1.7±0.3 [(b)]	HET/KON
030429	LONG	2.65	128±26	2.50±0.30	HET
040924	LONG	0.859	102±35[(b)]	1.1±0.12	HET/KON
041006	LONG	0.716	98±20	3.5±1.0	HET
050318	LONG	1.44	115±25	2.55±0.18	SWI
050401	LONG	2.90	467±110	41±8	KON
050525	LONG	0.606	127±10	3.39±0.17	SWI
050603	LONG	2.821	1333±107	70±5	KON
050922c	LONG	2.198	415±111	6.1±2.0	HET
051022	LONG	0.80	754±258[(b)]	63±6	HET/KON
051109	LONG	2.346	539±200	7.5±0.8	KON

Table D.1: 39 long burst used for the calibration of the Amati relation from Amati 2006 [1]

Bibliography

[1] L. Amati. *M.N.R.A.S*, 372(4):233–245, 2006.

[2] L. Amati, F. Frontera, M. Tavani, J. J. M. in't Zand, A. Antonelli, E. Costa, M. Feroci, C. Guidorzi, J. Heise, N. Masetti, E. Montanari, L. Nicastro, E. Palazzi, E. Pian, and P. Piro, L. andSoffitta. Intrinsic spectra and energetics of BeppoSAX Gamma-Ray Bursts with known redshifts. *A&A*, 390:81–89, July 2002.

[3] M. Arimoto, N. Kawai, K. Asano, K. Hurley, M. Suzuki, Y. E. Nakagawa, T. Shimokawabe, N. V. Pazmino, R. Sato, M. Matsuoka, A. Yoshida, T. Tamagawa, Y. Shirasaki, S. Sugita, I. Takahashi, J.-L. Atteia, A. Pelangeon, R. Vanderspek, C. Graziani, G. Prigozhin, J. Villasenor, J. G. Jernigan, G. B. Crew, T. Sakamoto, G. R. Ricker, S. E. Woosley, N. Butler, A. Levine, J. P. Doty, T. Q. Donaghy, D. Q. Lamb, E. Fenimore, M. Galassi, M. Boer, J.-P. Dezalay, J.-F. Olive, J. Braga, R. Manchanda, and G. Pizzichini. Spectral-Lag Relations in GRB Pulses Detected with HETE-2. *PASJ*, 62:487, April 2010.

[4] Z. Bagoly, L. Borgonovo, A. Mészáros, L. G. Balázs, and I. Horváth. Factor analysis of the long gamma-ray bursts. *A&A*, 493:51–54, January 2009.

[5] R. D. Blandford and R. L. Znajek. Electromagnetic extraction of energy from Kerr black holes. *M.N.R.A.S.*, 179:433–456, May 1977.

[6] L. Borgonovo, F. Frontera, C. Guidorzi, E. Montanari, L. Vetere, and P. Soffitta. *A&A*, (418):418–487, 2004.

[7] L. Borgonovo, F. Frontera, C. Guidorzi, E. Montanari, L. Vetere, and P. Soffitta. *A&A*, 465:765–775, 2007.

[8] H.-Y. Chang. Fourier Analysis of Gamma-Ray Burst Light Curves: Searching for a Direct Signature of Cosmological Time Dilation. *ApJL*, 557:L85–L88, August 2001.

[9] Li Chen, Y.Q Lou, M. Wu, J.L. Qu, and S.M Jia. *ApJ*, 619(1):983–993, 2005.

[10] B. E. Cobb, J. S. Bloom, D. A. Perley, A. N. Morgan, S. B. Cenko, and A. V. Filippenko. Discovery of SN 2009nz Associated with GRB 091127. *ApJL*, 718:L150–L155, August 2010.

[11] M. G. Dainotti, R. Willingale, S. Capozziello, V. Fabrizio Cardone, and M. Ostrowski. Discovery of a Tight Correlation for Gamma-ray Burst Afterglows with "Canonical" Light Curves. *ApJL*, 722:L215–L219, October 2010.

[12] A. de Ugarte Postigo, I. Horváth, P. Veres, Z. Bagoly, D. A. Kann, C. C. Thöne, L. G. Balazs, P. D'Avanzo, M. A. Aloy, S. Foley, S. Campana, J. Mao, P. Jakobsson, S. Covino, J. P. U. Fynbo, J. Gorosabel, A. J. Castro-Tirado, L. Amati, and M. Nardini. Searching for differences in Swift's intermediate GRBs. *A&A*, 525:A109, January 2011.

[13] Band D. et al. *ApJ*, 413:281, 1993.

[14] Barthelmy S. D. et al. *Space Sci. Rev.*, 120(5):143–164, 2005.

[15] Kouveliotou C. et. al. *ApJ L.*, 413:101, 1993.

[16] Mitrofanov I. et al. *ApJ*, 522:1069–1078, 1998.

[17] E. E. Fenimore, J. J. M. in 't Zand, J. P. Norris, J. T. Bonnell, and R. J. Nemiroff. Gamma-Ray Burst Peak Duration as a Function of Energy. *ApJ*, 448:L101, August 1995.

[18] N. Gehrels, J. P. Norris, S. D. Barthelmy, J. Granot, Y. Kaneko, C. Kouveliotou, C. B. Markwardt, P. Mészáros, E. Nakar, J. A. Nousek, P. T. O'Brien, M. Page, D. M. Palmer, A. M. Parsons, P. W. A. Roming, T. Sakamoto, C. L. Sarazin, P. Schady, M. Stamatikos, and S. E. Woosley. A new γ-ray burst classification scheme from GRB060614. *Nat*, 444:1044–1046, December 2006.

[19] G. Ghirlanda. Advances on GRB as cosmological tools. *ArXiv e-prints*, August 2009.

[20] G. Ghirlanda, G. Ghisellini, C. Firmani, A. Celotti, and Z. Bosnjak. The peak luminosity-peak energy correlation in gamma-ray bursts. *M.N.R.A.S.*, 360:L45–L49, June 2005.

[21] A. Goldstein, R.D. Preece, and M.S. Briggs. *ApJ*, 721:1329–1332, 2010.

[22] J. Hakkila, T. W. Giblin, J. P. Norris, P. C. Fragile, and J. T. Bonnell. Correlations between Lag, Luminosity, and Duration in Gamma-Ray Burst Pulses. *ApJLl*, 677:L81–L84, April 2008.

[23] D. W. Hogg. Distance measures in cosmology. *ArXiv Astrophysics e-prints*, May 1999.

[24] I. Horváth, Z. Bagoly, L. G. Balázs, A. de Ugarte Postigo, P. Veres, and A. Mészáros. Detailed Classification of Swift 's Gamma-ray Bursts. *ApJ*, 713:552–557, April 2010.

[25] I. Horváth, L. G. Balázs, Z. Bagoly, F. Ryde, and A. Mészáros. A new definition of the intermediate group of gamma-ray bursts. *A&A*, 447:23–30, February 2006.

[26] I. Horváth, L. G. Balázs, Z. Bagoly, and P. Veres. Classification of Swift's gamma-ray bursts. *A&A*, 489:L1–L4, October 2008.

[27] B. Link and W.C. Epstein, R.I.and Priedhorsky. *ApJ*, 408:81–84, 1993.

[28] J. S. Maritz. Distribution-Free Statistical Methods. *Chapman and Hall*, 1981.

[29] R. Narayan, B. Paczynski, and T. Piran. Gamma-ray bursts as the death throes of massive binary stars. *ApJL*, 395:L83–L86, August 1992.

[30] J. P. Norris, G. F. Marani, and J. T. Bonnell. Connection between Energy-dependent Lags and Peak Luminosity in Gamma-Ray Bursts. *ApJ*, 534:248–257, May 2000.

[31] B. Paczyński. Gamma-ray bursts as hypernovae. In *Gamma-Ray Bursts, 4th Hunstville Symposium*, volume 428 of *American Institute of Physics Conference Series*, pages 783–787, May 1998.

[32] Shi Qi and Tan Lu. *ApJ*, 717:1274–1278, 2010.

[33] E. Ramirez-Ruiz and E. E. Fenimore. Pulse Width Evolution in Gamma-Ray Bursts: Evidence for Internal Shocks. 539:712–717, August 2000.

[34] G.B. Rybicki and A.P. Lightman. Radiative processes in astrophysics. (Wiley-VCH), 1979.

[35] R. Salvaterra, M. Della Valle, S. Campana, G. Chincarini, S. Covino, P. D'Avanzo, A. Fernández-Soto, C. Guidorzi, F. Mannucci, R. Margutti, C. C. Thöne, L. A. Antonelli, S. D. Barthelmy, M. de Pasquale, V. D'Elia, F. Fiore, D. Fugazza, L. K. Hunt, E. Maiorano, S. Marinoni, F. E. Marshall, E. Molinari, J. Nousek, E. Pian, J. L. Racusin, L. Stella, L. Amati, G. Andreuzzi, G. Cusumano, E. E. Fenimore, P. Ferrero, P. Giommi, D. Guetta, S. T. Holland, K. Hurley, G. L. Israel, J. Mao, C. B. Markwardt, N. Masetti, C. Pagani, E. Palazzi, D. M. Palmer, S. Piranomonte, G. Tagliaferri, and V. Testa. GRB090423 at a redshift of z˜8.1. *Nat*, 461:1258–1260, October 2009.

[36] R. Sari, T. Piran, and Narayan R. *ApJ Lett.*, 497(L17), 1998.

[37] B. E. Schaefer, M. Deng, and D. L. Band. Redshifts and Luminosities for 112 Gamma-Ray Bursts. *ApJL*, 563:L123–L127, December 2001.

[38] Piran Tsvi. *Rev. Mod. Phys.*, 76(4):1143–1210, 2005.

[39] N. Vasquez and N. Kawai. volume 19 of *International Journal of Modern Physics D*, pages 997–1002, June 2010.

[40] N. Vasquez and N. Kawai. volume 1279 of *American Institute of Physics Conference Series*, pages 454–456, October 2010.

[41] S. E. Woosley, S. Blinnikov, and A. Heger. Pulsational pair instability as an explanation for the most luminous supernovae. *Nat*, 450:390–392, November 2007.

[42] K. Yamaoka, A. Endo, T. Enoto, Y. Fukazawa, R. Hara, Y. Hanabata, S. Hong, T. Kamae, C. Kira, N. Kodaka, M. Kokubun, S. Maeno, K. Makishima, R. Miyawaki, K. Morigami, T. Murakami, Y. E. Nakagawa, K. Nakazawa, N. Ohmori, M. Ohno, K. Onda, G. Sato, E. Sonoda, S. Sugita, M. Suzuki, M. Suzuki, H. Tajima, T. Takahashi, T. Takahashi, H. Tanaka, T. Tamagawa, M. S. Tashiro, Y. Terada, T. Uehara, Y. Urata, M. Yamauchi, A. Yoshida, K. Hurley, V. Pal'Shin, T. Sakamoto, and J. Cummings. Design and In-Orbit Performance of the Suzaku Wide-Band All-Sky Monitor. *PASJ*, 61:35, January 2009.

[43] D. Yonetoku, T. Murakami, T. Nakamura, R. Yamazaki, A. K. Inoue, and K. Ioka. Gamma-Ray Burst Formation Rate Inferred from the Spectral Peak Energy-Peak Luminosity Relation. *ApJ*, 609:935–951, July 2004.

[44] J. J. M. Zand and E. E. Fenimore. The autocorrelation function of gamma-ray burst time profiles. *ApJ*, 464:622–627, 1996.